Topologically close-packed phase development during solution heat treatment of rhenium containing single crystal nickel-based superalloys

JOHN MICHAEL HARRISON

A thesis submitted to the University of Birmingham for the degree of

DOCTOR OF PHILOSOPHY

UNIVERSITY OF BIRMINGHAM

School of Metallurgy and Materials

College of Engineering and Physical Sciences

University of Birmingham

June 2024

ABSTRACT

Superalloys, aptly named for their high-temperature performance, are at the forefront of materials technology for applications such as turbine blades in jet engines for both power and propulsion. Their complex chemistry, comprising often over a dozen elements, unique production methods, such as single-crystal casting, on top of their manufacturing complexity, with preformed cooling channels and coatings enable these materials to function in extreme circumstances.

However, their ever-growing complexity creates equally complex problems that are ever more unique to the alloys and harder to separate from all the different processes involved in the manufacture and operation.

Of these, topologically close-packed phases, or TCP phases, stand out as they are poorly understood in both why and how they form. It is known they are typically enriched in refractory elements, the same elements that provide the alloy with its superior high-temperature properties. However, the growing complexity of these alloys now see TCP phases occurring not just in-service conditions, but during manufacturing, in the as-cast state, heat-treatments and the focus of this work; the solution heat-treatment stage. The occurrence of these phases during solutioning is particularly problematic, as this stage is intentionally included to homogenise the alloy into a single phase, not introduce additional detrimental phases in a heterogeneous manner.

This work seeks to review past work on the study of nickel-based superalloys, in particular high refractory content alloys prone to TCP phase precipitation. As well as other works carried out to understand the occurrence of TCP phases. Through the casting of single-crystal alloys containing varying levels of Re; CMSX4, CMSX10K and CMSX10N, where Re is an element strongly associated with TCP phase precipitation, experiments

are carried out on the standard solutioning regime of these alloys to better understand the microstructural evolution during the solutioning process.

Through these experimental results, supported with modelling experiments primarily carried out using ThermoCalc software, efforts are undertaken to better the understanding of when; if at all, which TCP phases occur during the solutioning process. Calculation of volume fractions present, where in the microstructure they occur and expansion of the understanding of their initial formation, and why in some cases they appear to eventually redissolve or never form in the first place. The aspiration of this work is to inform future alloy development of the risk certain aspects such as composition and processing contribute to TCP phase precipitation during manufacturing and how, if at all, it can be avoided or minimised.

Through the experiments and analysis undertaken during this thesis, it has been shown that TCP phases; namely σ, do occur during solutioning in all the alloys studied during the solution process even in CMSX4, an alloy with significantly lower concentrations of Re. The kinetics of TCP phase precipitation are discovered; in these scenarios, to be substantially faster than previously reported. Evidence is presented that the variance of diffusion rates of Al and Re in particular, combined with the highly segregated nature of the as-cast material are the cause of this. Al diffuses into the dendritic core regions in significant quantities to promote the precipitation of γ', concentrating the already highly segregated refractory elements; namely Re, into the remaining γ matrix promoting the precipitation of TCP phases.

Modelling is shown to qualitatively predict the occurrence of TCP phases but is currently limited in its ability to quantify the volume of precipitation. Substantial discussion is made to understand the cause of these limitations and to understand the formation method of these TCP phases, the influence of their morphology and that of the temperature changes during the solutioning process.

ACKNOWLEDGEMENTS

My most sincere thanks goes to my academic supervisor, Professor Paul Withey. His humility, generosity and patience have made him the best supervisor I could have hoped for, and his encouragement and grounding I could not have completed this thesis without. His enthusiasm, technical insights and practical advice have allowed me to thrive and grow as an academic. His regular offers of coffee no doubt boosted my productivity throughout the course of my PhD. Furthermore his dedication to review and offer suggestions to this work and others is greatly appreciated.

An appreciation of my co-supervisor, Professor Nick Green's contributions to group discussions also receive my thanks.

Further thanks go to Keehyun Park and Dimitra Spathara for the contributions to group discussions, insights and recommendations made throughout the course of my PhD.

Extensive thanks go to Adrian Caden, Jonathan Davies, Grant Holt and Amy Newell for technical assistance throughout my experimentations.

The Innovative Metals Processing Doctoral Training Center's funding and support of casual but informative gatherings has been of immense assistance.

I would give thanks to Joseph Carter, Emma Young, Miles Fan and Alex Dickinson-Lomas for friendship and practical support throughout the course of my PhD.

Many thanks to my parents, Paula and Robert Harrison, my siblings and wider family without whom I wouldn't be where I am today without their unending love and support. A special thanks goes to my niece, Charlotte Thornhill, who insisted on helping me type up several sentences despite only being six years of age.

To the congregation of St.Mary’s Church Sileby for supporting me as I began my PhD, and Oasis Church Harborne, for always pointing me towards Jesus, constant moral support and copious amounts of food.

Furthermore I would like to dedicate this work to my grandfather, Robert Neil, who served as an inspiration to my younger self to pursue the sciences.

TABLE OF CONTENTS

List of Figures

List of Tables

List of Common Abbreviations

TCP - Topologically close packed
GTE - Gas Turbine Engine
TET - Turbine Entry Temperature
σ - Sigma phase (a type of Topologically close packed phase)
γ - Gamma phase, unordered FCC.
γ' - Gamma prime phase ($L1_{2)}$ (Ni_3Al)

1. GENERAL INTRODUCTIONS

Nickel-based superalloys are one of the most complicated materials developed by mankind, often containing over ten different elements from across the periodic table in varying quantities to achieve their desired properties.

Excellent creep life, high temperature strength and environmental resistance are amongst these desired properties, further enhanced by manufacturing techniques such as single crystal castings and internal cooling channels.

Whilst undeniably the best materials to employ for their applications the ever growing complexity of these alloys, notably the inclusion of rhenium, has been at the expense of their phase stability in regards to the precipitation of detrimental topologically closed-packed phases (TCP phases).

The issue of these TCP phases are detrimental enough to the properties of these alloys that the chromium content has been reduced in many alloys, at the expense of their corrosion resistance. Whilst this issue has been addressed with specifically designed coatings for these blades, the desire to continually improve the high-temperature performance of these alloys has left them so susceptible to TCP phases they now occur not just in-service but during manufacturing too.

The works of this thesis focus on the nature of these TCP phases during manufacturing, specifically the solution treatment post-casting. Whilst TCP phases have been observed at the as-cast stage, widespread assumption is the solutioning phase will sufficiently homogenise the material and thus removes any TCP phases present. However, some alloys, namely CMSX-10N are observed to still contain TCP phases after this

homogenisation, with no explanation to this behaviour so far being presented.

Attempts are undertaken to better understand the behaviour and mechanism behind their precipitation during this period, and why certain alloys are more susceptible to them then others.

The following chapter contains an extensive literature review of research on nickel-based superalloys, what makes them superior over other materials for their intended purposes. A breakdown of the individual elements typical of inclusion in these alloys is given, with their contributions to the overall alloy and specifically TCP phases is discussed.

The contribution of different phases to the overall alloy and relation to TCP phases is also discussed as well as the manufacturing process that these materials undergo to create the desired product, and their effect on the microstructure is also discussed.

Previous methods to predict and prevent TCP phases such as modelling are discussed including benefits and limitations. Specifically in regards to CMSX-4, CMSX-10K and CMSX-10N, the alloys that this thesis focuses on.

The third chapter of this thesis presents results previously published in 2023 in the Crystals Journal within Volume 13, Issue 519, under the title: Precipitation of Topologically Closed Packed Phases during the Heat-Treatment of Rhenium Containing Single Crystal Ni-Based Superalloys.

These contain micrographs during various sections of the solution-treatment process of the showing TCP phases present in different alloys at different stages, as well as volume fraction calculations to quantify the extent of these TCP phase occurrences. The significance of aluminium on the precipitation of TCP phases is discussed at length.

The fourth chapter of this thesis builds on the previous chapter with substantial modelling data, demonstrating the effectiveness of the ThermoCalc modelling software on qualitatively predicting the occurrences of

TCP phases during the solution-treatment stage. The quantitative deficiency of the modelling software is further discussed at length and why there is a difference between the modelling and experimental data is theorised.

The fifth chapter of this thesis focuses on the contribution of the individual stages of the solution-treatment cycle and how they each might contribute to the precipitation and growth of TCP phases. Varying discrepancies are discussed at length, particularly the probability of TCP phases forming and the potential contributions from different morphologies of TCP phases to the overall volume fractions.

The final chapters of this thesis present overall conclusions from this work, primarily the role of aluminium has on the precipitation of TCPs due to the initially heterogeneous nature of the solution-treatment. Avenues of further work to build upon the understandings gained from this work are proposed and how they might be carried out and what could be gained from such experiments.

2. LITERATURE REVIEW OF NICKEL-BASED SUPERALLOYS

2.1. Gas Turbine Engines

Gas turbine engines (GTEs); the centrepiece of electricity generation and propulsion for military and commercial aircraft, possess some of the most demanding requirements of their components. Specifically the turbine blades themselves. In the decades leading up to World War Two, there had been significant investment into improving the effectiveness of aeroplanes, this led to the invention of the jet engine, and from there a desire to operate at higher temperatures (C.T. Sims, 1984). Reed (R.C. Reed, 2006) explains that the 'turbine entry temperature' (TET) is where the greatest emphasis is placed when designing a GTE, the TET is pivotal in defining how much mechanical work can be extracted during the combustion process. Aerofoils are also designed to withstand high forces for the necessary 'lift' for either propulsion or electricity generation.

Gas turbine engines have been used for power generation since the turn of the 19th century, using the principles of the Brayton thermodynamic cycle to produce electricity (C.T. Sims, 1984). The design of gas-turbine engines will usually incorporate at a minimum the following stages: a rotating gas compressor at the gas entry point to the engine, a combustor, followed by a turbine that extracts work from the gases that have been compressed and heated via the combustor, before exiting the engine (F.Whittle, 1930). By 1939 this engine had been applied to the aeroplane. The addition of a propelling nozzle; which allows the internal energy to be converted into propulsive force, created what is now known as a jet engine. The principle of the jet engine was not new, but limited by technical

advances since its inception, and has always been pushing the limits of engineering capabilities.

Propeller-driven planes lacked efficiency at higher speeds and altitudes, for which the jet engine offers a solution. Within a decade they dominated military aircraft, and a decade after that commercial ones too, with the original piston and propeller designs now relegated to niche roles (C.T. Sims, 1984). Whilst jet-powered planes lacked the efficiency of their piston and propeller-powered counterparts at low speeds and altitudes this too was overcome with the creation of the turbofan, which essentially combines the two concepts into one.

A jet engine powers a fan; usually ducted, at the front of the engine, to bypass lower velocity but a higher mass of air (in comparison to the jet engine's exhaust) over the engine and out of the nozzle, these two components combine to produce the thrust of an engine (I.Henrich, 2024).

The efficiency of these engines is determined by two things, their propulsive (Froude) efficiency, and their thermal efficiency. There are numerous other practical aspects of engines that determine their overall efficiency, but propulsion and thermal efficiencies are of the most importance. Propulsive efficiency is determined by the following equation:

$$n = 2 / (1 + Vj/Va)$$

Where Vj is the velocity of the jet whilst Va is the velocity of the aircraft. As these velocities get closer together in value the propulsive efficiency increases (R.C.Reed, 2006).

In a turbojet, these velocities can be significantly different, due to the hot temperatures in the core converting thermal energy to kinetic energy. This difference is reduced in a turbofan as some of the jet passes over the engine and is not subjected to this heating and acceleration. To minimise this an increase in the contribution to the overall thrust from the fans, rather than the turbojet, is necessary (I.Henrich, 2024).

This can be achieved in two ways, increasing the size of the fans relative to the turbojet core, or reducing the size of the turbojet core. Both require turbo engine cores to create more power relative to their size. By increasing the thermal efficiency of the engine better performance can be achieved. This can translate into reduced fuel consumption or allow for greater power and trust.

Thermal efficiency is defined by the following equation:

$$n = Wout/Qin$$

Where the W_{out} is the work output of the engine, whilst Q_{in} is the energy input of the engine. A fundamental limit to this efficiency is determined by the second law of thermodynamics, where not all heat energy can be converted into work.

Carnot's theorem states this limit more precisely with the following equation for thermal efficiency:

$$n = 1 - (Tc/Th)$$

Where T_C is the temperature of the exhaust as it leaves the engine and T_H is the temperature the jet enters the engine.

To maximise this efficiency the disparity between T_C and T_H needs to be as high as possible. The lower limit of T_C has in an ideal system a lower limit of 0K and in a practical engine will be much higher, it also needs to be of a sufficient value to limit the conversion of thermal energy into kinetic energy to keep the jet velocity and aircraft velocity similar for the maximising of propulsive efficiency.

Therefore T_H is of utmost importance when designing an engine to maximise thermal efficiency. T_H in the example of a turbofan jet engine is the turbine entry temperature (TET), and in operation is limited by the materials used in the construction of the turbines that extract the work from the jet to produce power for the turbofan.

Not only must these materials be able to withstand the high temperatures of the engine; ideally as close to its melting temperature as possible, but they must be able to withstand the operating forces at these temperatures. They must be able to operate like this for extended periods of time with minimal degradation so that they can firstly achieve their practical purpose and secondly be economically viable in doing it. Thirdly, they must also be able to tolerate the environment of the engine, resisting oxidation and corrosion from sea-water and fuel impurities at these elevated temperatures and stresses. Other considerations to take into account are the affordability of the material for wide use in aerospace, as well as its weight, (R.C.Reed, 2006).

Initial development of the materials focused around steel, as chromium alloyed steels offered good corrosion resistance and affordability. However, their applications were limited to those below 600℃ due to a fall in strength past these temperatures.

Titanium alloys, which possess both excellent low-weight properties and strength find application up to 700℃, before they begin to suffer serious oxidation issues past these temperatures (R.C.Reed, 2006), whilst coatings could alleviate some of these issues the phase changes exhibited from $\alpha \rightarrow \beta$ is also a severely limiting factor (X.Lin, 2022)

Whilst iron and titanium provide the bases of some alloys used in the engine, usually contributing to the compressor and fan blades respectively, truly high-temperature alloys were needed to advance jet engine development. These demands were met by the discovery of superalloys, which meets the stringent demands needed in a jet engine, which are predominantly nickel-based, due largely to its ability to form the strengthening precipitate γ' [Gamma-Prime] which is looked at in more detail later.

Whilst cobalt superalloys exist, cobalt more often contributes as an

alloying element to nickel-based alloys. Makineni explains the phase changes that cobalt alloys undergo from their ambient HCP crystal structure do not impart good properties for high-temperature, high-stress applications (R.C.Reed, 2006)(S.K.Makineni, 2015). However, they still find applications even in aerospace, particularly in the turbine disks, where the different demands lend themselves to the use of cobalt superalloys more (B.Geddes, 2010).

Iron superalloys also exist and find uses within the industry, but these are often alloyed so significantly with nickel that they are referred to as nickel-iron superalloys. These are noted for the appearance of the γ'' [Gamma-Double Prime] phase, which takes the place of γ' seen in nickel-based superalloys as the major strengthening component of the alloy (R.C.Reed, 2006).

2.2. High temperature materials and superalloys

Therefore, any chosen material selected for use in gas turbines needs to accommodate the demand for high TETs, by being able to withstand significant mechanical forces close to its melting temperature. However, the conditions of operation for turbine blades demand many other mechanical and chemical properties as well.

For a material to be suitable for turbine blade applications it is necessary that it is resistant to creep; an inelastic deformation process that occurs at high-temperatures over time. Furthermore it must be resistant to chemical attack in these extreme conditions, from chemical attack and oxidation at high-temperatures.

Reed (R.C.Reed, 2006) defines a material that possesses these three qualities as a high-temperature material, however Geddes, (B.Geddes,

2010) makes a clearer distinction between superalloys; which possess these properties, and other materials that do not possess all of them.

This distinction needs to be made to better approach the subject of turbine blades made from superalloys. This is because numerous materials can function at high temperatures, such as ceramics, refractory metal alloys and platinum-group-metals (PGM). Yet none of them find use (beside alloying additions) in turbine blade applications. This is because they do not simultaneously possess all of the previously defined characteristics.

Ceramics; despite their high environmental resistance, lack fracture toughness, and therefore are limited in their applications in situations of a structural nature. PGM alloys such as platinum (Pt) also boast good environmental resistance, however their lack in the mechanical strength required to operate as efficient airfoils prevent their use. Refractory metal alloys such as tungsten (W) alloys possess high strength and creep resistance necessary; largely due to their high melting points (B. Geddes, 2010), but lack the environmental resistance of ceramics or PGM alloys. Furthermore PGM alloys typically imply high cost and density (R.C Reed, 2006).

It is these extra demands that distinguish superalloys from simply ‘high-temperature materials’. However, the term superalloy itself is not strictly defined, but an alloy based largely of nickel, cobalt, or nickel-iron, with the addition of various alloying additions to produce a material with the three necessary properties is commonly accepted as a ‘superalloy’.

The second need for a distinction between superalloys and high-temperature materials is that whilst GTEs are the most common application of superalloys they are not limited solely to high-temperature applications, such as the petrochemical industry where they are valued for their very high resistance to chemical attack. The variety of alloying additions that; whilst creating some of the most complex alloys ever

developed, allow a wide range of potential applications if optimised, producing numerous different alloys for use not just in GTEs but other applications such as nuclear reactors and rocket components.

Thus, Geddes' definition of a superalloy, containing all three features simultaneously, is correct. They are superior over any other alloys or materials because of this, making them super alloys. The terms high-temperature material and superalloy should therefore not be used interchangeably, all superalloys are high-temperature materials, but not all high-temperature materials are superalloys.

2.3. Nickel

The requirements for a high-temperature material are both considered extreme and numerous, many materials fail to fulfil all these qualities. Ni(nickel) is one of the few candidates that fulfil this role. It has a melting point of 1455°C (1728K), significantly higher than that of Al(aluminium), a widely used material in aerospace, although its density is much higher than that of Ti(titanium), another aerospace material with a higher melting temperature than Ni.

Nickel (Ni) is a transition metal element with atomic number 28, a density of 8.9g/cm^3. As part of the VIIIB group of elements, it has a face-centred cubic crystal (FCC) structure, which lends to its ductility and toughness, as well as reduced diffusivity at high temperatures (R.C.Reed, 2006).

It is the 23rd most abundant element in the Earth's crust, despite significant content being trapped in the core of the planet it's still abundant enough through its deposition from meteorites that it is economically viable to extract and manufacture in its pure form on sufficient scale to be a major component of many modern-day materials.

As discussed Ti suffers from much poorer oxidation resistance than Ni. Unlike titanium's $\alpha \rightarrow \beta$ phase change a significant advantage of Ni is that it maintains its FCC γ structure from ambient conditions to its melting point. An FCC structure is ideal as it will possess ductility and toughness, also lacking the ductile/brittle transition seen in BCC materials. Reed goes on to explain how any phase transformations that occur do not promote good high-temperature properties (R.C. Reed, 2006), this is due to the volume changes usually associated with phase changes during heating of a material (J.Emsley, 2011). Makineni et al states that is why typical Co(cobalt) alloys cannot compete with Ni alloys in high stress high-temperature applications (S.K.Makineni et al, 2015)(B.Geddes, 2010). However Co alloys are used in certain situations which Geddes et al. go on to explain are in low-stress structural situations but are generally more expensive than their Ni counterparts, therefore, are generally unsuitable for the high-pressure turbine blades.

This FCC structure is so desirable, that even in iron and cobalt-based superalloys, significant proportions of nickel are often added to suppress any transformation away from the FCC structure throughout its temperature application range (B.Geddes, 2010).

Nickel is also magnetic, along with iron and cobalt, however, it possesses the weakest magnetism of the three elements, with cobalt being used for stronger magnets and iron being used for more mainstream purposes due to being cheaper, however, there is still a variety of applications for nickel.

Stainless steels often have around 10 wt% Ni content, and this popular alloy sees the majority of nickel's usage, however, it has been used to colour glass and electroplating of silver (Ag). Its ductility makes it easily drawn into and used as wire, and its considerable corrosion resistance; when combined with elements such as chromium and copper (Cu), allows it to be used

corrosion-free at high temperatures such as in toasters, ovens, as well as in seawater, and resist acids used in the food industry (J.Emsley, 2011).

Other applications include dentistry, batteries, and memory materials, such as NiTi which attempts to revert to its original shape when changed and is used in crumple zones of cars to minimise accident crash damage.

Because of these advantages Ni-based superalloys stand as the superior choice over all the major alternatives. Whilst a number of platinum-group-metals such as Re(rhenium) and Ru(ruthenium) demonstrate the necessary properties they are expensive and therefore limits their use on large scale applications. Tc(technetium) and Os(osmium) are also insufficient due to their respective radioactivity and poisonous oxide (R.C. Reed, 2006).

This phase; the γ phase, typically contains; besides Ni, Cr, Co, Mo, W, Re and Ru (E.C. Caldwell, 2004). Unlike the ordered FCC phase (LI2) of γ' the unordered FCC phase is more able to accommodate varying compositions of elements, however the solubility of these elements can vary based on temperature (R.C.Reed, 2006). Leading to super-saturation of certain elements within the γ matrix.

2.4. - The γ’ Phase (Ni_3Al) [Gamma-Prime]

Nickel’s most fascinating application; for its use as a high-temperature material, is when it is alloyed with aluminium. Nickel aluminide (Ni_3Al) possesses an ordered array of atoms, their bonding is directional and covalent, creating precise stoichiometry such as shown above. The Ni_3Al in particular is the most important in regard to superalloys. It displays a primitive cubic crystal structure; $L1_2$. In the context of nickel-based superalloys, this Ni_3Al phase is referred to as γ’ a precipitate of which its formation is significant in providing the alloys with its desirable properties.

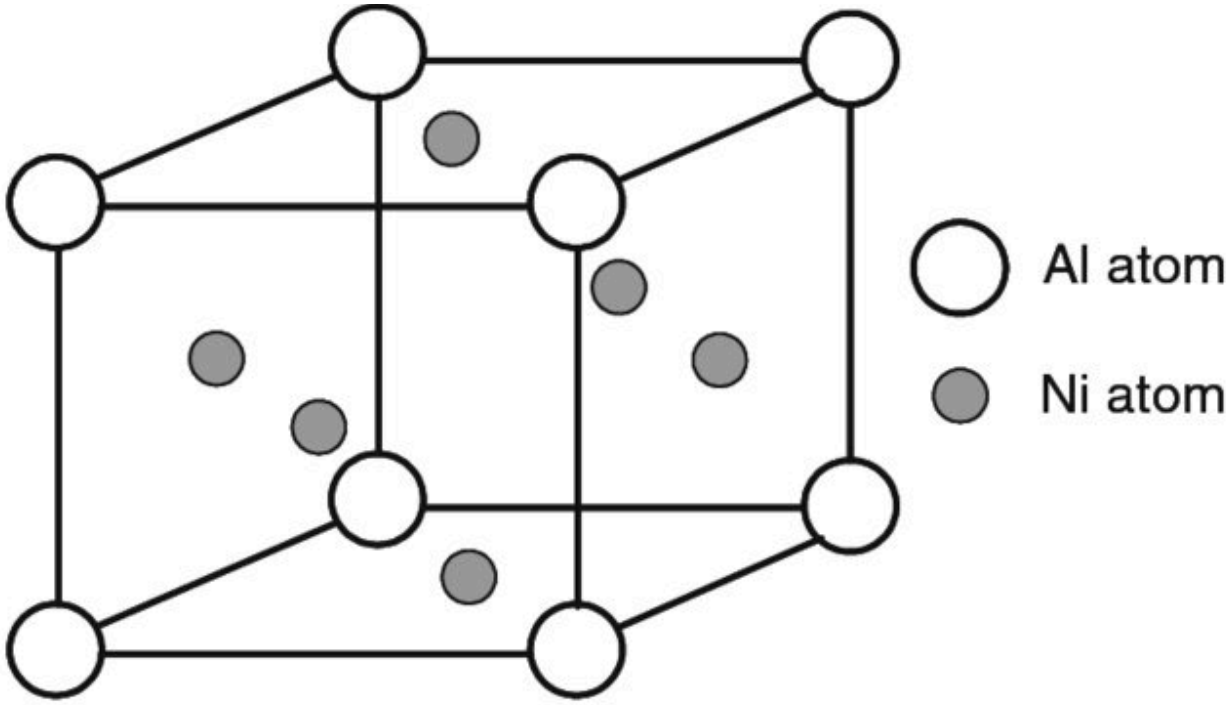

Figure 1: Showing the $L1_2$ crystal structure of nickel aluminide, with Al atoms at each of the corners, with 12 Ni atoms at their nearest neighbours, whilst Ni atoms occupy the faces, with 4 Al atoms and 8 Ni atoms as nearest neighbours. (B.Gleeson, 2009).

The ordered nature of pure Ni_3Al has been determined by extrapolation to remain so up to 1375°C, above its melting temperature. Its truly remarkable property is not only its high strength; several times that of stainless steel, but that it increases with temperature, up to 800°C, where it is up to twice as strong. Most materials decrease in strength with temperature (B. Geddes, 2010). As noted earlier steels are often limited in use to below 650 degrees, but nickel-based superalloys can operate well over 1000 degrees, with both high-strength and corrosion resistance (R.C.Reed, 2006)(J.Emsley, 2011).

γ′ possesses a unique planar defect; the anti-phase boundary, which is of great importance to superalloy metallurgy as it vastly changes the way the phase deforms compared to the FCC matrix.

Due to the ordered nature of γ′s $L1_2$ structure where Al bonds solely with its nearest neighbouring 12 Ni atoms, Al-Al bonds less formable, as well as Ni-Ni bonds. Therefore if a dislocation enters the matrix and displaces a layer, forbidden bonds can occur, which carry with them associated energy; an Anti-Phase-Boundary (APB) energy, which is quite substantial. This ABP energy is anisotropic, as depending on the plane the dislocation occurs in will affect the number of forbidden bonds occurring. The {001} plane for example, at the first order, does not cause any forbidden bonds, therefore having the lowest associated APB energy (R.C.Reed, 2006).

This energy penalty for a dislocation to enter γ′ is so significant that dislocations must move in pairs through γ′, and are referred to as super dislocations, or super-paritals in the case of the individual dislocation. For particle cutting to occur, stresses of approximately 400MPa would be needed, showing that for nickel-aluminium alloys order strengthening is the significant strengthening mechanism in the alloy (R.C.Reed, 2006).

The need for these super-partials to pair is considered the primary factor in why nickel-aluminium alloys exhibit an anomalous yielding pattern; that is that its yield stress increases with temperature before decreasing when in excess of 800℃.

Through γ′ dislocations tend to travel through the {111} slip-plane, however some will attempt to cross-slip onto the {100} plane, but as soon as a super-partial makes this jump it lacks it's pair, and has a ABP energy requirement to continue moving. These then become Kear-Wilsdorf locks, which in a more typical work-hardening fashion leads to increased strength(H.K.D.H. Bhadeshia, 2003). This cross-slipping mechanism has a thermally activated component, increasing in frequency with an increase in

temperature, leading to increased strength, until the 600°C-800°C range where the dislocations have enough energy to overcome these Kear-Wilsdorf locks (R.C.Reed, 2006). However, this mechanism is considered to be insufficient in explaining the strengthening behaviour of these alloys, as it occurs at lower temperatures that should be expected for a thermally activated process, and has varying responses in compression and tension.

The ɣ’ precipitate is so effective in providing high-temperature strength that one would expect at high a fraction as can be obtained, since increasing volume fraction of ɣ’ increases the Orowan stress values in turn increasing the yield. However an optimal volume fraction stands not at 100%

The ɣ/ɣ’ interface also imparts resistance to creep deformation, Reed suggests a volume fraction of up to 70% (R.C.Reed, 2006). The major reason to prevent 100% ɣ’ volume fraction is the strengthening that the interface between the two phases provides, particularly in regards to creep (T. B. Gibbons & B. E. Hopkins, 1984).

The coherency of ɣ’ with the ɣ matrix produces only a small misfit and associated interfacial energy between the two phases, this, in turn, promotes microstructural stability in the alloy and resistance to the formation of precipitates and their coarsening at these boundaries (H.K.D.H. Bhadeshia, 2003), however, to maintain this coherency the ideal morphology for the ɣ’ is that of cubes, like most precipitates they start as spheres, and eventually coarsen into cubes to mitigate this misfit strain. A significant amount of effort, in both the processing methods and composition of these alloys is carried out to ensure this cuboidal morphology and high volume fraction is achieved (R.C.Reed, 2006).

γ' coarsening leads to loss of coherency and therefore significantly contributes to loss of strength. To reduce this coarsening reducing the γ/γ '

misfit strain and modulus misfit is suggested (M.V. Acharya, 2004). Which can be done by increasing Al/Ti ratio as well as the introduction of slow diffusing elements to partition to γ'. Re has also been shown to slow γ' coarsening rates (R.C.Reed, 2006). This coarsening occurs at significant rates above 0.6Tm (B. Geddes, 2010).

Pivotal to the morphology of γ' precipitates is the lattice mismatch between the γ and γ'. Geddes (B. Geddes, 2010) reports that a mismatch below 0.2% produces spherical precipitates; which minimises the surface energy, whilst these become cuboidal particularly between 0.5% - 1.0%, minimises elastic energy as it becomes larger than the surface energy.

This interface 'is a barrier to mobile dislocations and a hindrance to plate thickening due to dislocation pile-up at the interface' (B.Geddes, 2010).

2.5. - Creep

Creep is time-dependent plastic deformation that occurs at sufficiently high temperatures, and is of significant concern to the design and operation of turbine blades. At its extremes it can cause rupture of the blades, but even at its earlier stages, induced creep strain can change the dimensions of the blade, which have strict dimensions for their fitting and function into the engine housing.

Nickel's latent resistance to creep deformation is very temperature sensitive, with a 25°C temperature increase effectively doubling the creep strain (R.C.Reed, 2006), strictly limiting the effective operating temperature range of it, therefore the alloy has needed its creep resistance properties improved.

The strengthening of a material to minimise creep can be achieved via two methods, precipitation strengthening, and solid solution strengthening.

An increase in the ɣ’ volume fraction has a direct increase to creep strength (T.B.Gibbons, 1984), and whilst it is significant increase eventually the movement of dislocations is limited to the ɣ phase. Here, solid-solution strengthening is required, which contributes a significant number of the alloying additions seen in nickel-based superalloys.

The inclusions of atoms into the primary phase of an alloy to prevent the movement of dislocations are seen in many alloys. With the ɣ phase, a strong positive correlation to improving creep-strength between the size difference between the solid-solution atom inclusion and nickel, as well as the concentration of the element in question (R.C.Reed, 2006), Gold (Au) for example was shown to be effective in increasing the creep resistance, however not only is it uneconomical it's low melting temperature would impede its high-temperature capabilities.

However, there are other elements that also possess high atomic radii that are economical to include, some of which also possess very low diffusion rates in nickel, which is ideal for minimising creep, a diffusion-based mechanism.

Refractory elements in particular have since the 1940s been used to vastly improve the strength of nickel-based superalloys through both solid-solution strengthening as well as have potential for precipitate strengthening, particularly in the form of carbides (C.T.Sims, 1984). The initial element of inclusion in these alloys was molybdenum (Mo).

Specific to these ɣ’ containing alloys in regards to creep is the process of rafting, where there is a disruption to the evenly distributed cuboidal ɣ’ precipitates that coalesce via the process of ‘rafting’ into plates.

Rafting is associated with a negative misfit between the two (which itself occurs when ɣ’ has a smaller lattice parameter than ɣ)(H.K.D.H.

Bhadeshia, 2003). A rafted structure is often considered to directly impact the creep properties of the alloy, such as creep hardening (R.C.Reed, 2006).

2.6. - Other phases

Many other phases, such as borides, carbides, γ'' and topologically close-packed (TCP) phases can occur, however in this work only TCP phases are relevant, some consideration for the other phases are discussed in later sections, however TCP phases are discussed in detail in section 2.4.

2.7. Alloying additions

Even though it is advantageous over its counterparts Ni still suffers from setbacks, mostly in its creep-resistance that limits its performance at high-temperature (C.T. Liu, 1995). The addition of numerous alloying elements has been the method to improve these properties; a characteristic of the continual development of superalloys, creating very complex materials. Around the 1970's saw the development of what is often referred to as second generation superalloys. Second generation superalloys have been characterised by the addition of the refractory element rhenium (Re) (M.Pessah, 1992)(W.S. Walston, 1996).

Third generation single crystal superalloys follow a similar suit by continuing to increase the refractory element content; specifically rhenium, to further improve the operating temperatures and properties of the alloys (W.S. Walston, 1996)(A.S. Wilson, 2017). This is characterised by not only increasing the refractory elements weight percentage but also the number of different elements introduced. Furthermore, the introduction of elements such as hafnium and yttrium, as well as the reintroduction of boron and carbon (P. Caron, 1999).

Numerous papers have discussed at length the effects that different refractory elements have on improving mechanical properties of nickel-based superalloys.

However, the increase of presence of refractory elements in these alloys leads to the production of TCP (topologically close-packed) phases. (M. Pessah, 1992)(M.S.A Karunaratne, 2001)(C.M.F Rae, 2000)(F. Sun, 2011)(A.S. Wilson, 2017). These are formed from the elements Ni, Cr, Co, Mo, W and Re. (R.C. Reed, 2006)(F. Long, 2009)(F. Sun, 2011), and so in designing these alloys limitations are placed on the use of these elements to prevent or limit the formation of TCP phases (M.Pessah, 1992).

2.7.1. Aluminium

Aluminium is an important addition to nickel-based superalloys, as the primary element involved in the production of the strengthening phase γ′ as discussed in **1.3**. This is due to aluminium's preference to partition to the γ′ phase (E.C.Caldwell, 2004). This has meant Al has been included in nickel-based superalloys since the first generation and have been kept at roughly the same concentrations (6wt%) throughout their evolution (P.Caron, 1999)(B.Geddes, 2010).

Aluminium is useful in addition to its alloying effect with nickel. Its low density of 2.7g/cm^3 with good strength sees extensive use throughout aeroplanes mostly for fuselage. Its low melting temperature of 661°C limits its use in hot sections of the engine, besides as an alloying element. The oxide film that forms from Aluminium, Al_2O_3, whilst not as potent as Cr_2O_3, grants the alloy considerable resistance to environmental degradation and is particularly effective at stopping corrosion. Aluminium is also abundant, and whilst still intensive to produce virgin material it's highly recyclable and cheap (J.Emsley, 2011).

Because of Al’s tendency to form ɣ’ its concentrations have to be tightly controlled, as the volume of ɣ’ significantly affects the overall strength of the alloy, as well as other properties such as weldability (B.Geddes, 2010). Furthermore, whilst Al is a major element in forming ɣ’ it is limited in its solubility in Ni below the quantities needed to form the satisfactory ɣ’ necessary (R.C.Reed, 2006).

For these reasons Al concentrations of 5-6wt% are typical of the majority of superalloys (Cannon-Muskegon, 2023), this is a lower concentration that would be needed to achieve the ideal volume fraction of ɣ’, but increased Al contributes to lower ductility in the alloy as well as poor weldability (B.Geddes, 2010), several processing concerns also lead to the reduction and replacement of Al in these alloys, which are considered in greater depths in later sections.

Therefore, nickel-based superalloys have to also include other ɣ’ formers. Aluminium has been included in nickel-superalloys since their inception for the above reasons, but as discussed in later sections aluminium segregates substantially, lowering the local incipient melting temperatures and as discovered in this work, it's substantially faster diffusion rate than other alloying elements indirectly contributes to the precipitation of TCP phases. While it may always be necessary further research for it's replacement by other ɣ’ such as titanium and tantalum could offer promising results to improving specific properties of these alloys.

2.7.2. Cobalt

Cobalt is used in a base metal for cobalt-based superalloys, possessing some of the properties needed for superalloy applications, specifically high environmental resistance and good performance at high temperatures (S.K. Makineni et al, 2015), however suffer from poor hardenability and can be

expensive (B.Geddes, 2010)(R.C.Reed,2006). Despite this cobalt is still used as an alloying element as it still possesses many of the desired properties of superalloys.

The role of cobalt in alloys appears to be rather disputed, Geddes (B.Geddes, 2010) reports that the literature has conflicting reports on the stress rupture life, and Caron (P. Caron, 1999) states 'the role of Co on the precipitation of TCP phases is still very controversial'.

However, it is agreed that cobalt does improve the creep life of nickel-based superalloys at intermediate temperatures, as well as increases the volume fraction of the γ' (B.Geddes, 2010).

Cobalt additions to nickel-based superalloys have varied, in part due to its contribution to TCP phase precipitation. (G.Erickson, 1996) describes how the cobalt content was kept low in CMSX-10 to reduce the tendency of TCP phases forming. Yet (W.S.Walston, 1996) describes how cobalt is kept high in Rene 6; which is seen in many 3rd generation alloys , to improve phase stability.

(P. Caron, 1999) describes how cobalt, along with other γ-forming elements must be kept low to avoid TCP precipitation due to Rhenium's preferential partitioning to the γ-matrix. However (E.C. Caldwell, 2004) showed that rhenium's segregation coefficient is significantly reduced with increasing cobalt content (up to 12%) which would explain how such high cobalt content can exist in nickel-based superalloys without excessive TCP precipitation.

It is clear that cobalt's contribution to the nickel-based superalloys phase stability is not fully understood, it is apparent that it can be included in alloys in substantial quantities without deteriorating its properties. It is clearly beneficial and so further research to understand how it can be included guarenting benefits whilst preventing detriments would be beneficial to continued alloy development.

2.7.3. Chromium

Chromium, along with aluminium, contributes to the corrosion resistance of nickel-based superalloys by the production of protective oxide scale; Cr_2O_3. However, chromium also partitions to the γ phase and contributes to the precipitation of TCP phases. Therefore it has been reduced in its content in nickel-based superalloys as rhenium has increased, but at the expense of its corrosion resistance (P. Caron, 1999).

Despite not being present in sufficient quantities to provide environmental resistance through Cr_2O_3 it does have an effect upon the aluminium activity, causing the latter to form Al_2O_3 protective oxide at much lower concentrations (B.Geddes, 2010). Therefore chromium can be found typically in the concentrations of a few percent in alloys to provide it with some environmental resistance.

Chromium is also a major component of carbides; many of which form at high-temperatures. Whilst these are very important in the strengthening of cobalt-based superalloys the effect is less in nickel-based superalloys; which depend on γ' for strengthening. However, in alloys that still contain, or have had carbon reintroduced these precipitates can still provide strengthening to nickel-based alloys (L.R. Liu, 2003). As well as reducing the coarsening rate of γ' (B.Geddes, 2010).

Despite this chromium's tendency to promote TCP phase formation, and it's strength reduction due to inhibition of γ' formation means chromium additions have continued to decrease over the years of nickel-based superalloy development (B.Geddes, 2010).

Whilst the loss of environmental resistance with the reduction of chromium seems like a significant drawback in the continual development of these alloys, the development of coatings has vastly outweigh this in recent

years, improving these coatings seems substantially more promising then trying to balance the composition of these alloys to retain their environmental resistances.

2.7.4. Refractory element contributions

2.7.4.1. Tantalum

Tantalum has been added to nickel-based superalloys for a variety of reasons, it shares some of the positive benefits of tungsten and molybdenum. Specifically it's solid-solution strengthening properties, however tantalum provides this strengthening to both γ and γ' phases (B.Geddes, 2010).

On Top of this it also improves corrosion resistance, specifically hot corrosion (P. Caron, 1999)(B.Geddes, 2010).

Unlike other refractory elements tantalum; along with niobium segregates strongly to the interdendritic region, increasing the alloy strength due to its positive effect on the γ' as well as being useful in reducing defects such as freckling and hot tearing(B. Geddes, 2010)(R.C.Reed, 2006), the former defect is prevented because unlike other refractory alloying additions tantalum partitions to the interdendritic fluid increasing it's density to become closer to that of the dendritic γ phase.

Karunaratne also states the use of Ta to offset the mismatch Re and W produce, (M.S.A. Karunaratne, 2001).

Specifically in single-crystal alloys tantalum is used to replace titanium, as it is both a γ' strengthener and also raises the solidus temperature, however another feature of single-crystals is that lack of carbon, which 'frees' some tantalum which is a potent carbide former increasing incipient melting temperature, although this could also be

because of the lack of carbon. Regardless, higher heat treatment temperatures can be used giving a better control of γ' size and distribution (B.Geddes, 2010).

Because of its beneficial effects on casting defects, incipient and solidus temperatures, strengthening of γ' and replacement of titanium, tantalum is now a crucial alloying addition to single-crystal superalloys, resulting in high levels (P.Caron, 1999).

Tantalum is highly beneficial to nickel-alloy development, and whilst it has seen some replacement by rhenium which contributes more to certain properties, rhenium appears to contribute more to deleterious properties too. Tantalum continues to be an effective way to balance out rhenium by conveying benefits without too many substantial negatives.

2.7.4.2. Niobium (or Columbium)

Niobium has been added to a variety of superalloys for a variety of reasons. It has seen addition in iron-nickel based superalloys for precipitation hardening, strengthening the alloys by forming γ'' (B.Geddes, 2010)(R.C.Reed, 2006), although this can also be present in nickel-based superalloys.

Geddes, (B.Geddes, 2010) states that niobium's large misfit can also provide solid-solution hardening to a greater extent that of tungsten, however, unlike other refractory elements niobium; along with tantalum, preferentially partitions to the γ' phase, and the interdendritic region (B.Geddes, 2010)(R.C. Reed, 2006).

Probstle (M. Probstle, 2016) states the importance of Nb additions in modern nickel-based superalloys, which is now present in most modern alloys due to its positive effect on the γ' precipitates that are vital to the mechanical properties of these alloys.

This is for many of the same reasons as tantalum, which share many properties, however niobium's density is lower, and it is cheaper and so is often used to replace tantalum. Like tantalum this precipitate orientated benefit comes about due to niobium's partition to γ' reducing coarsening and increasing the γ' volume fraction, both crucial in increasing alloy strength (B.Geddes, 2010).

However, niobium does suffer a few setbacks. It reduces hot corrosion resistance (B.Geddes, 2010) and its lower density means niobium likely exacerbates the freckling defect occurrence rather than improves it like tantalum does, meaning the latter cannot be completely replaced by the former.

Niobium currently does not see a large wt% contribution to rhenium containing alloys. However it's ability to offset some of negatives of rhenium and tungsten whilst maintaining some positives, and it's ability to from Ɣ' could be worth thorough investigation into a Nb-W-Re low Al alloy with maintained properties but reduced TCP phase propensity. What fallout such a system might have is also unknown.

The advancement of coatings may also negate the detrimental corrosion properties of niobium.

2.7.4.3. Molybdenum

Molybdenum, like many refractory elements is added to increase strength though solid-solution hardening, due to its large atomic radius; significantly larger than that of nickel, which has seen its increased addition to continually improve the operating temperature of nickel-based superalloys (B.Geddes, 2010)(C.M.F Rae, 2000)(A.S.Wilson, 2017)(P.Caron, 1999).

This large atomic radius; resulting in lowered diffusion rates, also serves to improve creep properties and reduce coarsening of γ', contributing

to improved strength and creep properties (P.Caron, 1999), the creep improving properties exceeding that of tantalum(B.Geddes, 2010)

Liu (C.T. Liu, 1995) discusses how Mo also improves strength and ductility due to its low solubility, furthermore studies the effects on many of these refractory elements on the properties of nickel-base superalloys. However Geddes (B.Geddes,2010) states that the solubility of molybdenum is significantly affected by other elements in the alloy and its own content. However, Mo solubility is generally low.

Furthermore, the addition of Mo to single-crystal superalloys has occurred for its ability to reduce the lattice misfit between γ and γ', which Reed states as 'critical to superior creep performance'. (R.C. Reed, 2006). Geddes (B.Geddes, 2010) also states the mismatch is effected, by increasing the lattice parameter of the γ phases, decreasing the mismatch since it is defined by:

$$Sigma = 2 * [(ay' - ay)/(ay' + ay)]$$

Reed goes on to explain that small misfits improve coherence between the phases, promoting preferred cuboidal γ' precipitates, with negative misfits also possibly improving the creep resistance of the alloy (R.C.Reed, 2006).

"Mo increases lattice parameter, solvus temperature and weight fraction of γ', by reducing Al solubility in γ, and Cr content in γ'" (B.Geddes, 2010). However, molybdenum also suffers some drawbacks, such as its reduction to corrosion resistance when used as an alloying addition to nickel (P. Caron, 1999).

Whilst Mo is an effective addition to nickel-based superalloys, its low solubility significantly limits the extent of its potential contribution. This work goes to show amongst others that Mo also contributes to TCP phase precipitation despite it's low content, and thus it's contributions should be

kept low, and there seems little benefit to further research on it in these rhenium containing alloys.

2.7.4.4. Tungsten

Tungsten, like many refractory elements is added to increase strength through solid-solution hardening, due to its large atomic radius that via increasing γ/γ' lattice misfit, which has seen its increased addition to continually improve the operating temperature of nickel-based superalloys (B.Geddes, 2010)(M.S.A Karunaratne, 2001)(C.M.F Rae, 2000)(A.S. Wilson, 2017).

This large atomic radius; resulting in lowered diffusion rates, also serves to improve creep properties and reduce coarsening of γ', and is a lower density substitute for rhenium if designed to keep high creep-resistance (B.Geddes, 2010).

Tungsten's preference to partition to the γ phase; whilst leading to solid-solution strengthening, also leads to a tendency to form TCP phases (B.Geddes, 2010).

Tungsten offers multiple benefits whilst also contributing to several negative features, such as freckling, segregation, and TCP phase precipitation. Its contributions are still vital to superalloys, and it seems unlikely viable non-tungsten alloys will be able to compete. Yet its wt% contributions vary from alloy to alloy by several percent, with some alloys such as first generation CMSX-6 having none at all (Cannon-Muskegon, 2023). Continued research on tungsten could be beneficial, but any benefits will likely come without drawbacks, most alloys have settled around 6-8wt% tungsten and this seems ideal for optimisation and attempting alloying outside of this range seems redundant.

2.7.4.5. Rhenium

Rhenium is considered beneficial to hot corrosion and oxidation resistance of nickel-based superalloys; despite the poor resistance observed in rhenium alloys, due to its effect on the diffusion of reactive elements in the alloy (P. Caron, 1999). However Geddes (B.Geddes,2010) notes that oxidation resistance in low-aluminium content nickel-based superalloys is degraded due to the presence of rhenium due to it preventing alumina scale forming.

Rhenium is also identified as a potent source in SRZ(Secondary Reaction Zone) production. SRZs and TCPs compete for the same elements from the matrix reducing chemical driving force for the other (W.S. Walston, 1996).

Rhenium positively influences the liquidus temperature of nickel alloys; much more than in comparison to other refractory elements, hence its use as an alloying addition in nickel superalloys. Reed suggests that rhenium along with ruthenium have this effect due to the significantly slower diffusion rates that these elements have in nickel; owing to the sizeable diffusion energy barrier they possess, causing what Reed describes as 'incompressible Ni-Re and Ni-Ru bonds that do not favour solute-vacancy exchanges' (R.C. Reed, 2006).

Geddes reports (B.Geddes, 2010) that rhenium's main purpose as an alloying addition is to increase the creep life, stating it can double to creep life with as little as 3% wt rhenium.

Furthermore, rhenium is a solid solution strengthening much like that of Mo and W, so it's content has been increased from 1st -3rd generation blades to improve the operating temperature of nickel-based superalloys (C.M.F.Rae,2001)(A.S.Wilson,2017). However its strengthening effect is significantly higher than that of other alloying additions added for solid

strengthening, such as tungsten and molybdenum, by at least a factor of 2 (E.Fleischmann, 2015). This effect occurs largely due to its preference to partition to the γ matrix
(P.Caron,1999)(E.Fleischmann,2015)(B.Geddes,2010).

Despite this preferential partitioning to the γ phase Re also exhibits an effect on the γ', namely increasing the γ/γ' misfit, as well as contributing to the γ' morphology, promoting the aligned, cuboidal precipitates as well as retarding the coarsening (B.Geddes,2010), yet does not appear to affect the volume fraction. The latter of these effects is likely due to rhenium possessing a very low diffusion rate, providing a limitation to the rate these transformations can occur.

Rhenium however, despite its great beneficial application to nickel-based superalloys suffers some drawbacks.

Like many of the refractory elements added to nickel-based superalloys, rhenium contributed towards detrimental TCP phase formation. Mainly the σ and μ phases, the former of which is considered the most detrimental to the mechanical properties (B.Geddes,2010). These phases are discussed in more detail in **2.10.**

Rhenium is often compared to tungsten, with its benefits often coming with drawbacks, but with a stronger relationship. Even small changes of rhenium content can have significant effects on an alloy's properties, even on rhenium's own partitioning (E.C.Caldwell, 2004). Because of this continued research in rhenium's contribution to alloy properties is essential, this work demonstrates that even a less than 1wt% increase in rhenium content significantly changes its TCP phase propensity in both volume fraction and kinetics. Its strongly segregating behaviour allows more micro-inhomogeneities, creating complexities that need to be understood and better predicted to enhance the application of nickel-based superalloys.

2.7.4.6. Ruthenium

Ruthenium is a more recent alloying addition to nickel-base superalloys and is what defines fourth and fifth generation single-crystal superalloys (B. Geddes, 2010). Geddes goes on to state 'Ruthenium suppresses dendritic segregation, promotes a more uniform distribution of alloying elements between dendrite cores and interdendritic regions and retards the formation of TCP phases'.

Ru also has a significant effect on the partitioning coefficient of Re, Cr and Mo (B. Geddes, 2010).

Ruthenium has similar effects on nickel-based superalloys as rhenium, likely due to its effect on diffusion as described under rhenium by Reed (R.C.Reed,2006). However it also reduced microsegregation, unlike rhenium which has the most significant partitioning, significantly reducing TCP phase formations and preventing casting defects such as freckling (B.Geddes, 2010).

Ruthenium appears to have a variety of promising effects upon nickel-superalloys. However being more expensive than rhenium and its highly volatile prices in general have seen it underutilised in industry. Further understanding the benefits of ruthenium, particularly its ability to reduce TCP phase propensity would still contribute to a better understanding of the nature of TCP phase precipitation. Furthermore, should ruthenium prices stabilise then the benefits of such research could immediately be implemented on larger scales.

2.7.5. Titanium

Titanium has seen use in nickel-based superalloys over their development, largely due to ɣ' forming abilities. However, Ti has an adverse

effect on the partitioning of Mo and Cr to the γ phase instead of the ɣ', therefore increasing the concentration of these TCP phase forming elements (W.T. Loomis, 1972). This, along with Ti being expensive to work and hot tearing contributions (B.Geddes, 2010) has seen its use decrease from 1st generation alloys to effectively nil in all but a few 3rd generation alloys (P.Caron, 1999). Its concentrations are so small in the alloys of this study, approximately 0.1% that it is largely ignored.

Titanium's ability to replace aluminium, whilst having a higher melting temperature is of interest, due to the drawbacks of aluminium seen in this work. Whilst titanium's should not be excluded from alloys entirely, it seems unlikely that any benefits are outweighed by the drawbacks of titanium that have seen it's contributions decrease over the generations. But further research into replacing Al to prevent TCP phase formation could still be promising, if only to understand the process better.

2.7.6. Other addition; carbon, boron, hafnium, iron

Whilst carbon has in the past been added to polycrystalline alloys for its ability to precipitate at the grain boundaries, reducing grain boundary slip (R.C. Reed, 2006), this is not necessary in single-crystal alloys. However, Liu et al (L.R. Liu, 2003) experimented with microalloying with carbon to prevent the formation of TCPs during thermal exposure, to which Geddes also agrees (B. Geddes, 2010).

However, these carbides that form instead of TCP phases still consume the other alloying additions that provide nickel-based superalloys with their high-temperature properties, creating undesirable depletion zones (B. Geddes, 2010). Furthermore Geddes (B. Geddes, 2010) states that due to the high coherency between the $M_{23}C_6$ carbide and the σ-TCP the latter can nucleate at the former due to their coherency, promoting TCP phases,

although it also consumes the same elements used in the formation of TCP phases (B.Geddes, 2010). Clearly the relationship between C and TCP phases is complex. And a trade off between the thermodynamic favorability and kinetics of TCP phase formation is apparent.

MC carbides are formed from Ta, Nb and Ti, depleting these from the surrounding areas leaving enriched areas of Cr, Re, Co and Mo (B. Geddes, 2010). These are the elements that form TCP phases. Producing a similar effect to γ' precipitation in concentrating TCP phase forming elements in the γ-matrix (B. Geddes, 2010-24).

Boron, carbon and hafnium added to improve production yields by strengthening subgrain boundaries; in much the same way at grain boundaries, increasing permissible misorientation tolerance (B. Geddes, 2010).

Iron is not used in nickel-based, superalloys as an alloying addition, but is sometimes used in large quantities creating nickel-iron-based superalloys, whilst saving costs iron tends to have significantly poorer performance at elevated temperatures, due to its tendency to form undesirable intermetallics (B. Geddes, 2010).

Hafnium confers numerous benefits to nickel-based superalloys, but primarily for improving mechanical properties such as improving ductility, grain-boundary strengthening and corrosion resistance (B.Geddes, 2010). Furthermore it improves the retention of coatings to the blades surface, however, it also reduces the incipient melting temperature, more significantly than it does the γ solvus temperature, narrowing the solutioning window (J.Wahl, 2018). Again the need to carefully tailor the concentration of an element to balance the positive and negative benefits is noted.

A number of reactive elements (like hafnium) are sometimes also added, these include: Yttrium, lanthanum and cerium, their additions are to

improve environmental properties of the alloy as well as adhesion of the protective scale to the alloy itself (B.Geddes, 2010).

2.8. Processing

2.8.1. Casting

Whilst specifics vary, typically ingots of the alloy material are induction melted before being poured into preheated investment moulds, grain selectors such as pigtails will be used to induce directional solidification or even single crystals with specific withdrawal rates being used to ensure the directional/single crystal nature (Q.Feng, 2003). In part due to the slow withdrawal rates required, casting is typically a long process over several hours, this enables a very segregated structure to form. As the liquid cools dendrites form of the highest solidus phase; ɣ, hence calls dendritic ɣ. These dendrites are typically enriched with denser, higher melting temperature elements such as rhenium and tungsten. A liquid front ahead of these dendrites is typically enriched in lower melting temperature elements such as Al, will continually be enriched with these elements as the alloy coosl, eventually forming ɣ’ alongside ɣ, producing eutectic mix of the two, or more accurately, interdendritic ɣ’ (N.Warnken, 2016).

Figure 2 demonstrates a typical as-cast structure. With dendritic ɣ in a typical dendritic cross shape, surrounded by ɣ’ and ɣ, with their sizes varying. The largest ɣ’ precipitates tend to form in the areas between two dendrites as the last to cool dumping large volumes of ɣ’ forming elements.

Figure 2: A typically segregated dendrite without any TCP phases present. CMSX-10K

The final product is a highly segregated mix of dendritic ɣ, enriched with ɣ forming elements, and interdendritic regions, enriched with ɣ’ forming elements, despite the alloy being designed to be entirely ɣ above its equilibrium solidus temperature. This requires substantial homogenisation via solutioning to create the correct microstructure from future heat-treatments to create the ideal distribution and volume fraction of ɣ’ for the alloy’s optimal performance.

The extent of segregation an element undergoes during casting can be summed up as **K’ (**Where **K’**=$X_{Dendritic}/X_{Interdendritic}$) the segregation; or partitioning, coefficient, specifically the ratio of an element in the dendrite core in contrast to the interdendritic regions.

K’	Al	Ta	W	Re
CMSX-4 (N.Wanderka)	0.75	0.69	1.35	2.7
CMSX-10K	0.72	0.60	1.25	1.98

(G.E.Fuchs)				
SX-1 (T.M.Pollock, 1992)	0.78	0.66	1.75	2.14

Table 1: K’ values of elements in different alloys vary significantly.

2.8.2. Solutioning

As mentioned, the as-cast structure is highly segregated in its microstructure, as well as substantial volumes of ɣ’ being present in the interdendritic regions. For optimal volume, distribution and sizes of ɣ’ throughout the alloy it is of best practice to put all of the ɣ’ into solution, hence the name solution-heat treatment. Afterwards lower temperature heat-treatment regimes can produce the optimal ɣ’ presence.

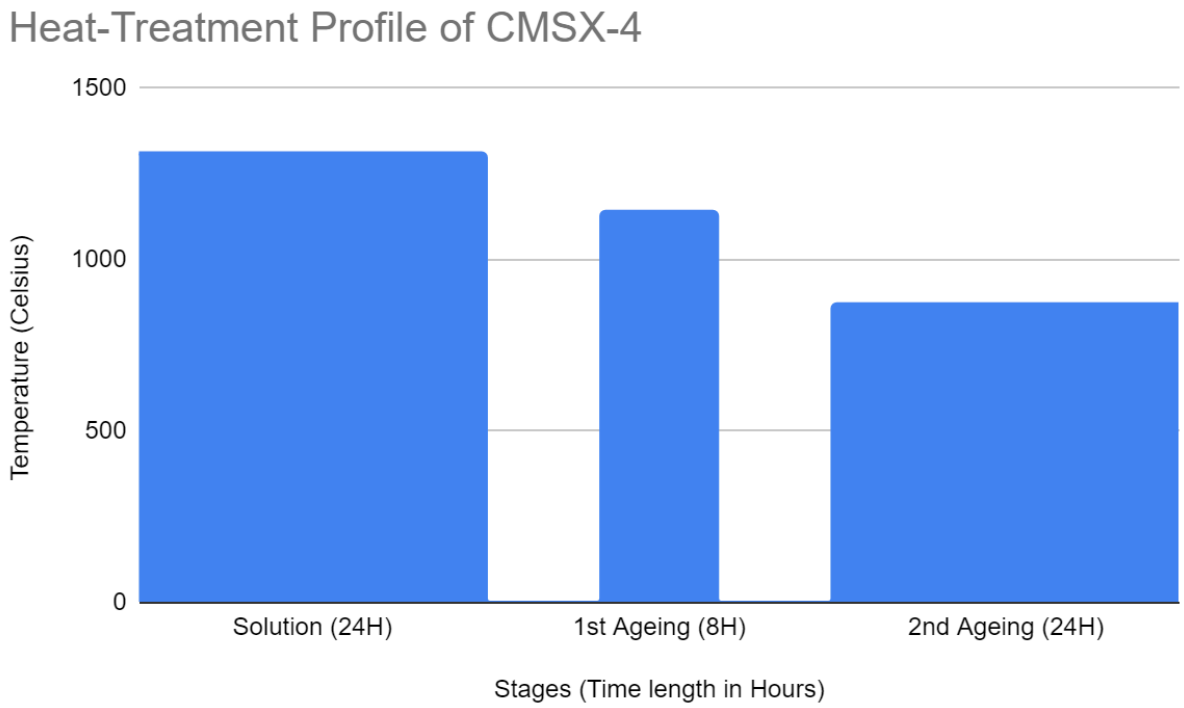

Figure 3: Heat treatment regimes vary in length and temperature.

This solutioning however is has a very narrow solutioning window, between the solvus of ɣ’, which needs to be reached to fully solution the ɣ’, and the solidus of the alloy, at which incipient melting will begin to occur and produce recrystallizations, this in particular would destroy this highly desirable single-crystal nature of blades (but is still detrimental to directional solidified blades, as the recrystallisation disrupts this too).

Furthermore the length of solutioning is significantly influenced by the composition of the alloy in question, as certain elements, (such as Re, W and Ta) can highly segregate to either the ɣ or ɣ’, and time is needed to homogenise them. Re in particular, with its low diffusion rate, requires substantial times to sufficiently homogenise (R.C.Reed, 2006).

2.8.3. Quenching

As the alloy is quenched, γ' forms, enriching γ in elements such as rhenium, tungsten and molybdenum which have large atomic sizes, increasing both the lattice parameter of γ and thus it's lattice mismatch with γ'. (A.Bezold, 2022) However, as the temperature rises during heat-treatments, the partial dissolution of γ' would reduce this misfit.

2.9. Recrystallisation and Freckling

Recrystallisation is the process of new grains being formed out of stressed grains, or in the case of single-crystals the original grain. This is most problematic in the case of turbine blades, as the desire for single crystals is due to the grain boundaries; especially high-angle grain boundaries, often being a site of failure (L.C.Zhou, 2015). Even in the case of directionally solidified alloys, the strengthening elements introduced, such

as boron and carbon, depress the melting point of the alloy and thus limit its maximum temperature regime. Removing these elements improves the high-temperature properties of the alloys, but if recrystallisation occurs, it is often fatal to the blade, causing them to be rejected if this occurs during manufacturing.

Two factors contribute significantly to recrystallisation, significant plastic strain and microstructural inhomogeneities (L.Wang, 2012). Wang et al showed that this is especially acute in the eutectic regions of nickel-base superalloys. Thus care must be taken in processing of the blades to prevent inducing stresses into them, whilst also stressing the importance of solutioning the homogenise the alloy.

Freckling (and mis-aligned grains) is often associated with convection of solutes within the liquid metal during casting, as the denser elements tend to solidify first in the dendrites leaving the liquid with significant imbalance (R.C.Reed, 2006)

Due to the precise nature of the withdrawing procedures during casting and the relatively large size of blades it has been a significant issue in the past (S.Tin, 2001). However, the introduction of tantalum especially, being a dense alloying addition that remains within the liquid preferring to segregate to γ' offsets much of the instability (P.Caron, 1999).

2.10. Topologically closed-packed phases (TCPs)

TCP phases are intermetallic phases that are rich in the elements, Cr, Mo, W and Re (especially with Re being particularly likely to enrich due to its propensity to replace nickel-sites during their formation (R.C.Reed, 2006). They also possess the following characteristics:

- High and uniform packing density
- A degree of non-metallic, directional bonding

- Complex crystal structures, built from distinct tessellated layers, consisting of arrays of hexagons, pentagons and triangles, stacked into a limited number of Kasper coordination polyhedra (name-sake) dependent on the specific phase. (R.C.Reed, 2006)

They possess the chemical formula A_xB_y where both A and B are transition metals, with A falling to one side of the chemical group VIIB column and B falling to the other. A and B display different electronegativity, suggesting electronic factors are important in determining their stability.

Compositions can vary significantly from those listed below, and they possess a very wide stoichiometry range. With the ones listed being the ideal stoichiometry.

TCP Phase	Stoichiometry	Crystal Structure	Cell Size	Examples
Mu (μ)	A_6B_7	Rhombohedral	13	W_6Co_7, Mo_6Co_7
Sigma (σ)	A_2B	Tetragonal	30	Cr_2Ru, $Cr_{61}Co_{39}$, $Re_{67}Mo_{33}$
P		Primitive Orthorhombic	56	$Cr_{18}Mo_{42}Ni_{40}$
R		Rhombohedral	53	$Co_5Cr_2Mo_3$, $Fe_{52}Mn_{32}$
M		Orthorhombic	52	$Nb_{10}Ni_9Al_3$

Table 2: Different TCP phases possess different crystal structures, stoichiometry and cell size.

2.10.1. TCP phase research

TCP phases are enriched from (Re, Cr, Mo, W,)(R.C.Reed, 2006) Co and nickel contribute to their composition as well, and as seen above, when present other elements also participate in their formation too.

The name TCP comes from the complex crystal structure exhibited, this consists of an array of hexagons, pentagons and triangles, building up in distinct tessellated layers. These layers are stacked into a limited number of Kasper coordination polyhedra. They also possess some non-metallic, directional bonding and a high, uniform packing density of atoms. Reed continues by suggesting that their stability is dependent on the electronegativity of the atoms involved (R.C. Reed, 2006).

Previous research in the formation and effect of TCP phases has mostly been researched when they are produced during service conditions. High temperature and stress conditions present during service is widely considered a major factor in their formation (F. Sun 2011). Rae explains this by stating TCP phases have very slow kinetics for formation, hence why they are more commonly observed in aged samples (C.M.F. Rae 2001)(A.S. Wilson, 2017).

However they have been identified in the as-cast state, through solidification from the liquidus (F. Long, 2009). Long continues to state that there has been very little research on occurance of TCP phases during solidification and that 'the precise transformation mechanism between σ and γ phase in nickel-based superalloys remains unclear', during the decomposition of metastable σ into the γ matrix.

2.10.2. Formation of TCP phases

Formation of TCP phases can be attributed to segregation of the alloy during casting ((B. Geddes 4.9, 2010), as TCP phase forming elements while overall may not have large enough concentrations to form TCP phases due to segregation can in localised areas have higher concentrations and form TCP phases. To describe segregation of elements there is a segregation coefficient (k') defined as the ratio of the concentration in the dendritic core over the concentration in the interdendritic region of the respective element (E.C. Caldwell, 2004).

Elements that prefer to partition to the interdendritic region typically are γ' formers such as Ni, Ti, Ta, Al and to smaller extends Cr. Whilst the elements that partition to the dendritic core are Re, W, Co and Mo (E.C. Caldwell, 2004).

Due to the volume fraction of up to 0.70 of γ' in Ni-based superalloys; which contain low quantities of refractory elements, they can suffer from accelerated TCP phase precipitation because of the now refractory rich γ matrix (C.M.F. Rae 2001)(A.S. Wilson, 2017)(R.C. Reed, 2006).This is further exacerbated if the alloy has a good lattice fit between the γ matrix and σ-TCP phase (C.M.F. Rae 2001). This is another limiting factor to how much of the strengthening γ' an alloy can possess as mentioned in **2.4.**

Certain behavioural aspects about TCP phases and their precipitation have been studied before. Such as σ have been identified as metastable (C.M.F. Rae 2000)(F. Long 2009). Wilson (B.C.Wilson, 2003) showing that TCP phases during heat treatments formed typically at the dendrite/eutectic borders.

Liu et al concluded that formation of carbides prevented the formation of TCP phases as they are competitive and therefore contributed to

maintaining good thermal stability (L.R. Liu, 2003). This occurs because the carbon combines with excess W and Re which are critical in the formation of TCP phases, similar to carbon's reduction of freckling defects (R.C.Reed, 2006).

The rhenium strengthening effect due to its low diffusivity is also its downfall as it causes any segregations of Re to only slowly diffuse giving the time and concentration needed to form TCP phases (P. Caron, 1999). This causes segregations in the alloys that are difficult to homogenise due to its as stated diffusivity, this also affects predictive methods such as electron vacancy (Nv) in predicting TCP phase precipitation (P. Caron, 1999). Furthermore the distribution of Re is inhomogeneous in nature, with areas close to the y/y' boundary typically being enriched (N. Koneva, 2021) and Re having a preference to diffuse to grain boundaries, where present (K.Park, 2021), with the later preferring to form rhenium rich, non-TCP phases, whilst the former could encourage their precipitation and growth.

Prevention of formation of TCP phases has been accredited to additions of Ru, although the reasoning for why this happens is still debated (R.C.Reed, 2006)(B. Geddes, 2010).

The dendrite cores; due to steep compositional gradients, are rich in TCP-forming elements and so tend to form these phases (B. Geddes, 2010). This is difficult to account for with heat treatments due to the low diffusion rates of Mo, W and Re. (B. Geddes, 2010).

Single crystal blades are grown with a [001] orientation, (Y.Wang, 2021)(H.P.Jin, 2007), whereas TCP phases have different orientations, varying on the type of TCP phase amongst other factors. H.Jin et al showed that even σ-phase can have different morphologies within the same alloy, with both needle-like and plate-like precipitations. With the former being (1$\bar{1}$0), and the latter (001) (H.Jin, 2022). Whilst the γ matrix being (111).

Jin reports that the a combination of planar mismatch and interfacial energy promotes either planar expansion or layer by layer growth, producing plate-like and needle/rod like respectively. Most interestingly is the presence of both in the same samples, with chemical compositions of the surrounding matrixes varying between the two different morphologies.

Interfacial energies between plate-like σ and the γ matrix are smaller than that of needle-like and the γ, requiring less driving force for formation (H.Jin, 2022). This also inhibits needle-like precipitate growth, where a redissolving of some of the precipitate occurs to minimise interfacial energy. Morphology type is also shown to be focused on reducing interfacial energy between γ and TCPs (H.Long, 2018).

2.10.3. Morphology contribution

The morphology of these TCP phases; needle and or plate-like precipitations, have preferred orientations. This could be key to understanding the timing of TCP phase precipitation, as the presence of γ' could help or hinder certain growth directions, therefore dictating whether TCP phases form first, and γ' around them, or γ' first then encouraging TCP phase formation from the enriched γ matrix.

Notably, Jin observed the plate-like precipitates to be larger than their needle-like counterparts, larger precipitates are identified more frequently in this work, possibly indicated the preference for plate-like TCP phases, and the smaller ones noted in the work, are σ-TCP precipitates too, but with needle-like morphologies, not different types of TCP phase (H.Jin, 2022). The same work does identify μ-TCPs alongside σ-TCPs, and this could also be the case, particularly in the case of the CMSX-4 alloy, where smaller precipitates are seen, in an alloy more associated with μ-TCPs (K.Cheng 2011).

Temperatures also impacts morphology, with higher temperatures showing a greater propensity to form plate-like precipitates over their needle-like counterparts (H.Long, 2018), combined with a need to reduce interfacial energy between the TCP phases and the γ matrix can help determine which morphologies might precipitate at the stages of solutioning.

Higher temperatures, would reduce the driving force for precipitation, which Jin, suggests favours plate-like precipitation (H.Jin, 2022). Lower interplaner mismatch would favour needle-like precipitates, as γ' dissolves, the γ lattice parameters would increase, becoming more similar to those of σ-TCPs, promoting needle-like growth, however, this requires temperatures sufficient to dissolve the γ', which as discussed, seems likely to encourage plate-like growth, these high temperature conditions would suggest a higher fraction of plate-like precipitates over needle-like ones.

2.10.4. Effect of TCP phases

It is widely considered that TCP phases have a deleterious effect on superalloys, this is primarily due to softening of the γ phase due to depletion of the strengthening refractory elements used to form TCP phases (C.M.F. Rae, 2000). Some have also suggested TCP phases act as crack initiation sites, as their precipitation leads to the formation of voids (C.M.F. Rae, 2000)(M.V. Acharya, 2004). However D.Wang and M.Pessah both report that neither creep or mechanical properties are negatively affected by the presence of TCP phases respectively(M.Pessah, 1992)(W.S. Walston, 1996) (D.Wang, 2010). Clearly, TCP phase influence on alloys is not simple, and is dependent on the type of TCP phase that forms as well as the effect their formation has on the matrix and γ'. Geddes, (B. Geddes, 2010) reports that the μ-TCP is detrimental in conflict with Pessash (M. Pessah, 1992) whom showed not mechanical properties changes. However, a study where this is

not the case; specifically in alloys MC2 and AM3, distinguish the effects of rafting from TCP phases and demonstrated rafting and γ' coarsening to be more significant in its effect on mechanical properties than TCP phase precipitation (B. Geddes, 2010).

Wang attributes the lack of recorded effect of TCP phases to the γ' film that often surrounds TCP phases. As TCP phases are rich in refractory elements the surrounding area becomes deficient in refractory elements as the TCP phases form. This deficient area favours forming the γ' phase; which does not contain refractory elements, suggesting that this film prevents the propagation of cracks (D.Wang, 2010). Acharya et al also observes these films, or envelopes (M.V. Acharya, 2004). However, due to the typical needle-like morphology of TCPs these films then to be long γ' structures interrupted the continuous matrix (B.C.Wilson, 2003).

TCP phase precipitation has also been suggested to reduce rupture life because of the reduced creep performance, Reed concludes that TCP phase formation is detrimental to properties (R.C. Reed, 2006), again due to the depletion of the γ/γ' which grants the improved creep strength originally. Acharya demonstrated that TCPs do alter the failure mechanism in CMSX-10, from porosity in no TCP phase containing samples to fracture surfaces matching the crystallography of TCP phases, however this did not embrittle the material, stating that TCP phases have been shown to improve the ductility of samples (M.V. Acharya, 2004), whilst Geddes (B. Geddes, 2010) reports that TCP phases reduce ductility. These conflicting reports reflect the complexity of the presence of TCP phases in alloys, both in how they affect nickel-base superalloys and to exact extent of the effects.

Others who have attempted to demonstrate the negative effect of TCP phases on mechanical properties have sometimes been unable to show it (S. Duval, 1994). One of the difficulties that arise when trying to produce TCP phases through ageing is because coarsening of the γ' also occurs during

heat treatment. This has been shown to degrade the properties of the alloy (M.Pessah, 1992)(M.V. Acharya, 2004), as the γ' phase is significant in providing nickel alloys with their strength. Therefore this coarsening either needs to be removed, or carefully calculated for in measuring any effect TCP phases have on an alloy.

This is further complicated by the type of TCP phase type studied, as Archarya's (M.V. Acharya, 2004) samples were shown to be predominantly σ-TCPs whilst Pessah's (M. Pessah, 1992) was μ-TCPs. Each producing different effects upon their respective samples, Geddes, (B. Geddes, 2010) reports that σ-TCPs are the most detrimental to nickel-base superalloys and so another area to be considered is the varying effects of different TCP phases.

Furthermore, an indirect effect of TCP phases, especially in 3rd and 4th generation blades is the intentional reduction of Cr. Because of the increase in Re content due to its creep strengthening ability and a desire to keep TCP phase formation down, designers have reduced Cr due to its contribution to TCP phase precipitation, therefore reducing the oxidation resistance and building a dependency on coating technology.

2.11. Modelling of TCP phases

2.11.1. Modelling background

To support and understand the experimental work carried out in this thesis, models were created using ThermoCalc software. This is also done to test how accurately the ThermoCalc software calculates the microstructural changes when compared to the experimental results acquired in the other sections. There are numerous modelling platforms available for the study of alloy microstructure, such as ProPhyPlus and OpenCalphad, Thermolib,

ProCAST and Crystal Manager. However, some of these have limited applications such as Crystal Manager or limited scope such as ProCAST, Nickel-superalloys often have nine or more elements in varying concentrations creating numerous phases that coincide, binary and ternary systems are far from sufficient in their ability to describe and predict properties in these alloys. A system is needed that can accurately describe the lower orders of a system and then build upon it to produce a reliable higher-order system. For this reason, ThermoCalc software has been the primary source of modelling data and calculations throughout this work.

2.11.2. ThermoCalc

The ThermoCalc software uses the CALPHAD methodology; a phased-based approach, using temperature and composition to model the properties of individual phases. However the extensiveness of the ThermoCalc software alloys for more than just thermodynamic calculations, allows combinations of data to enhance the larger picture of a material.

By using calculated thermodynamic properties, extensive high-quality experimental results, paired with ab-initio calculations from first principles, in-depth, thorough model parameters can be calculated with minimal uncertainty. This is primarily through Gibbs energy models, as it is fundamental to the thermodynamic properties of a material. These are validated by real-world data and optimised until there is agreement of the lower orders. From here higher order more complex systems can be predicted and extrapolated with high accuracy (ThermoCalc, 2021).

This ground-up approach is why ThermoCalc is an excellent choice for studying these nickel-based superalloys. Its well-validated databases, combined with sophisticated human judgments in their development all based on the fundamental principles of thermodynamics, leads ThermoCalc

to be a thorough and reliable software to model the development of these complex alloys (ThermoCalc, 2021)

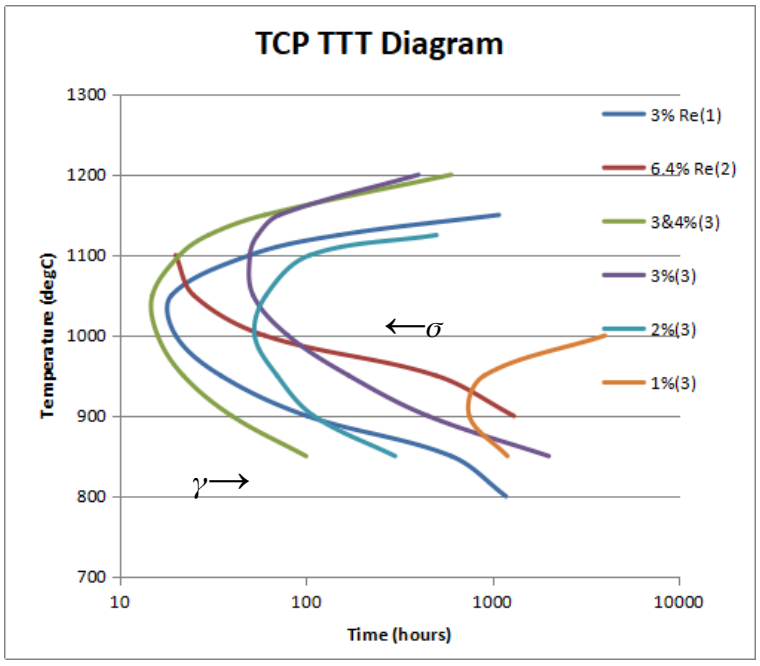

Figure 4: TTT curves taken from various sources, demonstrated the longer times typical of TCP phase precipitation at lower temperatures as a function of rhenium content. With regions to the left of the curve denoting pure γ whilst regions to the right of the curves contain σ-phase. 1 - Rae, C.M.F. (2000)**2 -** R.C.Reed, (2006)**3 -** Darolia, R (1988)

2.12. Alloy development in regards to TCP phase formation

The development of alloys has had to take TCP phases into consideration as a result of the detrimental effects they can have on the alloys. Whilst individual contributions of elements on the propensity to form TCP phases has been considered, ways to approach development of new alloys as a whole, whether via modelling or experimental methods will be briefly considered.

Modelling approaches to phase stability are considered in more depth in section **4.** However, it is worth noting the inherent difficulty in trying to predict numerous qualities such as: mechanical, castability, microstructural and solution heat treatability (K. Harris, 1984) while considering the contributions of more than 10 alloying elements.

Further difficulty with modelling also occurs with the bases of the modelling approach, any one base; such as phase equilibria, can neglect the other bases when then trying to predict microstructural evolution (T.D. Reynolds, 2019).

Furthermore, many of the alloying elements have significant effects upon one another, complicating attempts to easily adjust a model to compensate for this (D.Spathara, 2021), elements such as rhenium can even significantly affect their own behaviours at varying concentrations (E.C.Caldwell, 2004). In particular, traditional methods of predicting these deleterious TCP phases have struggled with the newer generational alloys (B.Seisser, 2011), in particular ones containing Re (R.Darolina, 1988).

Advantages of traditional alloy design; based on existing alloys and lessons learned, are a larger base of knowledge, with some alloys still in use to this day developed decades ago and have received significant study such as CMSX-4 (J.Wahl, 2018). This offers a degree of predictability and reasonable expectations with previous knowledge to lean on when deducing the cause of new effects, even if the qualitative properties of the alloy can only be deemed experimentally after some initial production.

2.13. Conclusion

TCP phases are detrimental to nickel based superalloys. Through removal of strengthening elements in the γ matrix, degradation of

mechanical properties and the reduction in beneficial elements such as Cr that no longer contribute their beneficial properties to the alloy.

Whilst numerous TCP phases exist, σ-TCP are generally considered one of the more detrimental phases, with higher propensity to form due to coherency with γ.

The occurrence of TCP phases has had minimal interest during the early stages of manufacturing, in particular the solutioning stage.

It is for these reasons that this work focuses on production alloys; CMSX-10K and CMSX-10N, using CMSX-4 as a base comparison due to its extensive literature. Modelling is considered in the section **4.**, but as supplementary to the experimental work presented in section **3.**, with more in-depth considerations of its approach addressed further on.

By thoroughly investigating the solution process and its effects upon these alloys can its influence of TCP phase precipitation be better understood, as well as the underlying nature of TCP phase precipitation during this process. Through this information potential process variations or design considerations can be suggested that would deter TCP phases from precipitating.

3. Precipitation of Topologically Closed Packed Phases during the Heat-Treatment of Rhenium Containing Single Crystal Ni-Based Superalloys Materials and Methods

3.1. Materials

The materials investigated in this paper are the third-generation alloys CMSX-10N and CMSX-10K, and the second-generation alloy CMSX-4, with their compositions (wt.%) shown in Table 3, containing the general composition of the three alloys used. CMSX-4 and CMSX-10 are registered trademarks of Cannon-Muskegon Corporation..

	Al	Cr	Co	Ti	Mo	Ta	W	Re	Ni
CMSX-4	5.6	6.5	9.0	1.0	0.6	6.5	6.0	3.0	Bal
CMSX-10K	5.7	2.0	3.0	0.2	0.4	8.0	5.0	6.0	Bal
CMSX-10N	5.8	1.5	3.0	0.1	0.4	8.0	5.0	7.0	Bal

Table 3: Showing composition in wt% of the alloys of interest.

3.2. Methodology

The superalloy castings used in this study were produced at the University of Birmingham School of Materials and Metallurgy using materials manufactured by Cannon Muskegon and provided by Rolls-Royce plc. For each casting, approximately 1100g of CMSX-10N was directionally solidified at a temperature of 1550℃ in a Retech Single Crystal Furnace with the use

of pigtail selectors to induce single crystal growth. This was achieved using investment casting ceramic moulds at a withdrawal rate of 229mm/hour, each producing two cuboid bars measuring 12mm in width and depth and approximately 180mm in length. These were then cut into smaller 20mm sections for further testing. This was repeated for the CMSX-4 and CMSX-10K samples.

The solution heat treatments were carried out in a type-1 TAV vacuum furnace, using platinum–platinum rhodium thermocouples to monitor the temperature to ±1 degree Celsius. Each test piece was heat treated individually. The furnace was heated to 1361℃, 1345℃, and 1310℃ for CMSX-10N, CMSX-10K, and CMSX-4, respectively. This was achieved over 90 min at a rate of 15℃/minute to prevent overshooting the solution heat treatment temperature. The samples were then held at these temperatures for times between 0 and 48 h before being quenched in Argon gas.

These samples were then subsequently prepared for SEM and BSE imaging using standard preparation techniques, finishing with a fine polish of OPA (oxide polishing alumina). The samples were then etched with Kaling's Agent 2.

Electron microscopy was carried out using a Jeol6060 microscope with an accelerating voltage of 20 kV and a working distance of 10mm. EDX maps were taken of 10 dendrite cores and analyzed with INCA software to measure the elemental make-up of the core and an average value used, whilst BSE images of the cores were analyzed using ImageJ software to calculate the volume fraction of the σ-phase in the cores.

Modelling was carried out using ThermoCalc software. By measuring the varying compositions of the dendritic cores and interdendritic regions throughout the solution process, phase occurrence and volume fractions can be predicted using ThermoCalc and compared to the experimental results. With no available way of imaging these alloys at their solution temperatures,

these methods are useful to determine the effect of quenching on the microstructure and what phases would be stable at the heightened temperatures.

3.3. Results

3.3.1. CMSX-4

CMSX-4 was chosen to be used as a baseline comparison of the other two alloys because it has been in use longer than the other alloys and the significant literature and data are available to allow comparison with the other alloys. BSE images were taken of samples throughout the solution process to see how the compositional makeup of the alloy changed throughout the solution process. EDX was used to quantify these data for use in graphs and modelling.

A segregated structure typical of this alloy can be seen in Figure 5a, where the lighter dendrite cores are significantly enriched in tungsten and rhenium while depleted in tantalum compared to the overall composition presented in Table 3, producing the contrast seen.

By 1h into the solution process, the dendritic structure is already homogenizing, yet by 8h, as seen in Figure 5c, TCP phases are present toward the centre of the dendrites. Figure 5d shows after 24h of the solution process, and in this case, the micrographs suggest an entirely homogenous structure (consisting of evenly distributed γ' surrounded with γ channels), with no sign of the dendritic structure left. No TCP phases were seen throughout the sample after this solution time.

Using ImageJ to calculate a volume fraction of TCP phases across the dendrite core region, an 8h sample was recorded with a 1.15% Vf. This solution time was the only one where TCP precipitates were found to be

present. Additionally, the volume fraction is considerably lower than that found in the CMSX-10N samples and only comparable to the CMSX-10Ks' lower recorded values.

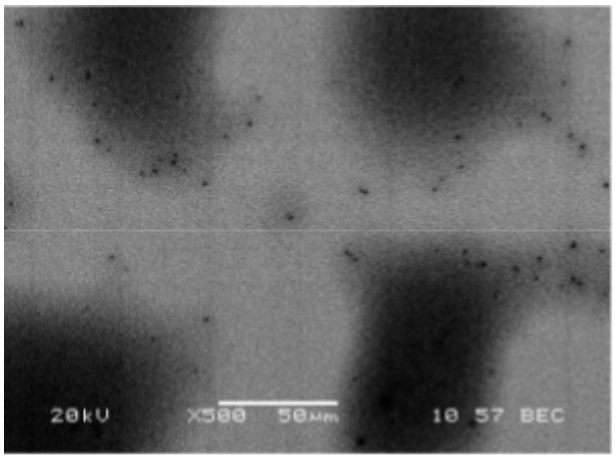

(**a**)

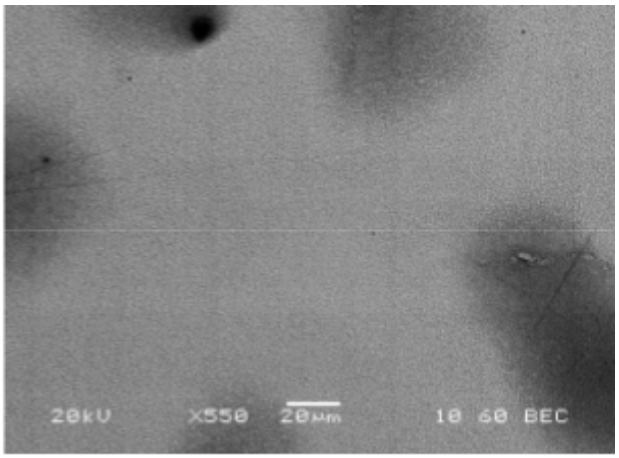

(**b**)

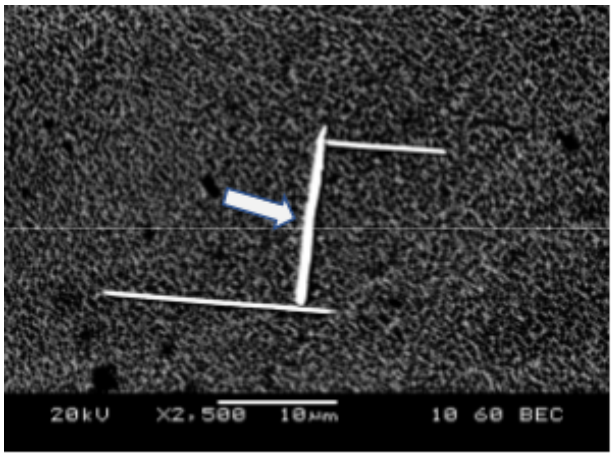

(c)

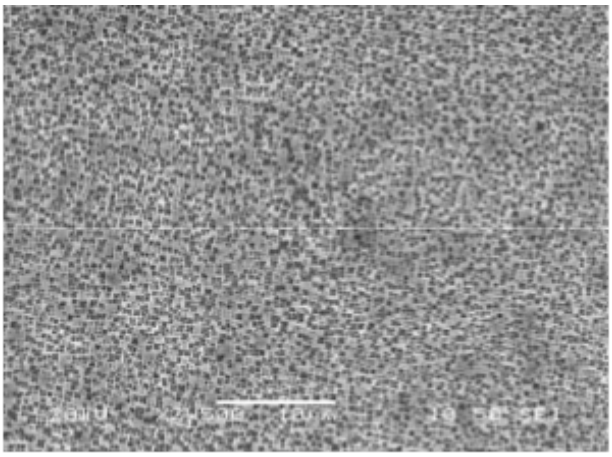

(d)

Figure 5: The microstructure of the dendritic cores of samples of different solution times: as-cast (**a**), 1h (**b**), 8h (**c**), and 24h (**d**). The TCP phases are clearly seen in (**c**) as white linear phases indicated by an arrow.

3.3.2 CMSX-10K

CMSX-10K was chosen for its similar composition to CMSX-10N, the only alloy that has been identified with TCP phases after solutions. CMSX-10N was developed from CMSX-10K, and a very similar behaviour was expected; apart from the rhenium content, there are only minor compositional differences between the alloys.

Figure 6 shows micrographs of CMSX-10K through the solution stages. Note that Figure 6b is labelled 0h; this refers to a sample that underwent the heating regime to the solution temperature of 1345℃ before immediate quenching, without holding at the temperature, to study the effects of the heating regime on the microstructure. The lighter regions are the dendrites, where the heavier elements are concentrated. The contrast within the dendrite arms indicates the underlying presence of interdendritic material separating the secondary dendrite arms.

A typical segregated dendritic and interdendritic region can be seen in Figure 6a, where the contrast is more significant compared to Figure 5a, as the dendrite contains significantly higher concentrations of tungsten and rhenium. Note that some of the dendrite arms have a feinter contrast, with some arms possessing a composition similar to that of the dendrite cores, whilst others vary significantly. The γ/γ' structure can be seen in Figure 6b as typical of an as-cast single-crystal material.

Figure 6b shows TCP phases already present, with varying morphologies, although typically long, needle-like structures (the images are only 2D, and therefore they could also be plate-like, as the literature would suggest (R.Darolia, 1988)(K.Kim, 2017)), they bridge across the surrounding γ/γ' structure and typically reside in the dendrite core, but in image 2c a small precipitate can be seen in the dendrite arm on the right-hand side of the image.

Figures 6d and 6e also show TCP phases, which tend to form in small clusters within a single dendrite core. Individual TCP phases are also common, but there are also many dendrites with no TCP phases, showing large variations in TCP-forming potential between individual dendrites. No TCP phases were observed in the interdendritic regions.

Figure 6f shows a dendrite after 24h of solutions; here the segregation is now minimal, and while some interdendritic regions can be seen on the edges of the image, a significant amount of homogenization has occurred, and the sample was absent of TCP phases throughout.

Figure 7 shows the volume fraction (Vf) of σ phase measured from the samples using ImageJ, compared to the value modelled from ThermoCalc using compositional measurements taken via EDX. The model assumed 30 min were available for precipitate formation, and although the quenching process would be much faster than this, the samples were kept in the furnace to prevent the sample from heating up again. Because of this, an overestimation in the model is expected.

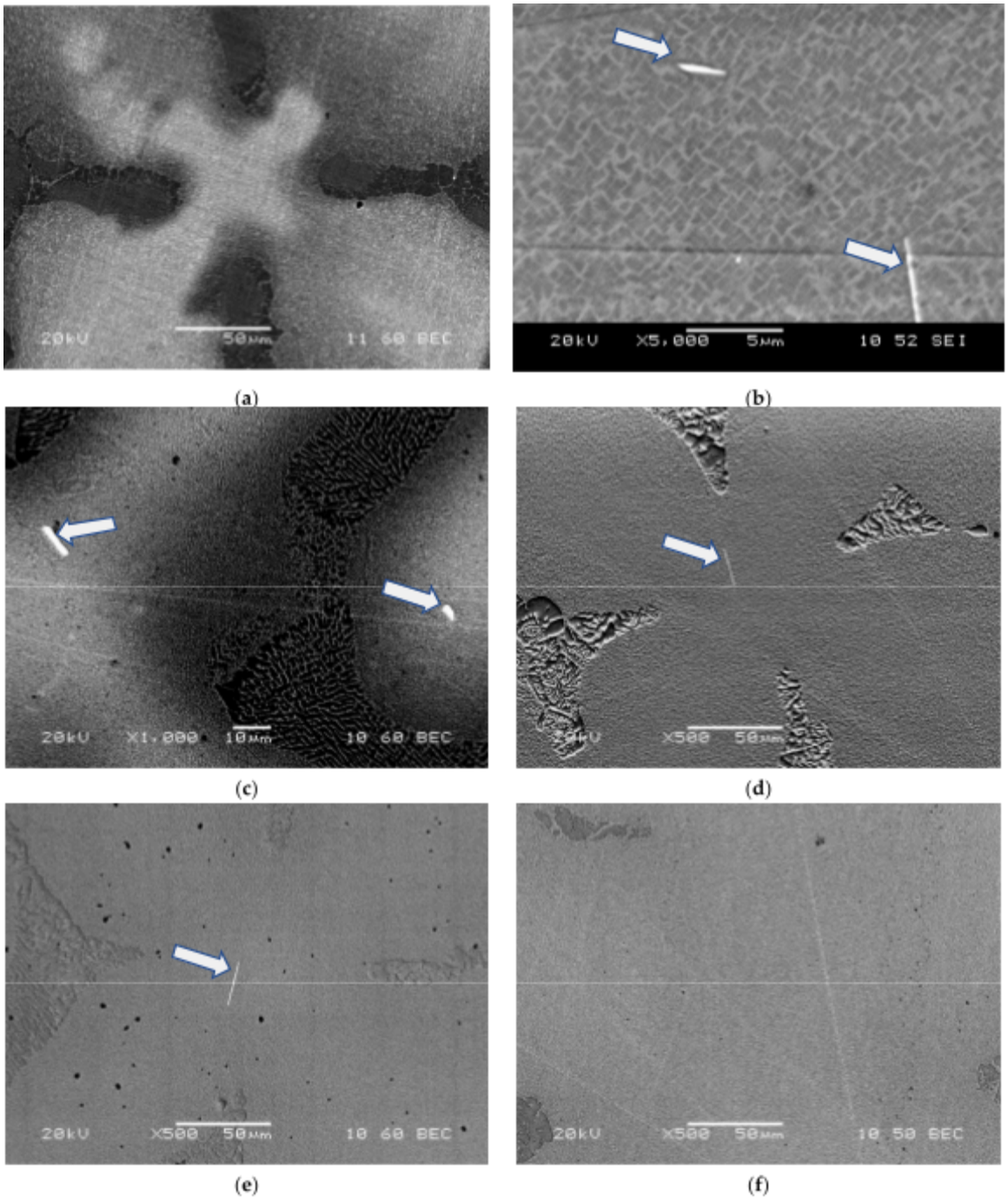

Figure 6: The microstructure of the dendritic cores of samples of different solution times: as-cast (**a**), 0h (**b**), 1h (**c**), 4h (**d**), 8h (**e**), and 24h (**f**). TCP phases are indicated by arrows.

In the as-cast state, the ThermoCalc models suggest there is a sufficient driving force (derived from the composition) for the precipitation of TCP phases; however, the sample did not undergo the same 30 minute quench but did cool from a molten state. However, no TCP phases were seen in situ, and so the circumstances of the cooling during casting appear sufficiently different from cooling from the process of solution to not promote the precipitation of TCP phases.

The modelling predictions were very similar to those measured, with the 1h measured and modelled values varying by less than a percent. However, at 24h, where none were seen, the modelling still predicted that some would precipitate. Some overestimation in the modelling data was expected, as it was known to overestimate the quenching time so that the results are so similar that one could argue the volume fraction of σ phase is higher than the composition alone could attest to.

Modelled alongside this is the time to the formation of the σ precipitates, also through

ThermoCalc in Figure 7. The times refer to the length of time for a 0.1% volume fraction to occur. Immediately it can be seen that the times to formation are very fast, significantly faster than is typically seen from in-service blades (R.C.Reed, 2005)(C.M.F.Rae, 2001)(R.Darolina, 1988). Their time to formation also increases with time, but still suggests a very rapid formation time at the end of the solution process, despite not being observed in practice.

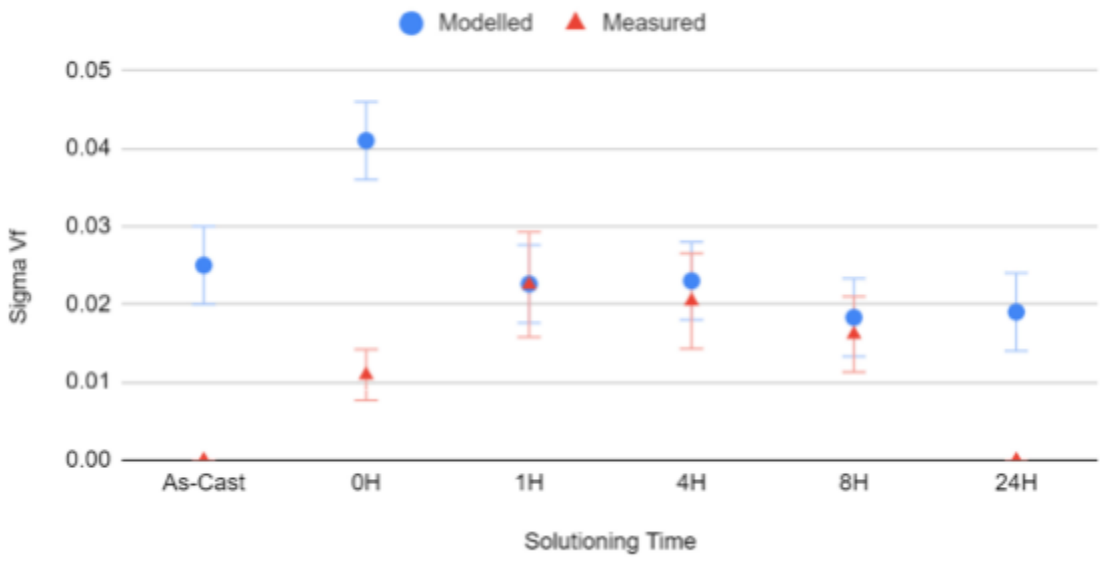

Figure 7: The calculated values of σ-phase volume fraction (Vf) using different methods for CMSX-10K.

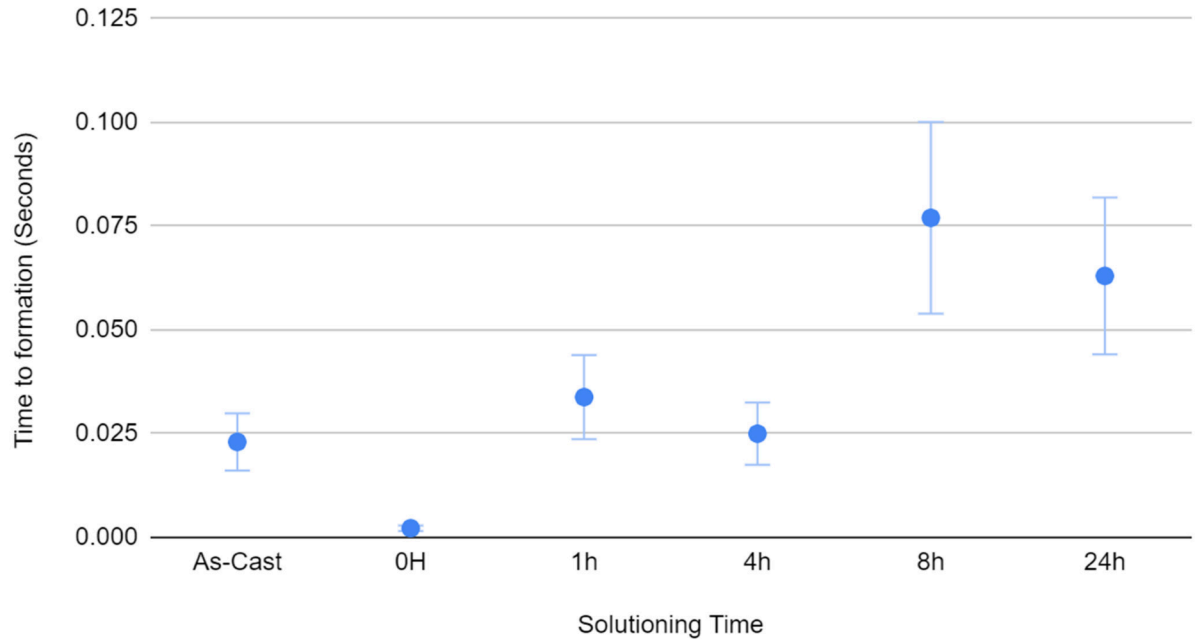

Figure 8: The time-to-formation of σ-phase modelled from 10 averaged dendritic core compositions taken via EDX for each solution time frame for CMSX-10K.

3.3.3. CMSX-10N

CMSX-10N is the primary alloy studied for this work, as it has been reported to contain TCP phases after the solution treatment (K.Kim, 2017). This previous work also demonstrates that the TCP phases seen in these alloys are σ-phase. More tests were carried out on this alloy because of this and its ready availability, as it is a widely used alloy (D.Spathara, 2021)(N.Warnken, 2016)(K.Park, 2022).

Figure 9 shows micrographs taken from each of the solution processes' ages, with many containing TCP phases; note that there are also 0h samples as part of this alloy-specific study. Figure 9a presents a very similar segregated microstructure as Figure 6a; however, Figure 9b lacks any TCP phases, and none were found throughout this early stage of the solution process for CMSX-10N. However, the cells in Figure 9c–h all contain TCP phases to varying degrees. Figure 9h, showing the microstructure after 24h of the solution process, shows that TCP phases remain, unlike CMSX-10K, and only after 48h are there no TCP phases present (Figure 9i), despite the microstructure not being fully homogenised.

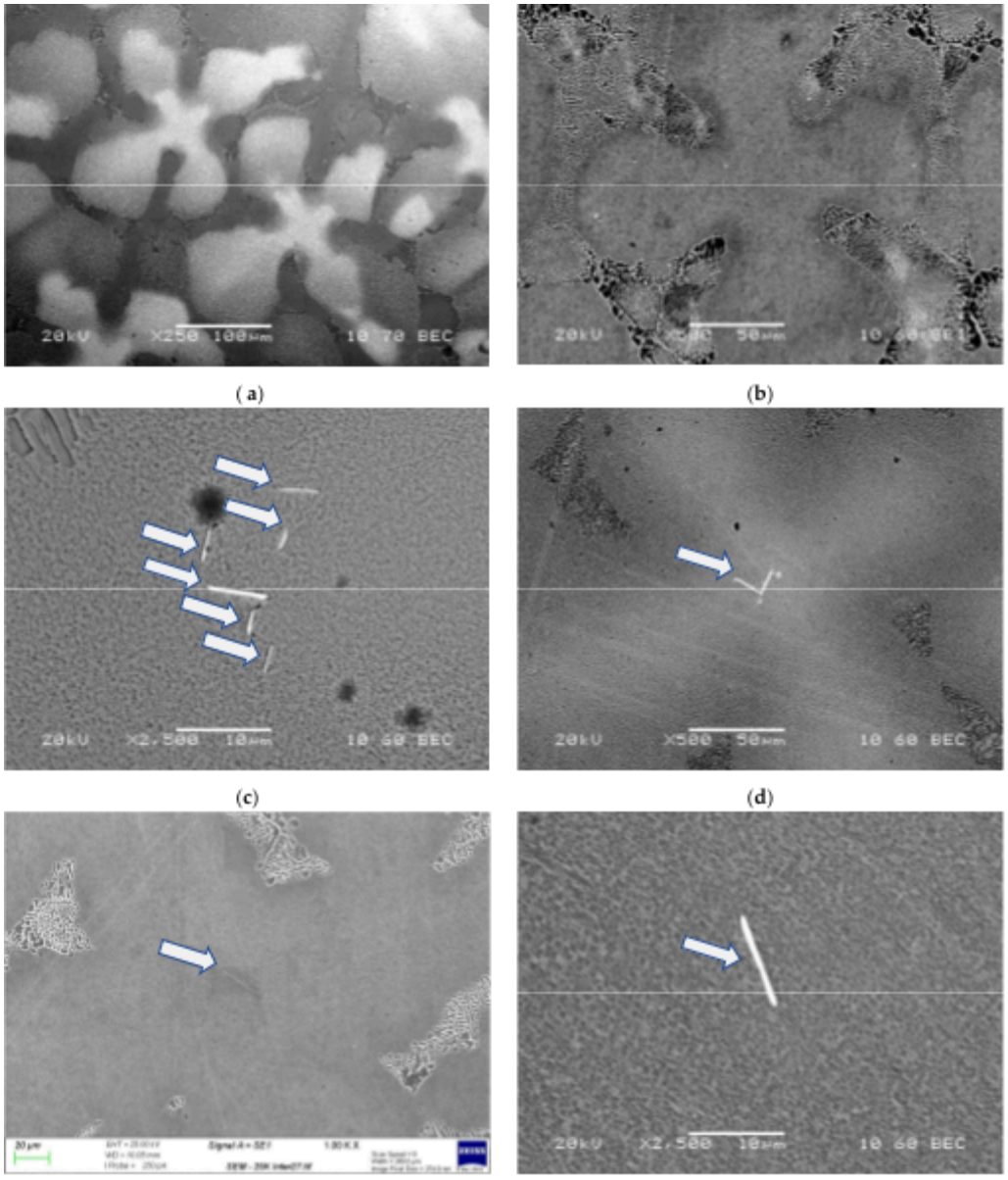

Figure 9: *Cont*.

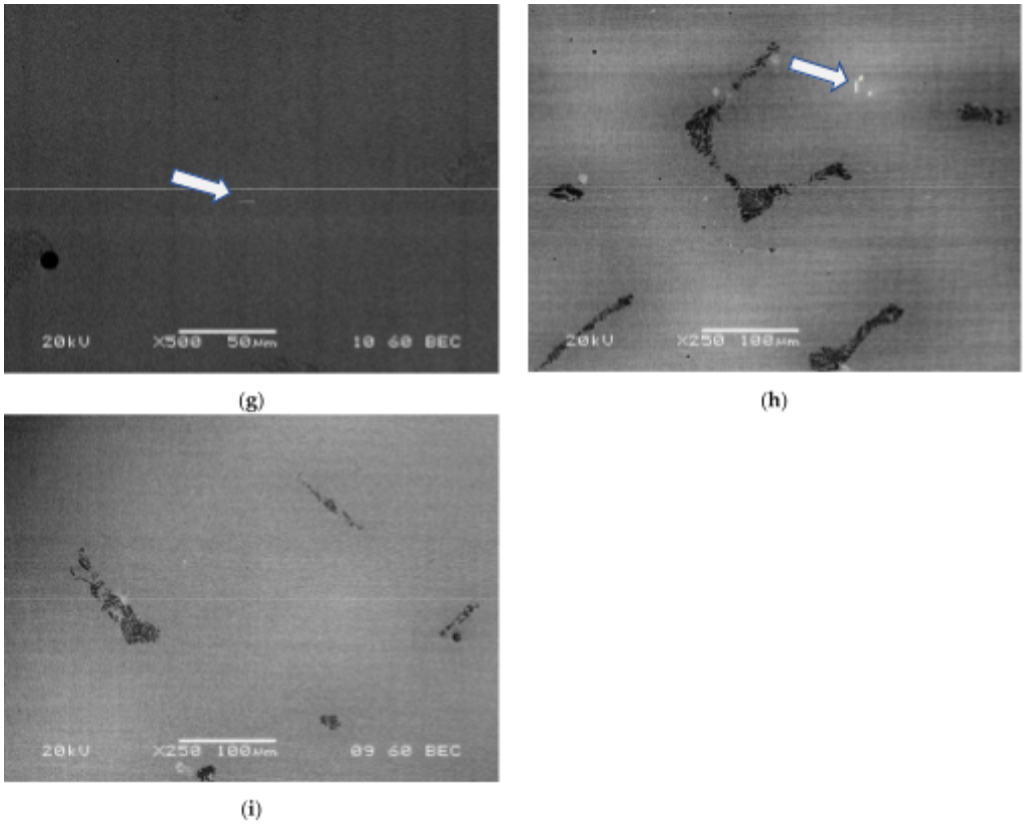

Figure 9: The microstructure of the dendritic cores of CMSX-10N samples of solution times: as-cast (**a**), 0 h (**b**), 1 h (**c**), 4 h (**d**), 8 h (**e**), 12 h (**f**), 16 h (**g**), 24 h (**h**), and 48 h (**i**). TCP phases are indicated by arrows.

The TCP precipitates present were seen to form either in clusters or as individuals, but almost always within the dendrite core, both as long needle-like precipitates and all smaller circular precipitates; however, these images only present a 2D insight into the material, meaning these needle-like precipitates could be plates and the circular precipitates needles if they were to extend into the depth of the material. This is seen in other works (K.Kim, 2017). Some TCP phases were observed in the dendrite arms, but none were seen in the interdendritic regions.

Figure 10 shows the volume fraction (Vf) of σ phase measured from the CMSX-10N samples using ImageJ, compared to the value modelled from

ThermoCalc using compositional measurements taken via EDX. The modelled assumptions were the same as those of Figure 7.

The as-cast modelling predicts the occurrence of TCP phases, although none were seen, and as with CMSX-10K, the model assumed the quenching behaviour it did not undergo.

An overestimate of TCP phases is seen again during the early stages of the solution process, with a very close alignment during the middle section. In contrast to CMSX-10K, the model underpredicted the volume of TCP phases at the later stages; however, at 48h, none were reported in the modelling (a non-zero value is shown to account for errors) nor were any seen during microscopy. Figure 11 shows a segment of a TTT curve for the surrounding temperatures of the solution profile, showing the rapid rate of formation for σ-phase is consistent at all surrounding temperatures.

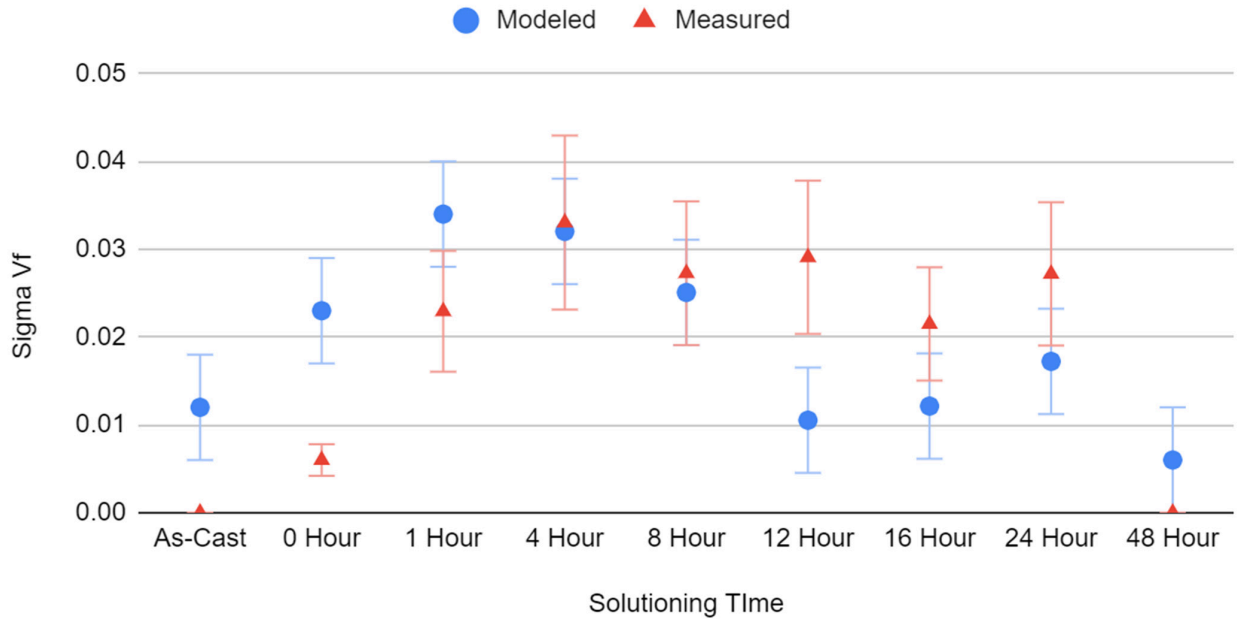

Figure 10: The calculated values of σ-phase volume fraction (Vf) using different methods for CMSX-10N.

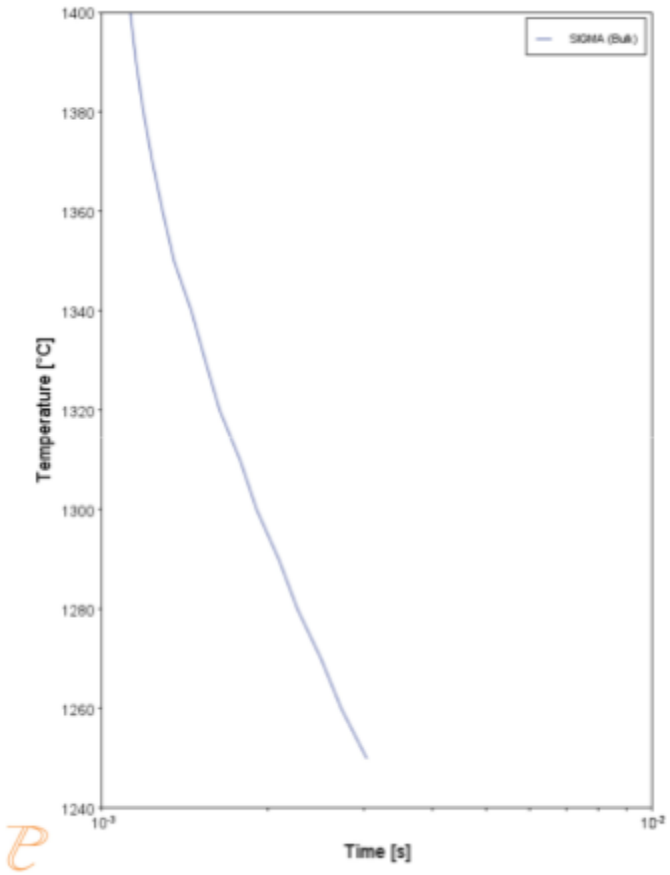

Figure 11: The time to the formation of a range of temperatures around the solution range of CMSX-10N.

3.4. Discussion

The immediate observation from the results is the appearance of TCP phases at all; whilst there have been some reports of TCP phases during the manufacturing process, they are limited. Long et al (F.Long, 2009) reported their occurrence in the as-cast structure, which then decomposed during the solution process; they also reported σ phase being present, along with η, however, Long's σ was nodular, whereas the η was platelet-like. Long did conclude that more σ precipitated from the platelet morphology of the decomposed sites of the nodular TCP phases during the solution process.

However, no TCP phases were seen in the as-cast state in these samples, and the same phenomenon cannot be used to explain their precipitation during the solution process. However, despite none being seen, there is a possibility they were not observed, and the modelling did suggest the possibility of TCP phases, although the modelling regime used did not replicate the solidification process. However, in this study, no platelet η was seen, nor did it appear in the modelling, suggesting that these two occurrences of TCP phases are rooted in different mechanisms.

Nader El-Bagoury et al (N.El-Bagoury, 2012) reported the occurrence of rhenium clusters in the as-cast state, as well as phases that possessed a needle-like morphology; however, neither of these phases was shown by TEM to be TCP phases; the needle-like particles were δ-phases, found alongside γ'', and contained Nb, neither of which are observed in the alloys in question here. The rhenium clusters are only a handful of atoms large and are a common occurrence in rhenium-containing alloys (G.A.Rao, 2004).

Fuchs suggested that TCP phases could occur during the solution process under certain circumstances (G.E.Fuchs, 2001), particularly if the solution process was shortened as it would lead to reduced homogenization. Fuchs reported that rhenium and tungsten diffusion was substantial only above 1340℃ This known behaviour identifies aluminium as the source of TCP phases, at least in the 0h treated sample. At these lower temperatures and shorter time frames, aluminium is the only element to undergo significant diffusion (Cr, Co, and Ni would diffuse at these temperatures too, but segregate relatively evenly on solidification).

As aluminium diffuses from the interdendritic region into the dendrite core, increasing the volume fraction of γ', this concentrates the Re and W, which have yet to diffuse, in the γ channels. Kim showed the composition of the γ and γ' is fixed (K.Park, 2022), severely limiting its ability to hold the excess rhenium and tungsten in solution. This oversaturation then

precipitates out as TCP phases, particularly as σ phase. Rae et al. reported that σ is typically the first to precipitate, but as a metastable phase that eventually returns to γ or a different type of TCP phase (C.M.F.Rae, 2001). However, the ThermoCalc models predicted σ would occur and would remain stable. The kinetics would lend itself to σ forming first, and the enriched concentrations would maintain the stability. This is reinforced by the dropping off of σ volume fraction with increasing solution time, as the Re and W have enough time to diffuse out of the cores into the interdendritic regions, with this reduction in σ volume fraction increasing with time.

The time to the formation of these TCP phases is of particular note, as Figures 8 and 11 show precipitation times of less than a second, almost instantaneous, far from the prolonged periods generally assumed for TCP phases (A.S.Wilson, 2017). These longer-to-form TCP phases are generally found at the surface, where there is an increased concentration of Al from the coatings (D.Spathara, 2001), whereas those in this paper are found within the bulk of the material, far from the surface, where the compositional non-equilibrium is the driver.

These data were modelled at the solution temperature, where the TCP phases formed and were stable, unlike the metastable σ reported elsewhere (C.M.F.Rae, 2001) and in the absence of γ'. These TCP phases could form during the heat-up cycle, and as Figure 6 shows, the time to the formation of TCP precipitates is fast at the surrounding temperatures too. Here the aluminium diffusion into the dendrite core causes an increase in γ' before its dissolution into γ, allowing a concentration of TCP phase forming elements in the core and allowing quick precipitation of TCP phases that are then stable throughout the solution process, continuing to grow until sufficient rhenium diffusion has occurred. Secondly, the TCP phases could form at temperature, despite no γ' being present, because the core regions would still be enriched in rhenium, with an increasing aluminium content in the early stages

oversaturating the γ matrix, which, as shown by Kim (K.Kim, 2017), has a fixed composition and must still reject the oversaturation of rhenium causing the precipitation of TCP phases. A third option is that the TCP phases form on quenching; as γ' forms during cooling, the γ is supersaturated with rhenium as it is rejected from the γ'; from here, the quick formation times of TCP phases at these compositions allow for the formation of TCP phases on cooling. Whilst this last theory does not reflect the modelling which suggests their stability at the solution temperature, it is hard to distinguish the methods without in situ imaging.

The first of these, where TCP phases form on heating, seems the most promising, as the still present γ' would still concentrate rhenium into the γ-matrix, increasing the driving force for TCP precipitation. However, precipitation and growth could still occur at this temperature, albeit to a reduced degree without the γ' concentrating effects, and furthermore, precipitation could occur on cooling too. If multiples of these effects are occurring, it would explain the discrepancy between the modelling data and experimental data, as the modelling only assumed at-temperature precipitation.

3.5. Conclusion

TCP phases precipitate during solution heat treatment of rhenium-containing alloys, particularly those of high concentration (6%wt or more).

- This occurs even at the earliest stages of the solution process, being present after the heating cycle to the solution window;
- This is most likely driven by aluminium diffusion into the dendrite cores from the interdendritic region before the other elements can homogenize, enriching the γ matrix and causing the rejection of the

rhenium, potentially from the formation of γ', which would further concentrate the rhenium in the γ matrix;

- Holding at the solution temperature for sufficient times allows sufficient rhenium diffusion so that TCP phases do not form. However, in the case of CMSX-10N, this time frame exceeds the 24h usually used for its homogenization in a production environment;
- Further work is needed to understand the mechanism behind the initial precipitation of TCP phases and how it varies across different alloys.

4. σ-TCP PHASE EVOLUTION DURING SOLUTIONING USING MODELLING

A comprehensive ability to model the phase stability of these alloys is essential, as they are expensive to develop, and if their production or use is limited by unforeseen issues it would considerably limit the alloy's potential to refund its investment. A successfully developed alloy can exceed expectations and be highly desirable (Y.Pei et al, 2009).

Despite the success of 2nd and 3rd-generation alloys they still suffer from numerous issues, from processing difficulties to undesirable properties in other areas, and in some cases, older alloys are still used or are being redeveloped to create an optimisation of the properties across the different generations (J.Wahl 2018).

Section **3.** shows the presence of TCP phases during the solutioning stage, and notably that this is relatively novel and unexpected. Whilst modelling data alongside these experimental results agreed with general trends, there were still significant variations. This section aims to delve deeper into these modelling discrepancies, to understand where the limitations lie, and how accurately modelling can predict TCP phase precipitation.

4.1. Alloys

The same three alloys were looked at throughout modelling as in the experimental side of this Thesis outlined in section **3.**, namely: CMSX-4, CMSX-10K, and CMSX-10N. See Table 3 for compositional data.

4.2. Methodology

ThermoCalc's extensive databases contain much of the fundamental information such as Gibbs energies for nickel alloys and the ability to extrapolate these into more complex higher-order systems. Thus, this work focuses on the input of compositional data, along with temperature and times (such as holding times) variables throughout the heat-treatment process to produce results (such as volume fractions and time to precipitation).

Initially, compositional data was gathered through experimental means, primarily electron-diffraction spectroscopy, this will focus on the dendrite core regions as the location where TCP phases are noted for their appearance.

However, this data will be compared to their equivalents in literature, to gauge how similar expected results should be to similar works. However, there is limited literature on compositional data during solutioning on these alloys. Comparing the as-cast state of these alloys, which are significantly more studied in literature, is necessary to be confident in the accuracy and repeatability of this work.

The alloys used are typical alloys used for comparisons or the base alloy for much of the work seen in literature, however, in this work, two similar alloys, CMSX-10K and CMSX-10N are used, this distinction is often not seen in literature, largely due to their compositional similarity, and that CMSX-10N is used in industry significantly more than CMSX-10K. However, this work is interested in the effect the small rhenium difference makes on the alloy. Thus the two alloys will be compared to literature simply as CMSX-10 and any differences will be discussed.

Area maps through electron-diffraction spectroscopy, as well as line scans, were carried out on the three alloys to measure the compositions of

the dendritic and interdendritic regions and calculate their **K'** value with the formula:

$$\mathbf{K'} = X_{Dendritic}/X_{Interdendritic}$$

The values calculated for each of the alloys are shown in Table 4 in comparison to those taken from literature of similar alloys; these values are all for the as-cast state of the alloys in question.

K'	Al	Ta	W	Re
CMSX-4	0.95	0.78	1.47	1.87
CMSX-4 (N.Wanderka)	0.75	0.69	1.35	2.7
CMSX-10K	0.88∓0.02	0.72	1.45	2.14∓0.07
CMSX-10K (G.E.Fuchs)	0.72	0.60	1.25	1.98
CMSX-10N	0.80∓0.02	0.69∓0.01	1.34∓0.03	2.73∓0.11
SX-1 (T.M.Pollock, 1992)	0.78	0.66	1.75	2.14

Table 4: Showing K' values for each majorly segregating element in the alloy, with results taken from literature for comparison.

SX-1's composition sits between that of CMSX-10K and CMSX-10N

There is significant variation in segregation values in literature and those present in this work, in particular, the Al content is less segregated whilst the W content is more segregated than the same alloys in literature.

However, other alloys such as SX-1 do show heightened levels of segregation too, suggesting it's possible for such values.

There is, however, a large degree of deviation between the measured results and those seen in the literature. In the case of CMSX-10N, which shows significantly more segregation of rhenium than the other alloys, Caldwell's work (E.C Caldwell, 2004) demonstrated Rhenium's strong relationship between its own segregation and concentration, where rhenium strongly segregates at low and high concentrations, with a minimum at approximately 6wt%, as in the case with CMSX-10K, and affects other elements too, thus explaining the strong segregation of Tantalum too.

These values are within the range seen within the literature but do raise the question of why there is so much variance between similar alloys. In part this is down to the individual dendrite variance; which is discussed later, but suggests a systematic difficulty in predicting TCP phases if they are dependent upon local concentrations since these concentrations can vary significantly between samples of the same material.

Table 5 shows how the segregation varies with time, showing how effective the 24-hour solutioning time is in homogenising these alloys.

K'	CMSX-4	CMSX-10K	CMSX-10N
As-Cast	1.87 (5.32wt% Re)	2.14 (12.82wt% Re)	2.73 (13.18% Re)
24 Hours	1.21 (3.64wt% Re)	1.76 (10.57wt% Re)	1.80 (10.70% Re)

Table 5: Rhenium segregation at the as-cast state compared with the fully solutioned (24H) treated samples for all three alloys with maximum dendritic Re concentrations shown in brackets.

A B

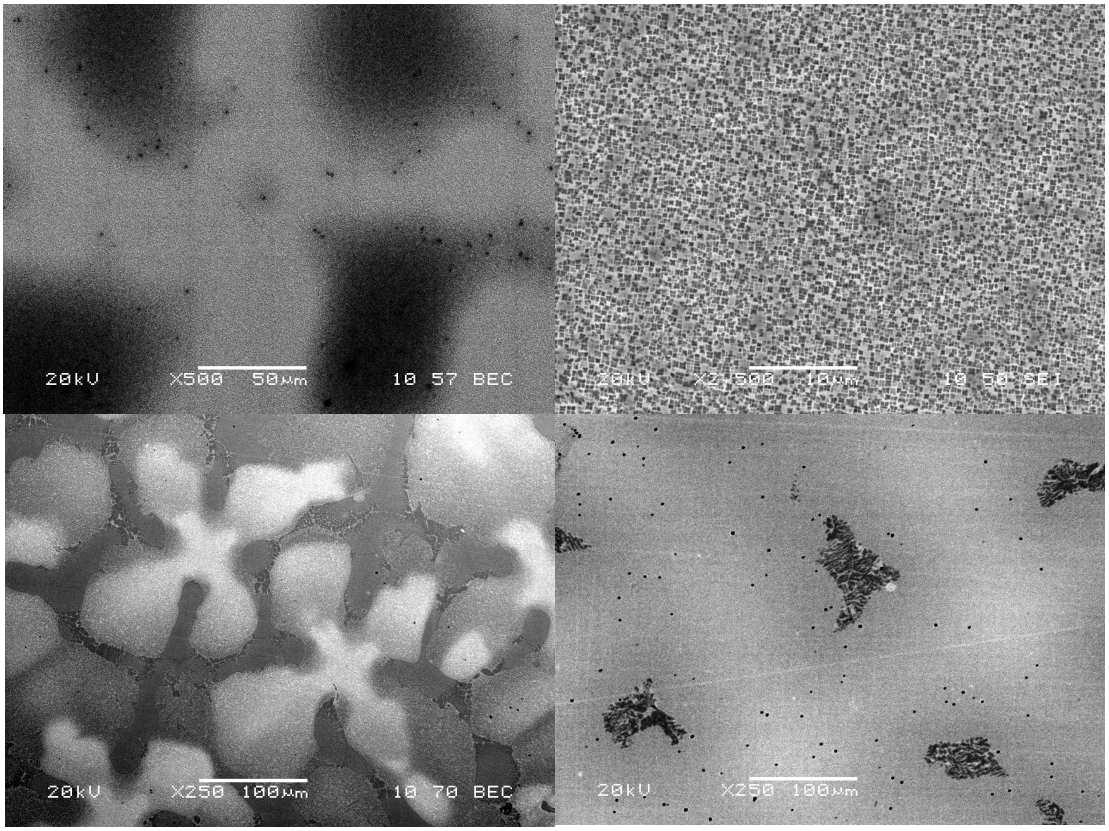

C D

Figure 12: Images A and C with microstructure of as-cast CMSX-4 and as-cast CMSX-10N respectively, and Images B and D showing CMSX-4 and CMSX-10N after 24 hours of solutioning at 1310℃ and 1361℃ respectively. (Images B and C are identical to those found in figure 5D and 9A)

As can be seen, whilst the solutioning process does improve the segregation of these alloys, the highly segregated CMSX-10 alloys end the process with a similar degree of segregation that CMSX-4 possesses in its as-cast state. This can be seen in figures 12a and 12d, showing the similar

microstructure of CMSX-4 in the as-cast state and CMSX-10N after 24 hours of solutioning.

Using electron diffraction spectroscopy the composition of the dendrites can be measured. However, the INCA software used to carry this out offers many ways to measure the regions. Initially, line scans were used, measuring from the centre of the dendrite core into the interdendritic regions. This was done to see how the composition changed between the regions, but also within the region, as TCP phases are primarily seen within the centermost region of the dendrite core and less frequently in the dendrite arms. This data could also provide information about not just how effective segregation and successive solutioning treatments were, but also the extent of diffusion of elements into and out of the dendrite.

However, a limitation of this is the interaction volume of the electron beam. To sufficiently excite the rhenium's electrons for detection an operating voltage above 17kV is needed, but this relatively high value produces a larger interaction volume and reduces the spatial resolution of the images. Casino simulations have shown that these high operating voltages can create interaction volumes of the order of $1_{\mu m}{}^2$ (Plymouth, 2021).

Figures 13a and 13b demonstrate that this scale interaction volume is too large to accurately measure this difference between γ' and γ channels, as they would overlap with each other. Furthermore, even large TCPs possess a width of less than 1um (appendix A). Whilst measuring this would give a reasonable estimate of the composition there would be some overlap of the surrounding regions, reducing the accuracy of these readings. Combined with the interaction volume being concentrated below the surface, it would also make it less accurate for these smaller particles.

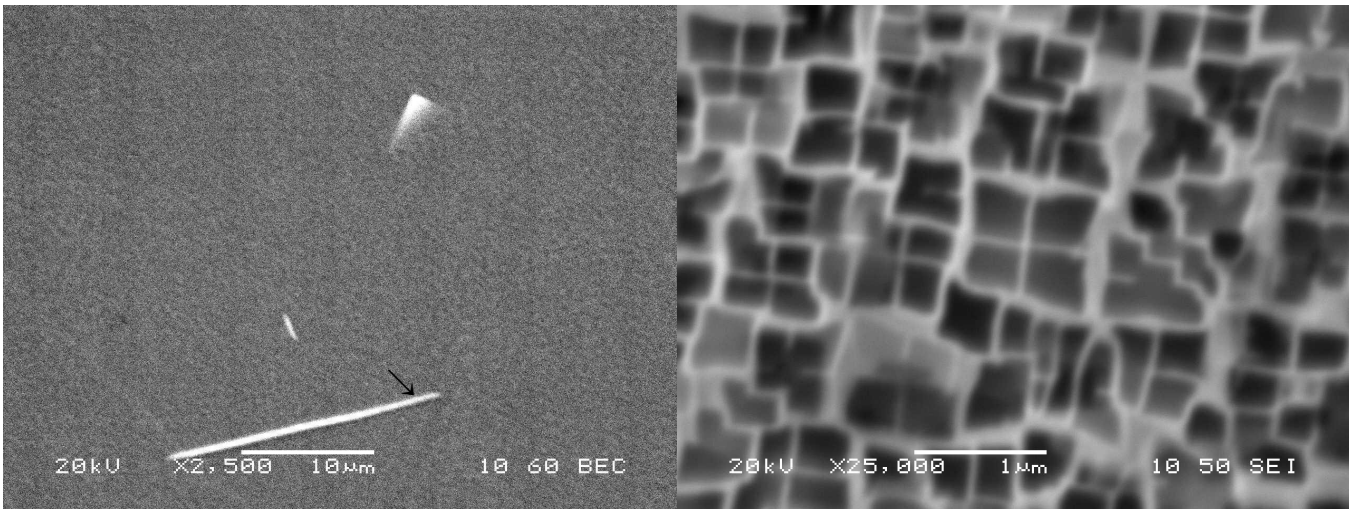

Figure 13: The small sizes of TCP phases (13a) indicated by an arrow and even smaller scale of the γ/γ' structure (13b) can be seen, showing the limitations of BSE measurements.

Despite this, the INCA software's area modes are sufficient to measure the composition of the much larger dendrite and interdendritic regions, even distinguishing between the dendrite arms and the dendrite core. As well as other large features.

This composition data can be used in ThermoCalc in several ways. Firstly, data gathered on the as-cast state can be used with ThermoCalc's databases on diffusion to predict the diffusion of elements over time, and then, using these predictions, produce expected volume fractions and formation times for TCP phases, notably σ. Secondly, compositions can be taken of the samples at each of the stages of the solutioning process, and this is used to directly produce volume fractions and formation times for σ.

To understand how accurate and where any shortfalls from the modelling lie it is necessary to compare these results to practical samples. The same samples from section **3.** were imaged using SEM and images of dendrite cores containing TCPs were taken. Using the ImageJ software the TCPs could be highlighted against the rest of the dendrite core and a volume fraction produced.

It is necessary to note not every dendrite core contains TCP phases (see Figure 2) and the proportions that do vary from alloy to alloy and solutioning time to solutioning time. The high temperatures of solutioning would provide a limited driving force for nucleation, but plenty for the diffusion of elements, and thus growth of precipitates. Therefore it would be expected to have fewer TCP phases that are larger in size, this in part would explain the lack of TCPs in every dendrite core. The influences of TCP phase nucleation variance is discussed later on in section **5.5**.

4.5. Results

Ten dendrite cores, taken from throughout the sample were used to produce an average composition of any one dendrite core for each solutioning time frame, compositional values were achieved through back-scattered electroscopy. Table 6 shows the calculated average of these results. This was repeated for all three alloys (1362℃ for CMSX-10N, 1345℃ for CMSX-10K and 1310℃ for CMSX-4). The volume of raw materials available was different for different alloys, allowing more solutioning times to be done for certain alloy compositions, with CMSX-10N having the most available material, allowing more solutioning times to be included.

CMSX-10K	Al (5.7)	Cr (2.0)	Co (3.0)	Ni	Mo (0.4)	Ta (8.0)	W (5.0)	Re (6.0)
As-Cast	5.00	2.24	3.57	Bal	0.56	5.77	7.26	12.82
0 Hour	5.52	2.33	3.37	Bal	0.62	7.03	7.33	13.37
1 Hour	5.07	2.29	3.42	Bal	0.47	6.88	6.74	12.10
4 Hour	5.13	2.515	3.56	Bal	0.54	7.18	6.27	10.79
8 Hour	5.50	2.46	3.49	Bal	0.56	7.87	6.20	10.60
24 Hour	5.6	2.42	3.42	Bal	0.53	8.48	5.76	10.57

Table 6: Dendrite core compositional variance with solutioning times, with nominal values in brackets in the headings.

0-Hour refers to samples that undergo the heating to solutioning temperature and quenching but held for no time at temp, hence 0-hour.

A general trend of γ precipitating elements reducing and interdendritic precipitating elements increasing can be seen as the solutioning times increase. However, a notable anomaly in this is the rhenium and tungsten concentrations increasing between the as-cast and 0-hour states. This is seen in CMSX-10N as well.

Aluminium and tantalum levels increase in this same period, suggesting not that more segregation occurs, but that this apparent increase in rhenium is likely the cause of the normalisation of the data to produce a

100% total of elements. As aluminium diffuses into the dendritic core, particularly before heavier elements such as tungsten and especially rhenium can diffuse out, the relative wt% contribution of these heavier elements increases, thus producing a result that suggests their concentrations have increased.

Using these compositional results as a basis, volume fractions and formation times of σ and other phases of interest can be calculated through ThermoCalc for the alloys at stages through their solutioning process. Alongside this a theoretical volume fraction can be calculated using ThermoCalc's database of diffusion rates, to compare the expected diffusion behaviours to that which is seen in the samples.

A modelled approach was taken to model diffusion and its effect on precipitation. By measuring the composition of the dendrite cores during the as-cast state its diffusion into the surrounding matrix was modelled aiming towards a complete homogenous structure. By recording the given value of each element at the same time frames as the practical experiments a composition can be gained for which estimated volume fractions can be calculated.

A more calculated approach was taken to model precipitation. By measuring the compositions of the dendrite cores during each of the solutioning stages, these were modelled to see each stage's potential to form the σ phase. This was achieved by leaving the dendrite core composition to reach equilibrium, without including the surrounding interdendritic regions as the material would diffuse across, changing the overall composition.

A measured approach was taken too. 25 images of numerous dendrites throughout the samples, the volume fraction of σ in cores that contained TCP phases by using ImageJ software was calculated, producing a value for TCP phases to compare to the modelled results.

The recorded σ values are as follows:

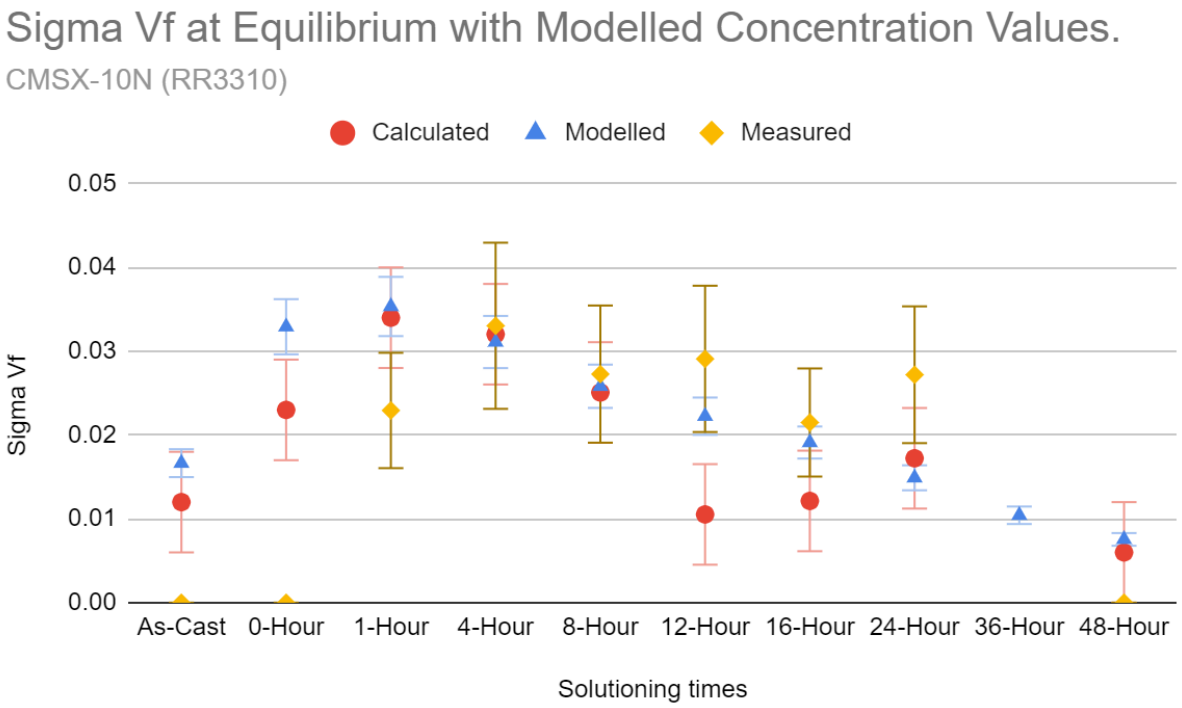

Figure 14: Calculations of σ volume fraction throughout the solutioning process for CMSX-10N, using different modelled, measured and calculated methods.

The practical calculated values demonstrated that initially, the potential to form σ phases increases up until 1 hour of the solution treatment, before dropping over and remaining relatively low for the rest of the solutioning process.

These values represent the potential to form σ phases if the dendrite cores were left to form an equilibrium mixture, without diffusing into the interdendritic spaces, or vice versa. Whilst this provides limited information into what the structure will look like during the more time-restricted

solutioning times, it does show whether the measured compositions still provide the chemical potential to form σ phases.

The theoretical values demonstrate that initially, the potential to form σ phases increases, however, it is important to note that the as-Cast and 0-hour values were used as a base for the diffusion profile, and therefore are the same values. At 1 hour, the potential σVf is still at its highest but lower than that of the 'practical' approach, however, these Vfs then begin to slowly decrease throughout the solutioning process, rather than a sharper drop that remains low.

The most notable feature that this graph provides, is that the potential to form σ phase initially increases throughout the solutioning process, before lowering again. This heterogeneous behaviour of the homogenization process is considered in further detail in section **5.2.**

The measured data shows the volume fraction of TCP phases present in the samples, the modelled and calculated values overestimate them at first, before underestimating them at the later stages. But during the midst of the solutioning, most are in occurrence with one another, even overlapping in the 4-8 hour range.

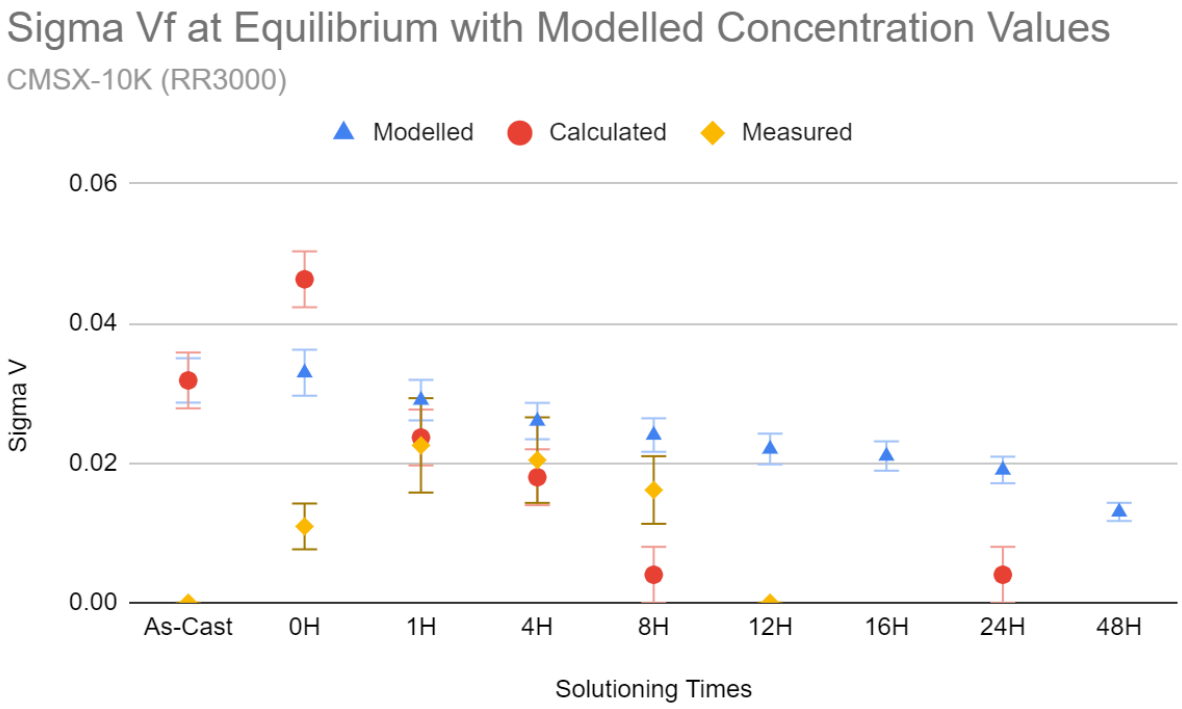

Figure 15: Theoretical and practical calculations of σ volume fraction throughout the solutioning process for CMSX-10K

The CMSX-10K results, like the CMSX-10N, show an increase in volume fraction in both the theoretical and practical approaches. Likewise, the theoretical results underestimate the practical approach in the earlier stages and overestimate at the later stages. However, a significant difference is the peak in the practical results for CMSX-10K occurs earlier, at 0 hours rather than 1 hour, this peak is also higher than the CMSX-10N peak, despite lower refractory content. This decreases faster too, with a near 0 value after only 8 hours.

Again the calculated values are lower than those of the modelled approach, except for the 0-hour samples in this case. Which increases considerably before dropping off into the later stages of solutioning.

The measured values are again undervalued by the other approaches in the early stage, whilst the measured and calculated approaches agree on

a near-zero content in the later stages. However, not enough data was available in the 12-16 hour range to determine when the cut-off exactly occurs.

Again the results are most in agreement with one another in the middle of the solutioning process, with the 1-4 hour range overlapping in this case of the CMSX-10K. It appears both precipitation and dissipation of TCP phases occur in a shorter time frame in the CMSX-10K alloy compared to those of the CMSX-10N.

The more distinct difference between the two alloys is that the CMSX-10N results had significantly more variance, with the errors on the results being larger. Whilst it is apparent rhenium plays a significant role in TCP phase precipitation, there also appears to be a strong probability spectrum that influences the location and scale of TCP phase precipitation. This is discussed further in section **5.5.**

In addition to this, timescales for precipitation were calculated with ThermoCalc, with the composition being used from each solutioning stage to calculate how long it would take for TCP phases to precipitate.

Due to the exponential nature of the results, the time values have also been shown as a function of Log (base 10) to better present the information.

It is noted that formation times for TCPs have long since been seen to vary significantly, and the temperature range of their precipitation increases, in varying alloys (R.Dreshfield, 1969).

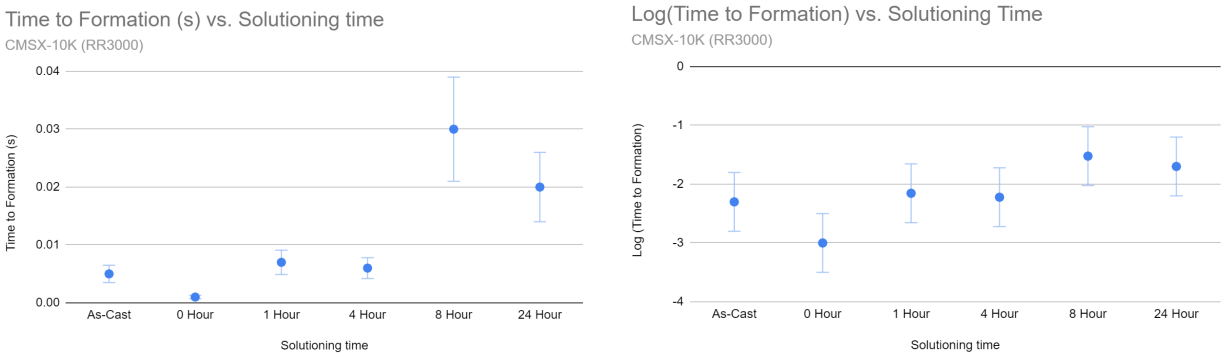

Figure 16: Time to the formation (16a) and Log(time)(16b) of σ phase in CMSX-10K

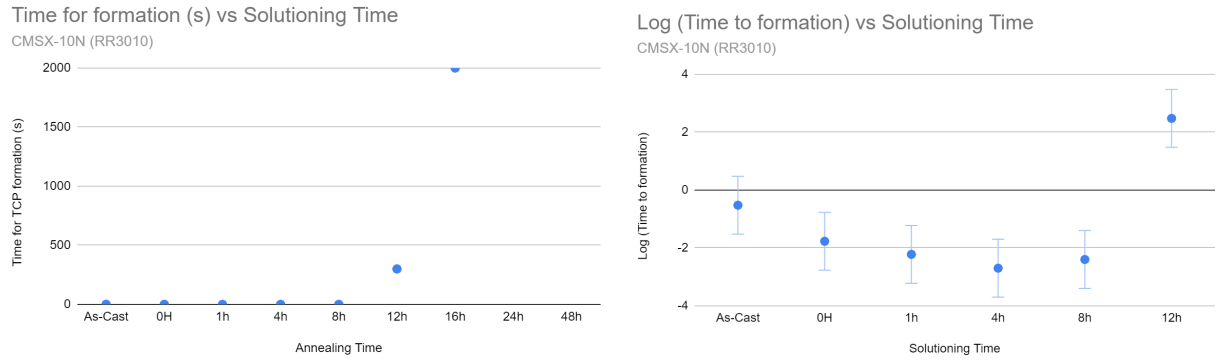

Figure 17: Time to the formation (17a) and Log(time)(17b) of σ phase in CMSX-10N.

Figures 16a and 16b demonstrate the exceptionally fast times to formation of TCP phases in CMSX-10K, interesting these times persist even until complete solutioning, whereas figures 17a and 17b, show the times to formation in CMSX-10N exponentially increases as solutioning times increase, but the 16-hour sample still records a time to precipitation of approximately 2000s, well below the total solutioning times.

These results suggest the kinetics favour TCP phase precipitating during solutioning, with the timescales allowing for precipitation during the

heat-up cycle or even the nearly instantaneous quenching process. These results thus fail to help identify where in the solutioning process that TCP phase formation occurs, merely stating that it is possible throughout the process.

Most interestingly, Figure 16 suggests that CMSX-10K has a longer period of potential precipitation of TCP phases, with Figure 17 showing a drop-off after 16 hours. This is unexpected, as the CMSX-10N experimental results showed larger volume fractions of TCP phases in the later stages of solutioning.

Time held at solution	As-Cast	1-Hour	4-Hour	8-Hour	24-Hour
Modelled σVf	0.00	0.0972	0.122	0.1648	0.00

Table 7: Modelled potential of σ-TCP in CMSX-4 at varying solutioning times.

ThermoCalc predicts the precipitation of σ-TCPs with the compositions at the respective solutioning times. This is unexpected, CMSX-4; chosen in the work to serve as a baseline, whilst not unknown to possess TCP phase these are associated with extended periods at operating conditions. As seen in section **3.,** TCP phases were observed, but only at 8-hours but not at other times. This suggests a potential for TCP phase precipitation, but possesses a barrier to it such as kinetics.

4.6. Discussion

The volume fraction results and the time to precipitation results leave questions to be asked. The measured TCP phase Vf in the earliest stages of

precipitation do not agree with the modelled or calculated results. Both of the latter suggest the possibility of TCP phases in the earliest stages, even in the as-cast state, and whilst the temperature of the casting doesn't correlate to the same for the solutioning stages, the time they take to precipitate; according to ThermoCalc, would leave the possibility of some being present in the as-cast state, as seen by Long et al (F.Long, 2009), and would expect to see them in the 0-hour state in both samples. Yet the measured results do not show them in both samples but only in the 10K sample and at the 0-hour sample with a significantly smaller volume fraction.

This discrepancy would suggest there are more factors influencing the precipitation of TCP phase than ThermoCalc accounts for. The model assumed homogeneous precipitation, whereas TCP phases have been seen to precipitate at boundaries and defects (K.Park, 2021)(R.C.Reed, 1999). This could lead to expecting more TCP phases in the measured values over their modelled counterparts. However, the occurrence of the opposite requires an explanation, that being that the model underestimates the energy for the formation of TCP phases in these particular systems. As an alternative; they have not had enough time to precipitate fully, which seems futile in the face of the time-to-precipitation results which expect precipitation in a matter of seconds.

Antonov et al (S.Antonov, 2017) showed that ThermoCalc was fairly accurate in its prediction of the σ-TCP phase, whilst falling short in regards to other TCP phases. These precipitations were primarily in and around grain boundaries; absent in this work, and thus suggests there is an emphasis on the precipitation method itself where ThermoCalc might be lacking.

The reasoning behind this is that eventually the modelled results and measured results agree, although most prominently in the middle stages of solutioning, the volume fractions overlap. Suggesting ThermoCalc has a

stronger prediction capability for the growth of TCP phases than their initial precipitation periods.

This accuracy falls off in the latter stages of the solutioning. Differently for the different alloys, however, overestimating the volume fraction in CMSX-10K whilst underestimating it in CMSX-10N. It is of interest, that two alloys, fairly similar in composition can vary so much in both the results they produce, and the way they are presented by modelling software (at least ThermoCalc), and that the small change in rhenium content (as well as the smaller changes in other elements) causes large changes in the stability of the alloy in regards to TCP phases. Small changes in composition have been seen to vastly change the partitioning behaviours, γ/γ' fractions, and now TCP phase precipitation too (A.S.Wilson, 2017).

Harder to understand is the time to precipitation results. The time scales; less than a second, for precipitation, are exceptionally fast compared to those found in literature. Typically TCP phases' ideal propensity to precipitate is considered to be at lower temperatures, hence much longer times to formation as seen in figure 4. However, these times have been seen down in the 10s of hours (over the usual hundreds or thousands)(R.Dreshfield, 1969).

Reed et al reported seeing TCP phases; at least in comparison to carbides, increase in volume fraction with temperature (R.C.Reed, 1999), but that the rate of formation drops after a certain optimal temperature; a typical C curve of TTT graphs. However, they did report on the rate of formation between the two alloys analysed in their work, to have formation rates varying by two orders of magnitude. It can be assumed that temperature and composition would affect the propensity for TCP phase formation, but the extent a small change on either function can produce

such large changes in volume fraction, time to formation, and the temperature range in which it can occur is significant.

Reed et al also report that tensile stresses can contribute to TCP phase precipitation, a potential cause of increased volume fraction, however, stresses have already been seen to cause recrystallisation during the manufacturing of blades (L.Zhonglin, 2016), and attempts to reduce this to prevent it are already implemented. It is worth noting that both have been seen in conjunction (L.Zhou, 2015)(L.Wang, 2012), however, Zhou reports P phase TCPs forming after recrystallisation, whilst Wang reports them before recrystallisation. Regardless, stresses can also increase the propensity for TCP phase formation, whilst appearing to have a symbiotic relationship with recrystallisation. However, the scale of the stresses to promote TCP phases and the stresses needed for recrystallisation are not necessarily of the same magnitude, with relatively high stresses necessary for recrystallisation to occur, there is potential for a region of stress, insufficient for recrystallisation and yet sufficient to contribute to the precipitation of TCP phases, a region not necessarily already addressed with current manufacturing methods.

Since the samples were cast into simple cuboidal samples, the only source of potential stresses was the cutting of the large samples into smaller ones, and from polishing and grinding. However, potential stresses from cutting would be localised, and initial grinding would remove much of the areas. No signs of recrystallisation were seen in any of the observations of the samples. And so the possibility of this contributing to the heightened volume fraction and kinetics of TCP phase precipitation would be minute at most.

Uniquely, ThermoCalc predicting σ-TCP in CMSX-4 varying stages of solutioning. Yet TCP phases were seen at 8-hours as seen in Figure 19.

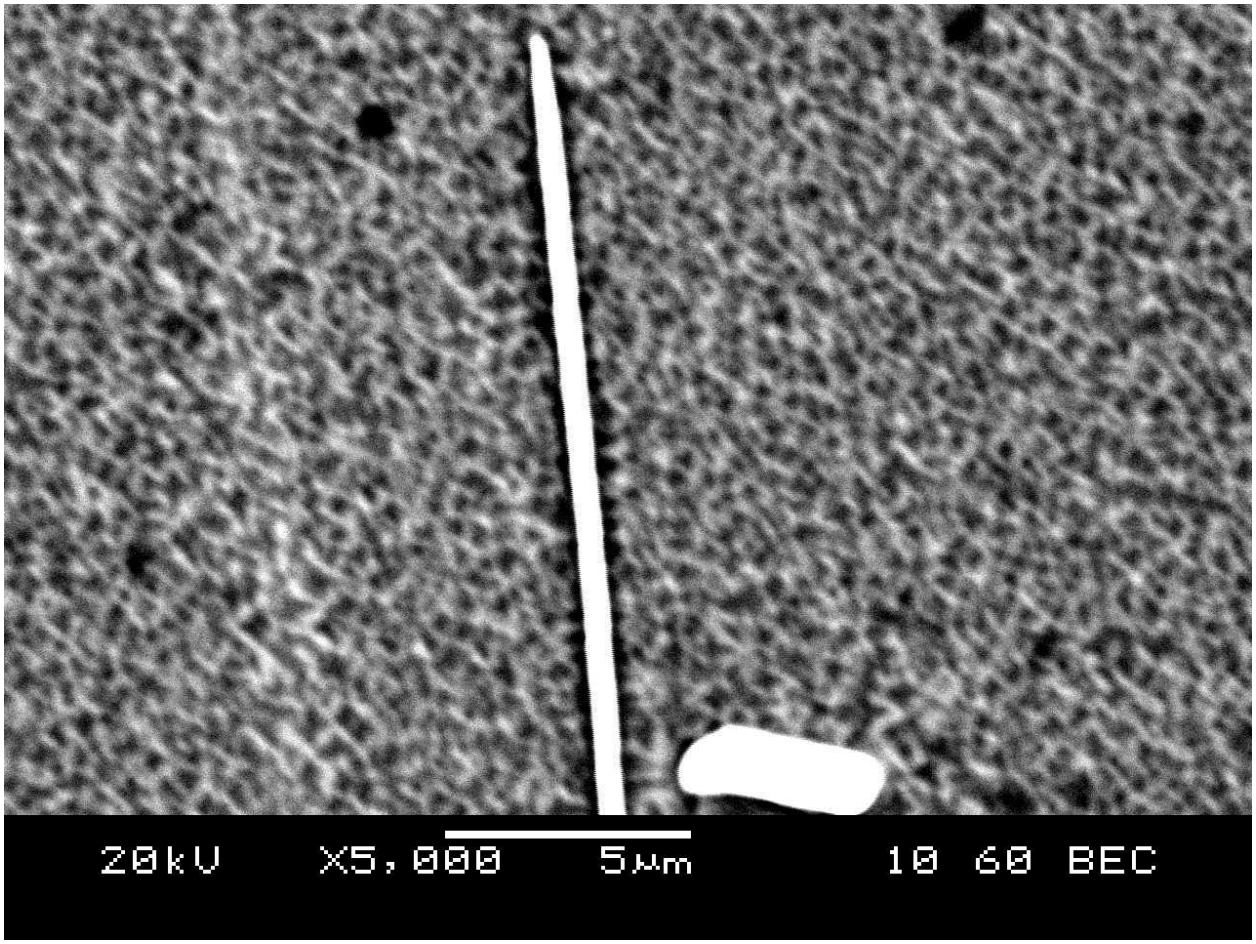

Figure 18: TCP phases present in CMSX-4 after 8 hours at solutioning conditions. A plate/needle like precipitate can be seen beside a more nodular precipitate.

CMSX-4 has seen more associated with μ-TCP (K.Cheng 2011) but a high occurrence of plate or needle like precipitates was observed in the CMSX-4 samples as seen in appendix A, whilst the modelling specifically predits μ-TCP and no μ-TCP. Why more volume fraction of σ-TCP is expected by the modelling is not immediately clear, however ThermoCalc is seen to underestimate volume fraction of TCP phases in certain circumstances and overestimate it in others as discussed in **4.5.**, and thus this issue could be more prevalent in CMSX-4. Kinetics could play a large part of this, as they are expected to be slower in CMSX-4 due to its lower refractory element

content, particularly rhenium, however it is still clearly sufficient for some precipitation after 8 hours.

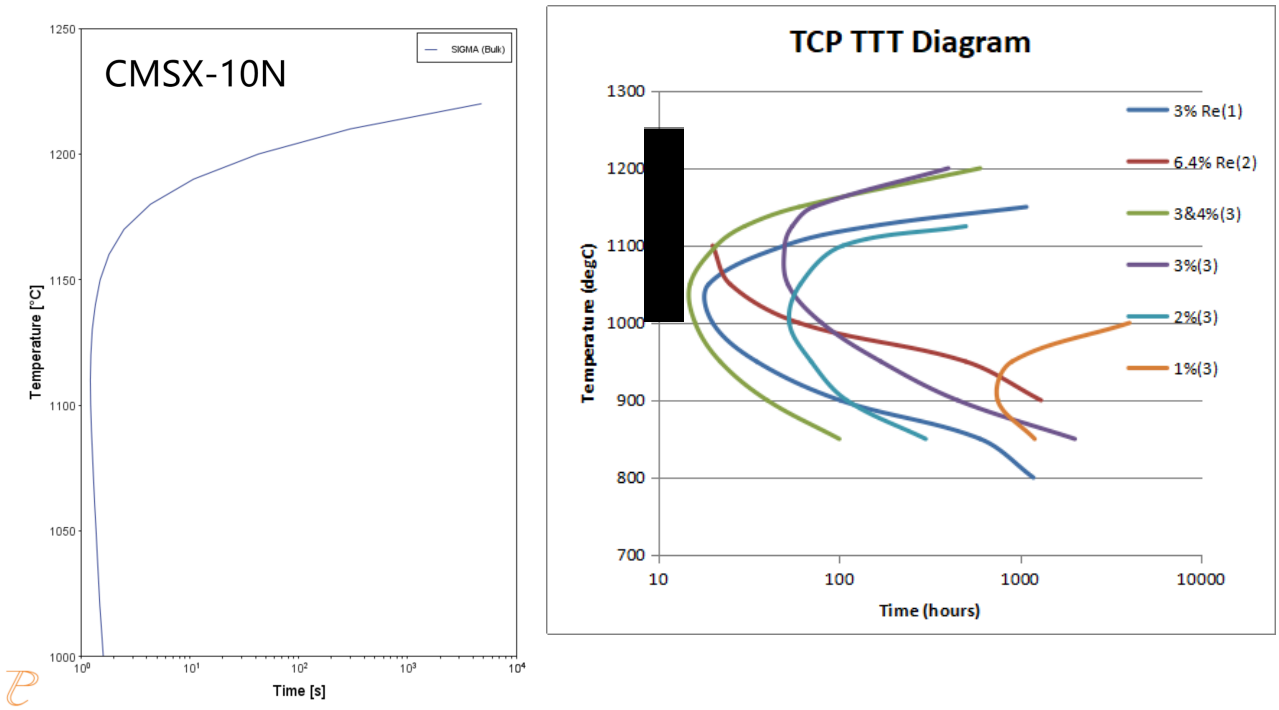

Figure 19: CMSX-10N formation times and temperatures. Compared to an edited Figure 4, where a black line represents Figure 19 imposed into Figure 4.

Figures 19 show TTT graphs for the precipitation of TCP phases in the 4-hour samples of CMSX-10N and shows rapid formation rates at a range of temperatures, only dropping off at considerably low temperatures (temperatures above the γ' solvus could not be calculated).

These rapid formation rates, order of magnitude higher than in-service rates for TCP phase formation seen in Figure 4, demonstrate the futility in direct comparison of the two different precipitation conditions, at least in regards to time to formation. Where one would expect to see only γ in the

alloys present in Figure 4, σ could be present during solutioning conditions of CMSX-10N.

The forwardmost point of the curves sits below the maximum temperatures, instead peak TCP phase precipitation rates occur in the 1050℃-1150℃ range. This is of particular interest, as this is in the vicinity of peak operating temperatures of turbine blades. An insufficiently solutioned blade would likely suffer extensive TCP phase precipitation early into its service.

A second problem these results imply is the unavoidable occurrence of these TCP phases in current processing methods. These high temperatures where TCP phases most rapidly occur are necessary to dissolve γ'. Whilst these results do not consider temperatures in the solution heat treatment window, any alloy would spend sufficient time just below those temperatures; mostly on heating but even briefly on cooling, that the rapid rate of formation would permit TCP phase precipitation. This issue is enlarged in CMSX-10N, which requires a stagnated solution heat treatment, as it suffers so much segregation in the as-cast state, that the γ' solvus is higher than the incipient melting point of the interdendritic regions. Thus the gradual increase of temperatures in the solution heat-treatment window may temporarily offer greater support to the precipitation of TCP phases.

4.7. Conclusion

- ThermoCalc modelling is capable of predicting the occurrence of TCPs during solutioning of rhenium-containing alloys.
- Current ThermoCalc databases are insufficient to precisely predict volume fractions of TCPs during the same stages, but are within the same order of magnitude, making for a relatively reliable estimation.

- TCP precipitation and growth likely possess numerous defining functions, including local micro-segregation, heterogeneous defects, and local γ' volume fractions. The large variances in TCP volume fractions measured are likely to imply a probability function too.
- TCP precipitation rates are exceptionally fast during solutioning and would be largely unavoidable using the current manufacturing methodology. To prevent excessive TCP precipitation full solutioning must occur.
- Attempts to shorten solution times must consider the possibility of TCP precipitation, particularly in high-rhenium-containing alloys.
- ThermoCalc overestimates σ-TCP occurrence in CMSX-4, possibly due to other TCP phases being present, but likely due to underlying limitations in the softwares understanding of TCP phase precipitation.

5. EFFECT OF SOLUTIONING CYCLE ON TCP PHASE PRECIPITATION

Throughout the previous sections numerous limitations have been identified and new questions raised in response to results gathered. This section discusses the extent of these limitations, recommends potential avenues of investigation to address them as well as anomalous results and the implications of further experiments of this thesis.

Section **3.** identified that TCP phases precipitate in the earliest stages of solutioning, precipitating even after just the heat-up cycle and following quench. Section **4.** shows σ particles can be predicted qualitatively via ThermoCalc, however it is lacking in its ability to correctly quantify the volumes produced. Furthermore, even though CMSX-10N appears more susceptible to TCP phases, only the CMSX-10K alloy was seen to possess TCP phases at 0-hours.

Differentiating the stages of solutioning to determine which stages precipitation occurs; or the contributions of each stage to the total volume, proposes numerous challenges. Namely: TEM, Atom Probe, modified solution treatments, cyclic solutioning.

5.1. Methodology

The following sections use the same data collected through sections **3.** and **4.** These are then used to consider the individual contributions of the stages of solutioning.

5.2. Solutioning cycle

There is limited information to deduce when the precipitation occurs; during Heating, Holding Period, or Quenching, and thus which part of the

process to study more in depth to attempt to understand the nature of TCP phase precipitation during the solutioning process and hope to improve the alloy's response to TCP phase precipitation.

A contribution of all three stages of the solutioning cycle (These stages will simply be referred to as Heating, Holding Period, and Quenching) could also take place, their totals producing the TCP volume fractions seen.

As stated in the discussion of section **4.**, the initial Heating stage (heating from room-temp to solutioning temperature, a 90 minute period) seems possible for the onset of precipitation, the modelling data of section **4.** shows the time-scales to formation to be sufficiently quick to allow the precipitation of TCP phases in any of the timeframes of each stage. Whilst the major suspect; Al, is already largely diffused to promote the necessary γ' formation, as can be seen in Figure 20, where Al is already equalised, whilst Re does not see significant diffusion until 4 hours.

However, as the temperature approaches the solutioning window, the volume fraction of γ' decreases, reducing the Re saturation effect. The true time-frames of TCP phase formation during heating would require significantly more dynamic modelling calculations. However, the extended period of time with a supersaturated γ matrix still offers the possibility of TCP phase precipitation during heating. Methods of investigating this further are considered in section **7.**

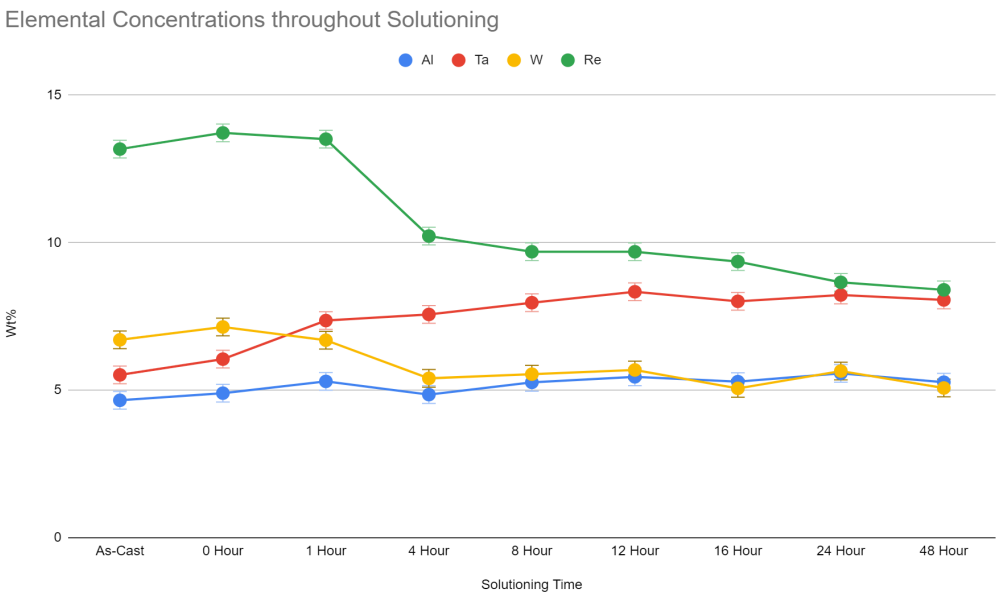

Figure 20: Average Wt% change with solutioning time of high partitioning elements in the dendrite cores of CMSX-10N, taken from section **3.**

In the Holding Period, within the respective solutioning windows for each of the alloys, ThermoCalc modelling predicts that σ phase to be stable at these elevated temperatures. The lack of γ' however would inhibit the driving force for formation, if the driving force is already sufficient to precipitate at these conditions it seems certain is would be initiated before this during the heating period. However, growth could still occur in this period if precipitates have already formed, the high temperatures enabling for the diffusion of rhenium without γ' to limiting its movements to gamma channels.

The lack of γ' would maximise the lattice parameters of gamma promoting needle-like precipitate growth, and it's following partial redisolving into the matrix (H.Long, 2018) could produce the few small

blocky TCP phases seen. However, there is much difficulty in determining such relationships on experimental characterization alone (H.Jin, 2022).

Quenching could either lock in the already precipitated TCP phases, encasing them in γ' envelope (C.Rae, 2005) or, with as γ' rapidly forms the slower diffusing Rhenium becomes supersaturating in the γ matrix, forcing the formation of TCPs after γ'. However, TCP phases are large, and their preferred orientations cut through numerous γ' precipitates and interrupting the continuous matrix (B.C.Wilson, 2003), it raises the question of how the TCP phases grow through the γ' due to its absence of TCP phase forming elements.

Thus again, it seem likely that the onset is during heating, the concentrated γ channels could nucleate small TCP phases, which are enabled to grow during the holding period after γ' dissolution, but with local concentrations remaining high in rhenium content, with the surrounding regions depleted of TCP phase forming elements and encouraging γ' films to precipitate around them.

5.3. Potential investigation methods

Furthermore, other features need to be discussed, the lack of TCP phases in the as-cast state and the statistical variation of TCP phase presence. It can be confidently stated that the solutioning stage, whilst may contribute to precipitation and growth, is not necessary, as the 0-hour samples (for CMSX-10K) contained TCP phases, despite not being held at solutioning temperature for any significant length of time.

To identify the stage in which precipitation occurs microscopy could reveal if TCP phases occur only during quenching. If they precipitated in the earlier stages they then would have to dissolve back into the matrix for the homogenous 24 hour samples in the CMSX4 and CMSX-10K samples to

occur, this would leave residual stresses in the matrix and potentially affect the surrounding structure, particularly the lattice parameter, which would be expected to be larger, if higher enriched in the large atomic radius elements typical of TCP phases. Whereas, if they only formed during quenching then in the 24 hour samples they would never form, leaving no trace and producing a ‘truly’ homogeneous structure.

The relatively small size of TCP phases would hinder this however, typical microscopy techniques would struggle to discover this. TEM would have the potential but numerous samples, potentially hundreds would need to be made and imaged to fully analyse the necessary number of dendrites to show there is no residual, and disproving a negative is an invalid alternative.

However, atom probe techniques could show the distribution in particular of rhenium, and more easily show the occurrence or lack of residuals from TCP phase dissolution. N.Wanderka et al showed that time of flight atom probe techniques can accurately measure features within single-crystals, identifying both the narrow γ/γ' boundaries, and rhenium clusters in the matrix (N.Wanderka, 1995). This was in CMSX4, which has a lower rhenium content. It could effectively detect the presence of rhenium particles. Whilst likely to be TCP phases, it would be hard to distinguish this from rhenium rich particles (N.Wanderka, 1995)(N.El-Bagoury, 2012), although TCP phases are typically much larger than these particles. Atom probe techniques would likely run into the same problems as TEM, with no guarantee that any particle needle contains TCP phases, making it hard to definitively demonstrate there are none, if there are none. However, it's excellent spatial resolution would allow the detection of an area enriched in rhenium from where a TCP phase had been present before dissolving, as it would contain a higher concentration than the surrounding matrix with diffusion both into the γ' regions and the surrounding less rhenium enriched

matrix. Atom probe has been used to identify elemental makeup across narrow regions similar to that of TCP/γ' and γ matrix (C.Rodenkirchen, 2023).

Alternative methods could also offer some insight, trying to quench the samples before they reach solutioning to see if they form on the heat up will allow γ' to remain, concentrating rhenium in the γ matrix allowing for conditions for typical TCP phase precipitation as in-service temperatures. The timescales of typical in-service precipitations are significantly longer, however the pre-solutioned conditions of the alloy would promote TCP phase precipitation, part of the reasoning solutioning is carried out in the first place. Distinguishing between TCP phases formed by these means, and any by the solutioning process would run into the same problems as the previous section identified. As both would still require quenching, which itself may contribute to the precipitation.

However, taking longer to the quench the alloys would also allow time reduction of saturation in the γ matrix, it would also prolong the time the alloy spends in the time where TCP phases are stable in tradition circumstances, distinguishing the effects of the experiments from that of the solutioning process itself would make it very difficult to determine when precipitation occurs, and especially the volume of TCP phases precipitated as functions of either the quenching or heating, or of a typical TCP phase producing regime.

This is demonstrated in the following graph:

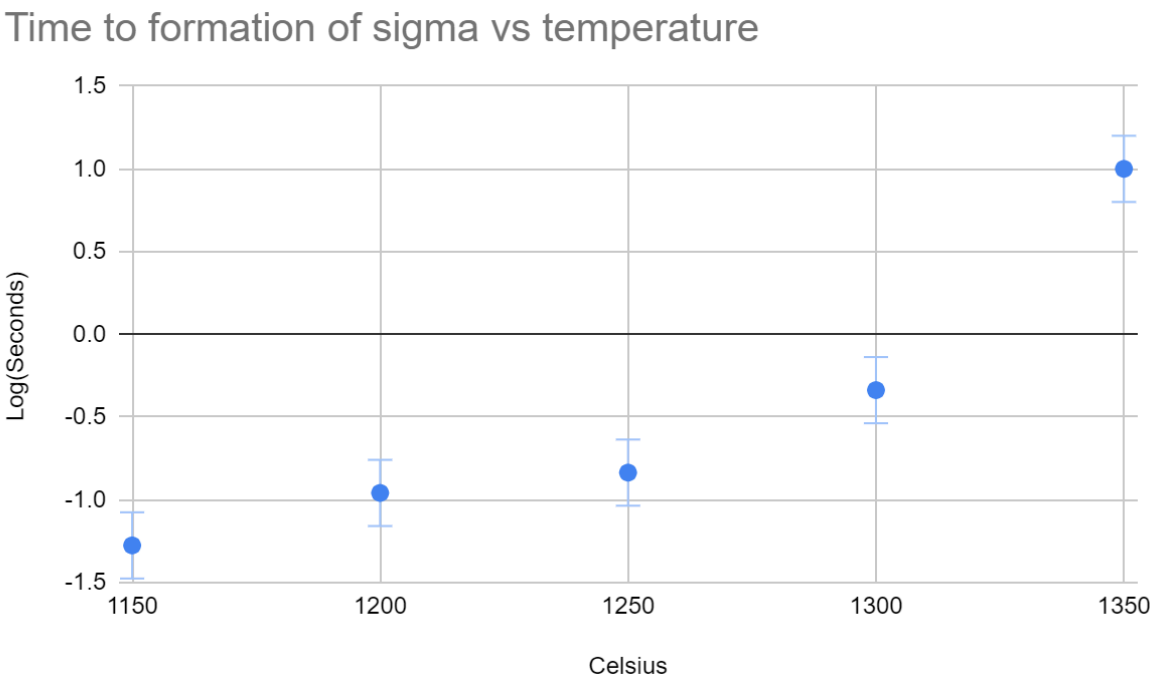

Figure 21: Decreasing holding temperatures promote decreased formation times for sigma-TCPs, data produced by ThermoCalc simulations.

Figure 21 demonstrates that not only are σ-TCPs stable in the solutioning temperature range, but that at temperatures just below these ranges TCP phase formation becomes exponentially faster.

5.4. CMSX-10N vulnerability

This raises a potential issue with CMSX-10N. The dendrite cores; containing such high refractory element content, require temperatures sufficiently high to dissolve the γ'. These temperatures are higher than the incipient melting temperature of the interdendritic regions. For this reason, the solutioning process is staggered to allow for the necessary solutioning window. The alloy is heated to just below the γ' solvus, allowing for sufficient homogenisation of the interdendritic that its incipient melting point

increases. Only then can the solutioning temperature be increased in steps, repeating the process, until the incipient melting point of the interdendritic is higher than the γ' solvus allowing for full homogenisation to take place. A schematic demonstrating this can be seen in Figure 22.

However, this would leave the alloy in a prolonged period where the temperature is high enough for minor rhenium diffusion (G.E.Fuchs, 2001), but where significant fractions of γ' would be still be present, this is represented by the areas under each line in Figure 22. Thus the alloy possesses more kinetics, driving force and time for potential TCP phase precipitation. This means the CMSX-10N manufacturing process would leave it even more exposed to the potential of TCP phase formation than just from its increased rhenium content. As the incremental solutioning window would produce longer conditions where TCP phase precipitation can occur.

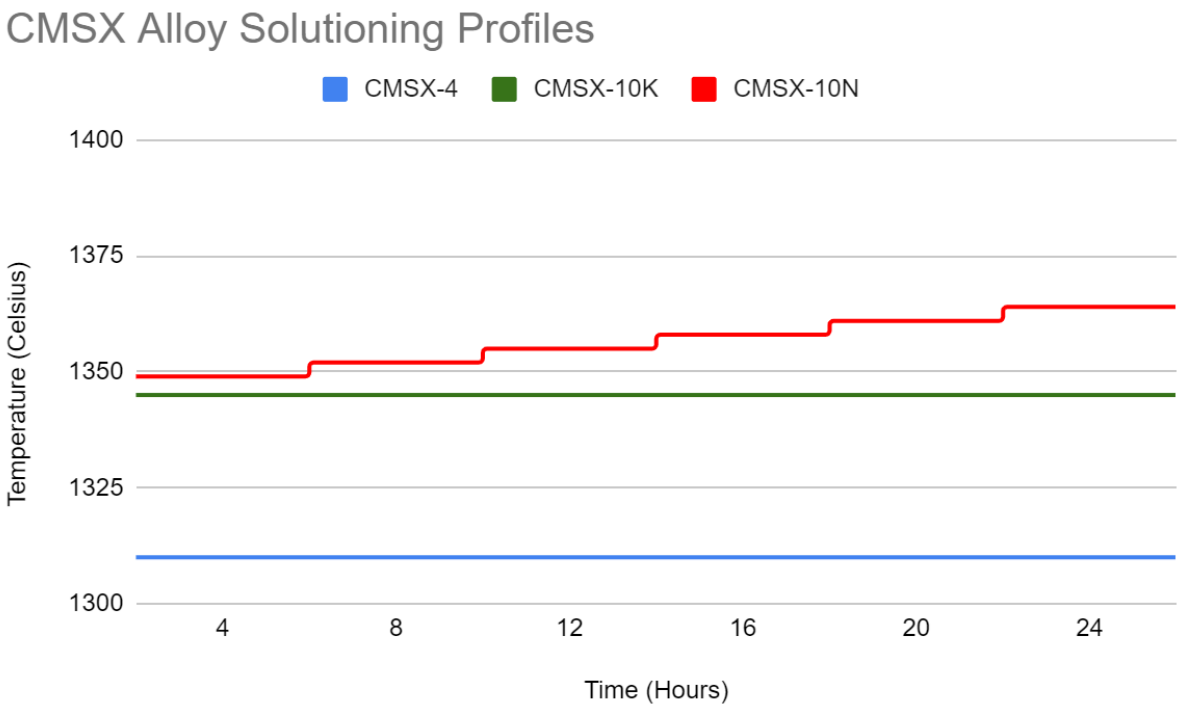

Figure 22: CMSX-10N incremental steps for solutioning and compared to the simple holding temperatures of CMSX-10K and CMSX-4.

5.5. Probability and Solutioning cycle contribution

Also of necessary explanation is that the volume fraction of TCP phases in the dendrite cores matches the modelled data, however the modelled data is based on compositions across numerous dendrites including those without TCP phases present. The experimental volume fraction is only measured from dendrite cores containing TCP phases, whereas the compositional data was taken from an average of dendrite cores, both those with TCP phases and those without.

This disparity must again be linked to the fundamentals behind their formation. The modelling showed the equilibrium content of σ-TCPs, which

the samples have enough time to reach according to Figure 21, hence why some of the dendrites contained them.

However, not every dendrite core had the initial conditions (whatever they are) to precipitate TCP phases, and therefore prevent them from reaching their equilibrium, either by lack of kinetics or driving force. Jin showed that local composition variations can influence the morphology of TCP phases (H.Jin, 2022), if this can influence the preferred growth mechanism of these phases, whether planar or layer-by-layer, it could affect its propensity for growth at all.

The modelling of this average composition suggests σ-TCPs form and are stable up to and at solutioning temperature, but only some dendrites contain TCP phases, even in dendrites containing lower concentrations of TCP phase forming elements than some TCP phaseless dendrites. It is suspected the solutioning cycle plays a crucial role in enabling individual dendrites to form TCP phases, as discussed later.

Since the heating conditions were uniform across the sample, and macro concentrations seemingly independent of which dendrites did and did not possess TCP phases, local variations; with a scale of micrometres, must be responsible for whether TCP phases nucleate or not. The locations within dendrites that TCP phases occur also vary, whilst the majority occur around the core of the dendrite, some precipitates are also seen in the dendrite arms (appendix B). Wilson reports TCP phases in the as-cast state of CMSX-4 along the dendritic/eutectic border (B.C.Wilson, 2003), here, Al diffusion from the interdendritic during cooling could increase the local γ' volume fraction, saturating the matrix with enough Re to force the precipitation of TCP phases. With longer periods of time, the local region would relax as rhenium diffuses into the neighbouring eutectic. The Al would diffuse further into the core, where the rhenium is most heavily concentrated, and has the further distance to diffuse. But could also provide

the rhenium with sufficient energy to group together, but not enough to diffuse out, producing a heterogeneous middle ground effect promoting precipitation in the dendrite core over the borders. Means of quantifying this are discussed in section **6.**

Another possibility is that TCP phases precipitate on localised, micro defects, such as dislocations combined with areas of microsegregation where sufficient elements are already present pre-diffusion. This would produce a probability effect, where a dendrite has a chance of possessing enough micro segregations and defects interacting to promote nucleation.

Only by varying the sections of the solutioning cycle can this effect be quantified better, whilst potentially also alluding to which part of the cycle nucleation occurs.

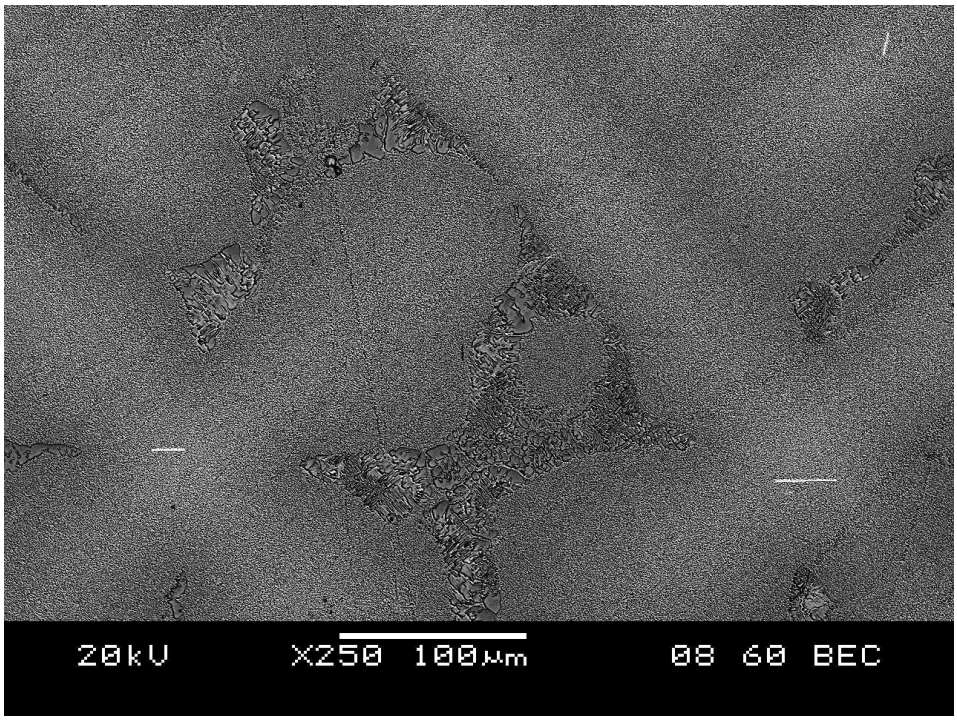

Figure 23: Higher frequency of large TCP phases and increased volume fraction are present within this double-heated alloy sample in comparison to single-treated alloy samples.

An alternative avenue of investigation to understand TCP phase formation is seen in Figure 23.

Figure 23 is the result of a sample undergoing two solutioning treatments. It is a CMSX-10K sample solutioning at 1345℃, firstly for 2 hours before quenching, and then again for 4 hours before quenching. This occurred to equipment failing to carry our solutioning fully. However, since the heating cycle and quenching process are the culprits behind TCP phase precipitation efforts were taken to study it to see what effect this has on the TCP phase precipitation behaviour.

Throughout the sample TCP phases are more numerous, with dendrites having numerous TCP phase precipitates with the number of dendrites containing TCP phases increasing too (More micrographs and given in appendix C). Figure 20 showed the aluminium is predominantly homogenised during the initial heat up cycle, thus numerous cycles shouldn't enhance its effect on γ' formation and matrix saturation effect. The increased number of TCP phases seen would suggest the heating cycle promotes nucleation of TCP precipitates, whilst there is an increase in the number of larger TCP precipitates their maximum size does not appear to exceed that of those seen in section **3.** Suggesting that the time for growth is the same, or in both situations maximum growth has been achieved.

It is worth noting that these micrographs provide only 2D pictures of the dendrites. Beneath the interaction zones there could be TCP precipitates undetected. However typical TCP phases seen are plate-like, suggesting any 2D slice would still observe them. However, using more 3D methods of investigation, such as atom-probe or TEM would confirm whether or not this is the case. Furthermore morphology is shown to vary even within the σ phase, with needle-like precipitates occurring in some instances. Means to measure this component, and achieve a better understanding of how frequently dendrites produce TCP phase is discussed in **7.1.**

Figure 24 shows the volume fractions of alloys CMSX-10K and CMSX-10N from early sections imposed with the volume fraction from the 6-hour sample, denoted at K+ to represent its altered solutioning process.

Notably its volume fraction exceeds that of CMSX-10N samples with similar time periods of treatment, despite 10K lower overall propensity to form TCP phases.

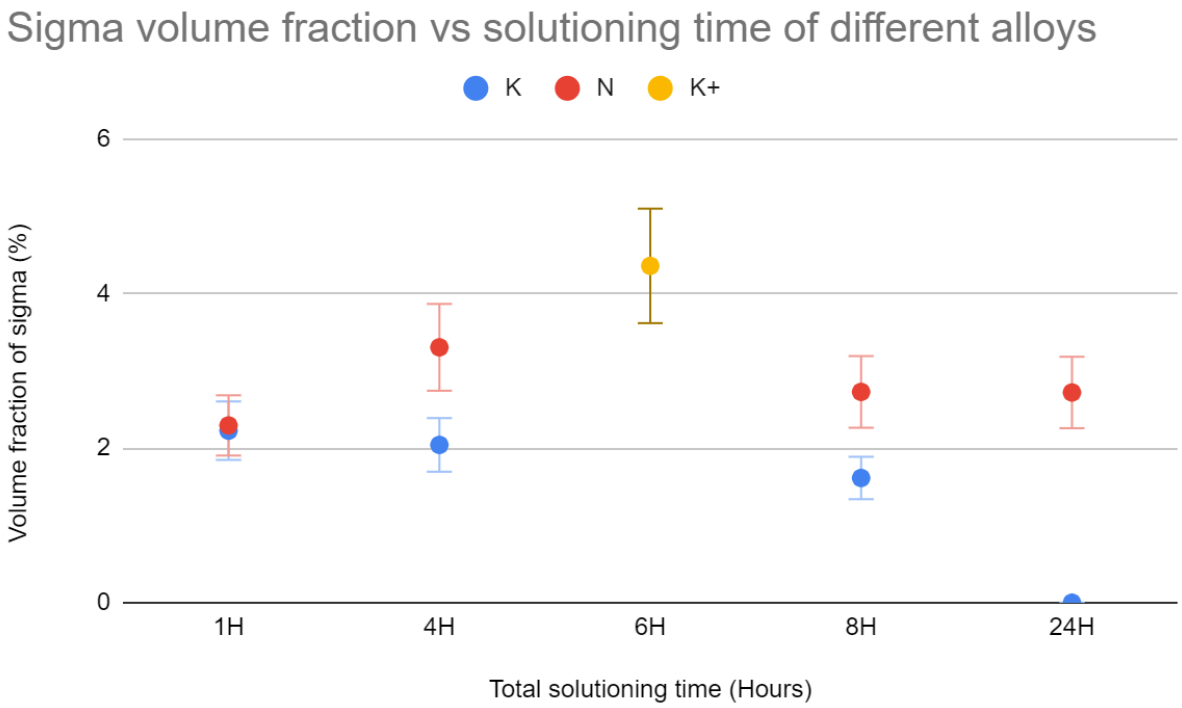

Figure 24: Volume fractions of σ in alloys 10K and 10N in comparison to the altered 10K regime.

Higher TCP phase volume fraction occurred in the double heat-treated 6 hour sample, this initially seems to contrast with other works, such as Park, who reported that Rhenium rich particles can be removed with additional heat-treatments, as it reduces the driving force for their precipitation (K.Park, 2021). However, this simply shows that after such short treatments the driving force is still present, and two high-temperature cycles increases the time the microstructure is at sufficient temperatures for

TCP phase precipitation (both in the typical TCP phase formation range, and the higher temperatures for formation seen in these highly segregated samples), whilst insufficiently reducing the driving force to prevent their formation. It would however, explain why once the microstructure is sufficiently homogenised, TCP phases stop appearing and the microstructure remains this way; at least until late in-service conditions promote the formation of TCP phases via different conditions (A.Bezold, 2022).

Repeating this process more times could confirm that the cycling promotes TCP phase nucleation, although eventually it can be assumed a saturation would be achieved and thus the process would have a diminishing effect.

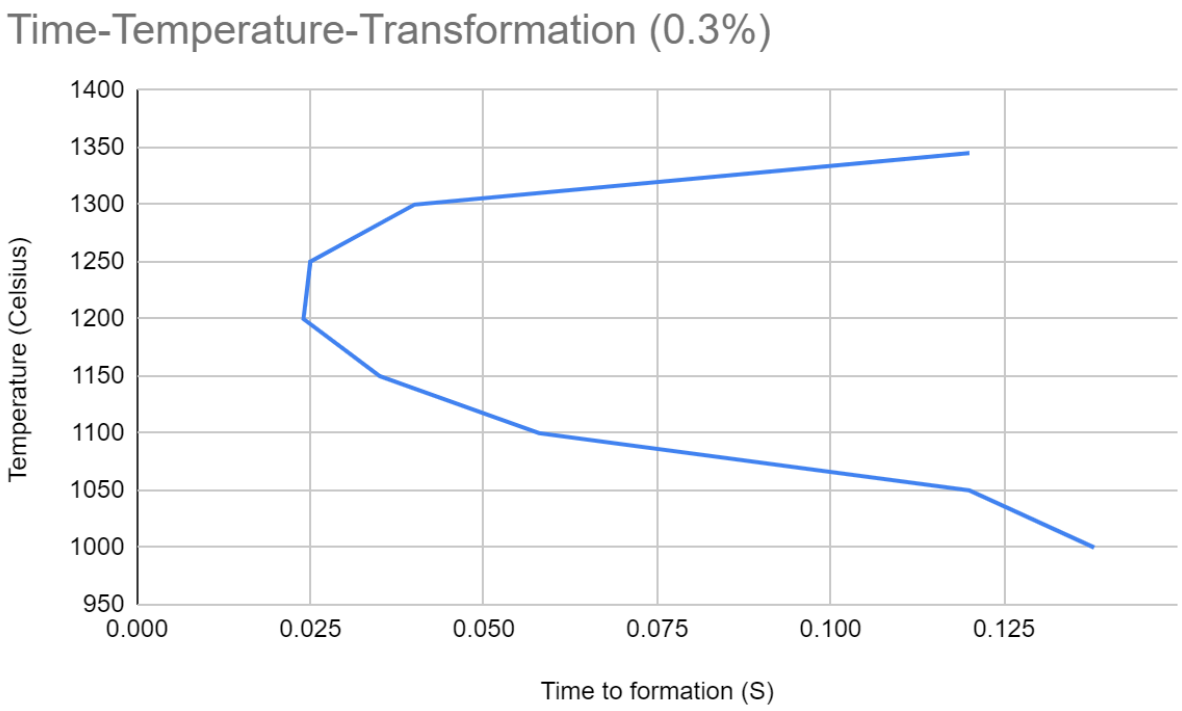

Figure 25: The time-temperature transformation of σ (0.3% vf) at varying temperatures, with minimum time to formation at the 1200℃ region. Data taken from twice treated K+ sample.

Figures 24 and 25 show the kinetics and potential for TCP phase formation are not perfectly aligned, with the fastest formation times occurring at a lower temperature regime then where the maximum potential volume fraction occurs. Compared to Figure 4, these results are shifted up and to the left.

By undergoing two heating cycles, the 6-hour sample would spend longer in the kinetic maximum region before reaching solutioning temperatures, where the higher equilibrium potential could maintain TCP phases and promote their growth.

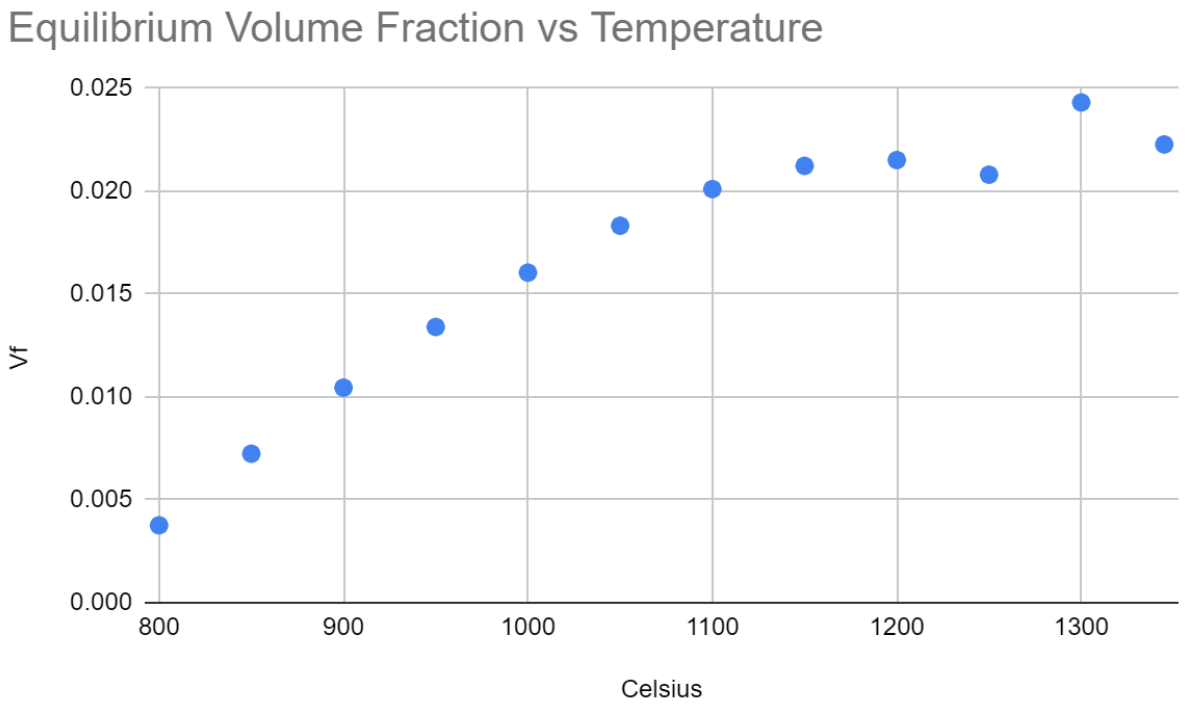

Figure 26: Modelled maximum volume fraction as a function of temperature, with a double peak, at 1200℃ and 1300℃.

The equilibrium values in Figure 26 show a double peak for maximum potential volume fraction, the reason for this is uncertain, but perhaps has to do with the dissolution of γ' prime, of which it's volume fraction would

decrease as it approaches its solvus temperature, potentially allowing for the larger matrix to remain saturated with rhenium without TCP phase precipitation. Alternatively, or in combination, each peak could represent the maximum potential for the different morphologies of σ, as discussed earlier, both morphologies can be encouraged at higher temperatures but by different mechanisms. It is worth noting one of the peaks, at approximately 1200℃, synchronises with Figure 25.

5.6. Conclusion

- The presence of TCP phase at 0 hours demonstrates that the heating or quenching regimes of the solutioning process must be when TCP phase precipitation occurs, however it cannot be ruled out that holding at solutioning temperature also contributes.
- σ-phase morphology could help reveal with section is responsible for TCP phase precipitation, or confirm that both contribute to their occurrence. However significant changes are posed in the methods to further investigate.
- CMSX-10N's precise solution heat treatment requirements leave it especially vulnerable to TCP phase precipitation due to its extended time in conditions promoting TCP precipitation, in addition to its heightened Re content.
- A statistical component, likely a probable function, of TCP phase precipitation is identified, with the cause of local variations being discussed at length.
- Repeated heating/quenching cycles promote TCP phase precipitation, producing more precipitates of larger size.

- Nucleation kinetics and formation potential do no align perfectly, likely creating a mix of overlapping contributions to the total σ-TCP volume fraction.

6. OVERALL CONCLUSIONS

A comprehensive literature review demonstrated that limited research has been carried out on the precipitation of TCP phases during manufacturing of Nickel-Based Superalloys, particularly during the solutioning stage. This thesis contributes to improving this knowledge base using both experimental and modelling results.

TCP phases were identified during solutioning of three alloys, CMSX-10N, CMSX-10K and in particular CMSX-4, initially chosen as a base alloy to its previously assumed stability in regards to TCP phases during its manufacturing.

This precipitation occurs during the earliest stages of the solutioning, as the faster diffusing aluminium diffuses into the dendrite core from the surrounding interdendritic regions it increases the volume of γ', refractory elements; most notably rhenium, already enriched in the dendrite core due to the high segregation from casting, are concentrated further into the γ matrix. When sufficiently enriched, a preference for the formation TCP phases, mostly likely σ-phase, occurs due to the saturation limits of rhenium in the γ-matrix. As shown in appendix E.

Modelling supports the conclusion of this new mechanism of precipitation of TCP phases, by suggesting fast precipitates rates of TCP phases within the solutioning timeframes and similar volume fractions of σ-phase compared to those measured from micrographs.

Which stage of the solutioning cycle the TCP phases form was discussed, and whilst currently it is indistinguishable via experimental results whether they form on heating and eventually dissolve back into the γ-matrix, or only form on quenching, through interpretation of modelling results TCP phases can be assumed to precipitate during heating, although each stage can contribute to the total TCP phase volume fraction.

Furthermore, the variance in TCP phases present in dendrites, from none at all to significant numbers of individual precipitates and total volume fraction is concluded to have a significant probability factor, with twice-treated samples containing significantly more TCP phases than those treated once. This is further concluded to be a result of micro-segregations and local defects lowering the energy needed for TCP phases to form, and that this might produce different morphologies of TCP phases influenced by the stages of solutioning.

The 24-Hour solutioning times for CMSX-4 and CMSX-10K are sufficient for the prevention of TCP phases, however this cycle is insufficient for CMSX-10N due primarily to its higher rhenium content. This is likely to be further exacerbated by its incremental heating during solutioning typical of industry.

7. FUTURE WORK

The previous sections, whilst illuminating the nature of TCP phase precipitation during the solutioning process of rhenium-containing alloys, raise numerous questions, or add to the need to answer long-standing ones.

This section considered avenues of investigation to acquire more information to determine the nature of TCP phase precipitation and growth, and experiments to distinguish some of the intertwined effects occurring during the previous work.

7.1. Quantify Morphology Contributions

Jin identifies that the same type of TCP phase can have different morphologies within the same sample (H.Jin, 2022). This is considered in section **5,** as a potential for varying locations of TCP phases, whether in the core or at the dendrite/eutectic interface, as well as for their relative size and potentially the cause of a double peak of maximum equilibrium.

Measuring the frequency of different types of morphology, as well as recording their locations within the dendrite (core vs arms), may allude to the understanding of some of the questions above. Deep etching would be sufficient to distinguish the different morphologies, (although TEM or other techniques should be used to confirm the crystal structure and identify of the TCP phases), calculating the volume fraction would be more complicated, as the image analysis software used in this work would be unable to distinguish the two. Individually calculating the ratio of the two, and their average size could be used to quantify each of their contributions to the total volume fraction.

However, TCP phases also vary greatly in location, from the dendrite/eutectic boundary (B.C.Wilson, 2003), to the centermost regions of

dendrites as seen in this work, to throughout the alloy (A.Yeh, 2006) to macro-regions such as the subsurface of the alloy (D.Spathara, 2021). These differing locations show varying TCP phases, with different morphologies, sizes, and volume fractions. Effectively cataloguing their occurrences; and the circumstances behind them: such as local compositional micro-homogeneities within the regional segregation, varying lattice parameters of the γ, γ', and TCP phases formed, potential stresses and times held at temperature (and the temperatures held at), a greater understanding of what factors influence which precipitates and to what extent. This can be combined with existing databases; such as those used by ThermoCalc, to improve their ability to model such precipitates, as seen in section **4.** current models; whilst capable of predicting their precipitation, fail to accurately gauge volume fractions and the timings of precipitation.

Only by extensive experimentation under these varying circumstances, such as proposed by Yeh (A.Yeh, 2006) can the mechanisms for the formation and growth of TCP phases be isolated and their individual contributions (if any) be better quantitatively measured.

However, one of the key issues addressed in section **5.**, is the inability to distinguish happenings at higher temperatures from one another. Typically samples are quenched to lock in the microstructure for an effective snapshot of their in-situ microstructure. Solutioning temperatures however are designed to remove the γ', which cannot be prevented by quenching, and as discussed the process of quenching in itself contributes to the precipitation of TCP phases via concentrating TCP phase forming elements in the reducing γ matrix as γ' precipitates out.

A highly ambitious attempt to understand the timing of precipitation during the solutioning cycle would be through in-situ imaging. By imaging the alloy during the stages of heating and quenching it could be more precisely determined when these TCP phases formed. However, currently,

there are no easy means to image these blades while undergoing solutioning. The 1300℃+ solutioning temperatures already impose difficulties in maintaining such temperatures for the process, introducing a microscope set up into this, whilst maintaining the strict conditions and enabling the microscope to operate and produce useful results would be a substantial task. These high temperatures would induce significant background noises, depending on the mechanisms used.

Currently x-ray diffraction and even heated TEM stages allow for analysis of materials at moderate temperatures in the region of 800°C. Whilst this is insufficient for a definitive understanding of where in the process TCP phases form, it could be used to understand the contribution of elements such as Al; that diffuse at these lower temperatures, towards elemental segregation and TCP phase precipitation. This region is also more synonymous with the follow-up heat treatment regimes post solutioning for the intention precipitation of γ'. Its contribution to TCP phase dissolution or precipitation post solutioning is also worth investigating within these TCP prone alloys to better understand the entirety of the manufacturing process of TCP phase content.

7.2. Component Geometry

Also of little investigation, is whether geometric features impact the rate and nature of TCP phase precipitation. Whilst the surface coatings have been studied extensively, whether features such as the root block or aerofoil possess more or less tendency to form TCP phases, despite being made of the same alloy. If so, this would reinforce the defect argument for TCP phase precipitation, as different areas undergo different stresses during casting and would have varying dislocations and other stress-induced defects. The thickness of the piece could also be responsible for this, as thinner sections

will have more surfaces which are also seen to be susceptible to TCP phases (D.Spathara, 2021). The thickness of the root block could cause local variations throughout the piece, inducing localised compositional changes, another potential for TCP phase nucleation as well as stresses from cooling as the thicker section contracts.

As discussed in section **4.**, this could produce a region susceptible to stress induced TCP phase precipitation whilst not sufficient for recrystallisation and thus being missed by standard manufacturing efforts.

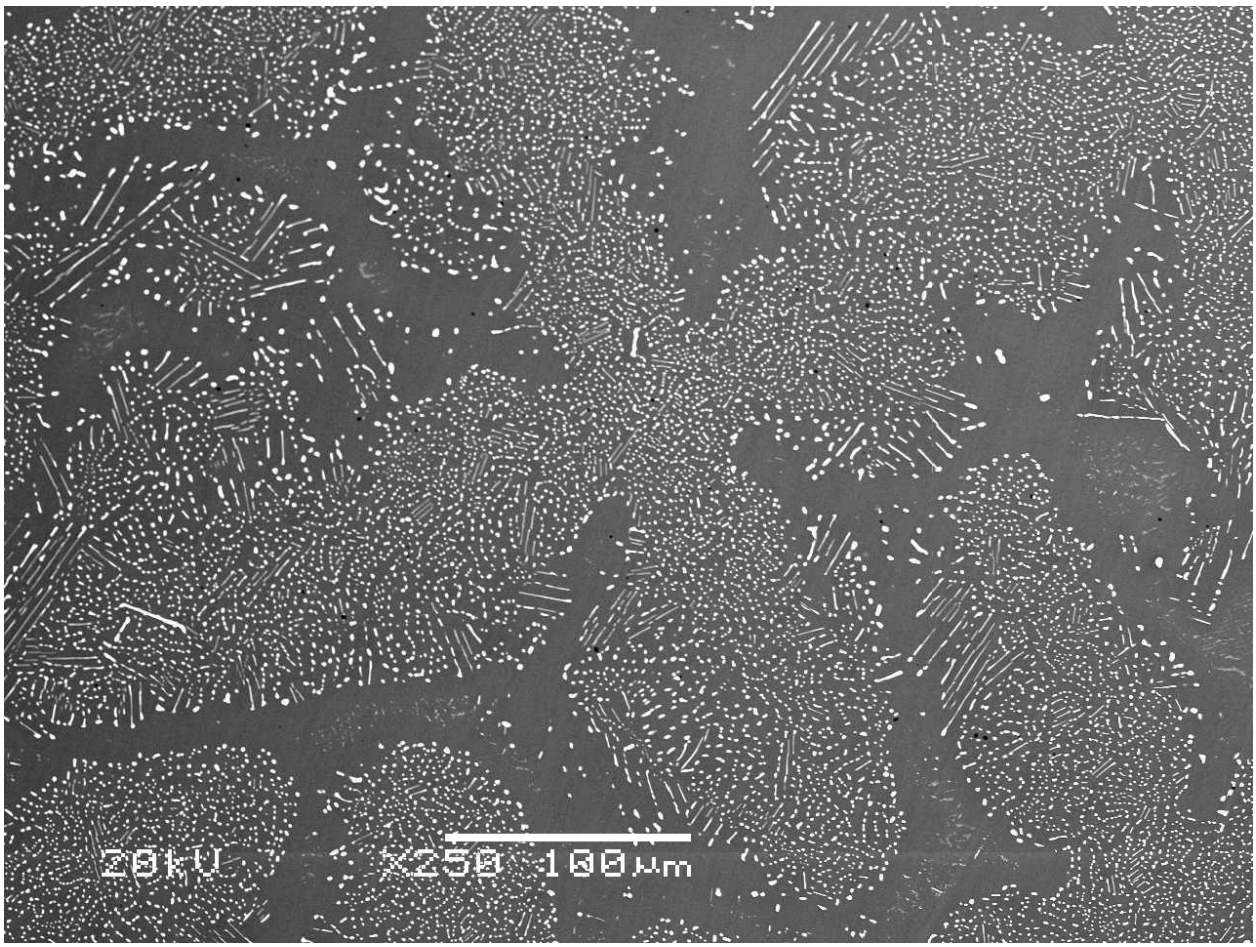

Figure 27: Large scale precipitation of refractory enriched particles throughout the dendritic regions of samples taken from the surface.

Images of samples from the surface of test pieces show a substantial difference in structure. Figure 27 shows numerous precipitates throughout dendrites. Large TCP precipitates can still be seen (more examples are given in appendix D), but these smaller particles had very similar compositions (they appear less concentrated in TCP phase forming elements, than typical TCP phases, but this is likely due to the interaction volume of the BSE being of similar scale to the precipitates, overlapping with the surrounding depleted matrix).

The boundaries for nucleation are substantially different at the surface. Significant study has gone into TCP phase formation at the surface, as this is the location where they are typically seen in-service due to the aluminized coating diffusing into the blade (D.Spathara, 2021), enhancing the effect of concentrating the Re into smaller and smaller volume fractions of γ.

However, no additional Al is present in the samples, with the test pieces exposed to an argon-filled atmosphere. If anything, Al sublimation from the surface would reduce the local Al concentration. Al might diffuse in from the bulk of the sample to fill this, this movement of Al could be the initiator for TCP phase precipitation. The varying atoms within the alloy have many different atom sizes, as they move they could create defects, some may remain persistent in the structure long enough for TCP phase formation, which is seen to be exceptionally quick, thus before these defects relax TCP phases could nucleate, this process would be exasperated at the surface due to sublimation and diffusion.

Furthermore this would support the extra TCP phase precipitation from Figure 27, as more Al diffusion has occurred without any other relaxation. However, Al diffuses at a low temperature relative to the solutioning temperature. Heating the sample at lower temperatures could reveal if this would promote TCP phases at a range of temperatures, however, this would run into some of the same issues described insection **5.** As alternating the

heating regime would affect the precipitation of TCP phases, it would be difficult to distinguish them from one another. However, precisely measuring the diffusion rates and distances of Al from the interdendritic into the dendrites may provide a base of data for in-depth simulations, where the heating regime can be carefully modelled to see if and when it produces TCP phases in light of the changing composition of the local region.

Alternatively, the surface region of Figure 27 could be enriched in TCP phase forming elements. As the dendrites solidify γ enriching elements; many which contribute to TCP phase formation, would be pulled in from the liquid into the dendrites, enriching the dendritic front, this would proceed until it reached the edges of the component, creating a localised enriched surface. This form of enrichment has been seen in the liquid enriched zones (D.L.Sponseller, 1996) but has not been a widely reported phenomenon, it would make for a better explanation of these extensive TCP phases at the surface and justified further investigation.

7.3. Optimise Chemistry

The as-cast structure lacks any TCP phases, whilst Al is not yet diffused into the core the cooling times; from post solidification but before cooling to room temperature, could enable some diffusion to happen, and due to the quick forming times of TCP phases seen in section **4.**, where the modelling also suggests a thermodynamic potential for TCP phases, it is surprising not to see any with so many later on based on these models alone and that TCP phases have been seen in casting by others (F.Long, 2009).

This could promote the defect precipitation hypothesis over the diffusion-only method, requiring some time before sufficient precipitation can occur hence why they are seen after some solutioning but not before. Understanding this is important, as TCP phases in other alloys have been

seen in the as-cast state (B.C.Wilson, 2003), why this variance occurs, and more importantly what causes could be beneficial to help prevent their occurrence altogether.

Some alloys are prone to TCP phase precipitation at the as-cast stage, such as Rae's (C.A.E.Rae, 2001), comparing the compositions of these alloys to those of this work to determine whether it is a product purely of segregation would further an understanding of TCP phase formation. Furthermore, creating dendrites with heterogeneous features, such as induced stresses, inclusions, porosities and measuring what increase; if any, this has on TCP phase precipitation at the as-cast stage, and during solutioning treatment, would further which if these contributes to TCP phase formation and if both, help quantity their individual contributions.

7.4. Quantify mechanical properties

Whilst there is a consensus throughout literature that TCP phases are certainly detrimental to desirable properties of these alloys, the extent of what is still poorly quantified. Attempts to determine this have even shown no reduction in properties in some circumstances (M.Pessah, 1992). However, Pessah et al focused on the μ-TCPs, largely absent in this work. As discussed the different types of TCP phases will have differing effects, and even the same phase can possess different morphologies. A more thorough investigation into quantifying how the types, location and quantity of TCP phases impact the overall performance of turbine blades is essential, especially in light of the conclusions of this work, that current alloy compositional complexity combined with current manufacturing processes still leave CMSX-10N prone to TCP phase precipitation. Being able to predict their effect on the properties of the turbine blades would enable further alloy

development with confidence about how much the properties would be impacted by the inclusion of TCP precipitates.

7.5. Additions

Of interest for future work, would be the diffusivity of Al in the specific alloy compositions. If the higher Re content in CMSX-10N, is sufficient to reduce the diffusion rate of Al in it, it could explain why it takes longer for TCP phases to form than in CMSX-10K, despite an overall higher propensity to form TCP phases. Regardless, since Al has been concluded to be very influential on the formation of TCP phases; despite not being a TCP phase forming element, a deeper understanding of its behaviour during solutioning and impact on the process is needed to better understand TCP phase formation during manufacturing.

Co concentrations were significantly lower in the precipitates compared to the alloy. Caron (P.Caron, 1999) reports that cobalt's contribution to TCP phase precipitation is controversial due to conflicting reports. Alloys vary substantially in their inclusion of Co, such as 3-4wt% in CMSX-10N whilst as high as 12% in Rene N6, yet both are sufficient for commercial application.

Whilst concentrations are lower in these precipitates, suggesting that it does not contribute to TCP phase precipitation Co has been shown to significantly affect the segregation behaviour of other elements, especially Rhenium (E.C.Caldwell, 2004), reducing the K value substantially.

How Co contribution affects the precipitation of these TCP like phases during solutioning would be of great interest, both as a way to see if these phases can be prevented from forming, and to bring clarity to cobalt's contribution to TCP phase precipitation.

Ru; an elemental addition seen in some newer generations of superalloy, has been shown to improve the segregation of Re in particular

(E.C.Caldwell, 2004). Furthermore the addition of Ru in place of Re has been shown to reduce TCP phase propensity whilst maintaining the properties of 3rd generation alloys (P.Caron, 2000), this suggests there are methods of maintaining the desired properties whilst reducing TCP phase occurrence. Further studies to better understand what properties of Re addition produce these effects may also boost the understanding of TCP phase precipitation, as well as predict other, more economical elements that could also have this effect, as Re has already seen efforts to replace it (Y. Mori, 2016).

8. REFERENCES

- M.V.Acharya, G.E.Fuchs, (2004). *The effect of long-term thermal exposures on the microstructure and properties of CMSX-10 single crystal Ni-base superalloys.* Materials Science and Engineering A, volume 381, issue 1-2, pp. 143-153.
- S.Antonov, J.Huo, Q.Feng, D.Isheim, D.N.Seidman, R.C.Helmink, E.Sun, S.Tin, (2017). *σ and η Phase formation in advanced polycrystalline Ni-base superalloys.* Materials Science and Engineering A, volume 687, pp. 232-240.
- A. Bezzold, H. Stone, C. Rae, S. Neumeier, (2022). *In Situ Investigation of TCP Phase Formation, Stress Relaxation and γ/γ' Lattice Misfit Evolution in Fourth Generation Single Crystal Ni-Base Superalloys by X-Ray High-Temperature Diffraction.* Metallurgical and Materials Transactions A: Physical Metallurgy and Materials Science, volume 53, issue 8, pp. 2890-2901.
- P.Caron, (1999). *Evolution of Ni-based superalloys for single crystal gas turbine blade applications.* Aerospace Science and Technology, volume 3, issue 8, pp. 513-523.
- P.Caron, (2000). *High γ' Solvus New Generation Nickel-Based Superalloys for Single Crystal Turbine Blade Applications.* Superalloys 2000, pp. 737-746.
- H.K.D.H. Bhadeshia, (2003) '*Nickel Based Superalloys'*, University of Cambridge, pp. 1-11.
- E.C.Caldwell, F.J.Fela, G.E.Fuchs, (2004). *The segregation of elements in high-refractory-content single-crystal nickel-based superalloys. JOM* volume 56, pp. 44–48.

- Cannon Muskegon (2023) *Product Catalog: Vacuum Alloys:* [accessed 16 May, 2024] https://www.cannonmuskegon.com/products/vacuum-melt-alloy
- K.Cheng, C.Jo, T.Jin, Z.Hu, (2011). *Precipitation behavior of μ phase and creep rupture in single crystal superalloy CMSX-4,* Journal of Alloys and Compounds, volume 509, issue 25, pp. 7078-7086.
- R.Darolina, D.Lahrman, R.Field, (1988). *Formation of Topologically Closed Packed Phases in Nickel Base Single Crystal Superalloys. Superalloys, pp. 255-264.*
- R.Dreshfield, R.L. Ashbrook, (1969). *Sigma phase formation and it's effect on the stress-rupture properties of IN-100.* Nasa Technical Note, TN D-5185, pp. 1-28.
- S.Duval, S.Chambreland, P.Caron, D.Blavette (1994) *Phase composition and chemical order in the single crystal nickel base superalloy MC2.* Acta Metallurgica et Materialia, volume 42, issue 1, pp. 185-194.
- N.El-Bagoury, A.Omar, K.Ogi, (2012). *Role of Rhenium on Solidification, Microstructure, and Mechanical Properties of Standard Alloy 718.* Metallography, Microstructure and Analysis, volume 1, issue 1, pp. 35-44.
- J.Emsley, (2011) *'Nature's Building Blocks' An A-Z Guide to the Elements.* New Edition, University of Oxford University Press
- G.L.Erickson, (1996) *The Development and Application of CMSX-10*. *Superalloys* 1996, pp. 35-44.
- Q.Feng, 2003. *Solidification of High-refractory ruthenium-containing superalloys.* Acta Materialia, volume 51, issue 1, pp. 269-284.
- E.Fleischmann, M.K.Miller, E.Affeldt, U.Glatzel (2015). *Quantitative experimental determination of the solid solution hardening potential of*

rhenium, tungsten and molybdenum in single-crystal nickel-based superalloys. Acta Materialia, volume 87, Pp. 350-356.

- G.E.Fuchs (2001). *Solution heat treatment response of a third generation single crystal Ni-base superalloy.* Materials Science and Engineering:A, volume 300, issue 1-2, pp. 52-60.
- B.Geddes, H.Leon, and X.Huang, (2010). *Superalloys: Alloying and Performance.* Materials Park, Ohio: ASM international.
- T.B.Gibbons, B.E.Hopkins, (1984). *Creep behavior and microstructure of Ni-Cr base alloys. Metal Science,* volume 18, issue 5, pp. 273–280.
- B.Gleeson, (2009). *Compositional factors affecting the establishment and maintenance of Al 2 O 3 scales on Ni–Al–Pt systems* - Scientific Figure on ResearchGate. Available from: https://www.researchgate.net/figure/A-schematic-showing-the-L1-2-crystal-structure-of-c-0-Ni-3-Al_fig2_248076132 [accessed 16 May, 2024]
- K.Harris, G.Erickson, R.Schwer, (1984). *MAR M 247 Derivations - CM 247 LC DS Alloy and CMSX Single Crystal Alloys: Properties & Performance.* Superalloys 1984, pp. 221-230
- Huixin Jin, Jianxin Zhang, Youjian Zhang, Wenyang Zhang, Shiyu Ma, Shengcheng Mao, Yiqun Du, Zihan Wang, Jingyu Qin, Qi Wang, (2022). *Effects of the orientation relationships between TCP phases and matrix on the morphologies of TCP phases in Ni-based single crystal superalloys,* Materials Characterization, Volume 183, Article 111609.
- H.Jin, J.Li, S,Liu, (2007). *Stress Rupture Properties of the Second Generation Single Crystal Superalloy DD6 after High Temperature Exposure.* Materials Science Forum, volumes 546-549, pp. 1249-1252.
- M.S.A Karunaratne, (2001). *On the microstructural instability of an experimental nickel-based single-crystal superalloy*. Metallurgical and

Materials Transactions A: Physical Metallurgy and Materials Science. volume 32, issue 10, pp. 2409-2421.

- N.Koneva, E.Nikonenko A, N.Popova, (2021). *Microstructural changes in ni-al-cr-based heat-resistant alloy with re addition.* Crystals, volume 11, issue 2, pp. 1-13.
- Xin Li, Qisong Zhu, Sinong Liu, Feng Li, Fuwen Chen, Hui Wang, Hui Chang, (2022). *Phase transformation and microstructure evolution of Ti6Al4V-0.55Fe alloy with different initial microstructure during continuous heating.* Journal of Materials Research and Technology, volume 18, pp. 1704-1716.
- C.T.Liu, J.A. Horton, (1995). *Effect of refractory alloying additions on mechanical properties of near-stoichiometric NiAl*. Materials Science and Engineering A, volumes 192-193 pp. 170-178.
- L.R.Liu (2003). *Microstructural evolution of a single crystal nickel-base superalloy during thermal exposure.* Materials Letters. volume 57, issue 29, pp. 2540-2546.
- F.Long, Y.S.Yoo, C.Y.Jo, S.M.Seo, H.W.Jeong, Y.S.Song, T.Jin, Z.Q.Hu (2009). *Phase transformation of η and σ phases in an experimental nickel-based superalloy.* Journal of Alloys and Compounds, volume 478, issues 1–2, pp. 181-187.
- Haibo Long, Yinong Liu, Shengcheng Mao, Hua Wei, Jianxin Zhang, Shiyu Ma, Qingsong Deng, Yanhui Chen, Ze Zhang, Xiaodong Han, (2018). *Minimum interface misfit criterion for the precipitation morphologies of TCP phases in a Ni-based single crystal superalloy.* Intermetallics, volume 94, pp 55-64.
- Isabel.Henrich, (2024). *How does a turbofan engine work - Ingestion* AreoReport, [last accessed, 14/06/2024] https://aeroreport.de/en/good-to-know/how-does-a-turbofan-engine-work

- W.T.Loomis, J.W.Freeman, D.L.Sponseller (1972), *Influence of molybdenum on the μ-phase in experimental nickel base superalloys.* Met Trans, volume 3, issue 4, pp. 989-1000.
- S.K.Makineni et al (2015). *Synthesis of a new tungsten-free c–c0 cobalt-based superalloy by tuning alloying additions.* Acta Materialia, volume 85, pp. 85-94.
- Y.Mori, T.Yokokawa, T.Kobayashi, H.Harada, S.Suzuki, Shinsuke, (2016). *Phase Stability of Nickel-Base Single Crystal Superalloys Containing Iridium Substituting for Ruthenium.* MATERIALS TRANSACTIONS. volume 57, pp. 1845-1848.
- K.Park, P.Withey, (2021) *General view of rhenium-rich particles along defect grain boundaries formed in nickel-based single-crystal superalloy turbine blades: Formation, dissolution and comparison with other phases.* Crystals, volume 11, issue 10, pp 1201-1217
- Y.Pei, Y.Zhao, C.Lu, C.Qin, W.Xiao, (2009). *The Development and Application of WACM*. Advances in Water Resources and Hydraulic Engineering. Springer, Berlin, Heidelberg. pp. 289-295.
- M.Pessah, E.Martín, P.Caron and K.Tasadduq (1992). *Effect of Phase on the Mechanical Properties of a Nickel-Base Single Crystal Superalloy.* Superalloys 1992: pp. 567-576.
- Plymouth (2021) *'Understanding Interaction Volume'* University of Plymouth, [last accessed, 17/06/2024] https://www.plymouth.ac.uk/about-us/university-structure/faculties/science-engineering/electron-microscopy-centre/understanding-interaction-volume
- C.M.F.Rae, M.Karunaratne, C.Small, R.Broomfield, C.Jones, R.C.Reed, (2000). *Topologically Close Packed Phases in an Experimental Rhenium-Containing Single Crystal Superalloy.* Superalloys 2000. pp.767-776.

- C.M.F.Rae, R.C.Reed (2001). *The precipitation of topologically close-packed phases in rhenium-containing superalloys.* Acta Materialia, volume 49, issue 19, pp. 4113-4125.
- C.M.F.Rae, M.Hook, R.C.Reed (2005). *The effect of TCP morphology on the development of aluminide coated superalloys.* Materials Science Engineering: A, volume 396, issue 1-2, pp. 231-239.
- G.A.Rao, M.Sirnivas, D.S.Sarma (2004). *Effect of solution treatment temperature on microstrucutre and mechanical properties of hot isostatically pressed superalloy Inconel*718.* Materials Science and Technology, volume 20, issue 9, pp. 1161-1170.
- R.C.Reed, N.Matan, D.C.Cox, M.A.Rist, C.M.F.Rae, (1999). *Creep of CMSX-4 Superalloys single crystals: effects of rafting at high temperature.* Acta Materialia, volume 47, issue 12, pp. 3367-3381.
- R.C.Reed, (2006). *The Superalloys: Fundamentals and Applications.* Imperials College of Science, Technology, and Medicine, London: Cambridge University Press.
- T.D.Reynolds, D.M.Collins, N.K.Soor, S.R.Street, N.Warnken, P.M.Mignanelli, M.C.Hardy, H.E.Evans, M.P.Taylor (2019). *Identifying heating rate dependent oxidation reactions on a nickel-based superalloy using synchrotron diffraction.* Acta Materialia. volume 181, pp. 570–583.
- C.Rodenkirchen et al (2023) *Effect of Alloying on the Microstructure, Phase Stability, Hardness, and Partitioning Behavior of a New Dual-Superlattice Nickel-Based.* Metallurgical and Materials Transactions A: Physical Metallurgy and Materials Science, volume 54, issue 5, pp. 1902-1923.
- B.Seiser, R.Drautz, D.G.Pettifor, (2011). *TCP phase predictions in Ni-based superalloys: Structure maps revisited.* Acta Materialia, volume 59, issue 2, pp. 749-763.

- C.T.Sims, (1984). *A HISTORY OF SUPERALLOY METALLURGY FOR SUPERALLOY METALLURGISTS.* Chester T. Sims General Electric Company Schenectady, New York 12345
- Dimitra Spathara, Dmitry Sergeev, Dietmar Kobertz, Michael Müller, Duncan Putman, Nils Warnken, (2021). *Thermodynamic study of single crystal, Ni-based superalloys in the γ+γ′ two-phase region using Knudsen Effusion Mass Spectrometry, DSC and SEM.* Journal of Alloys and Compounds, volume 870, pp. 159-175.
- D.L.Sponseller, (1996) *Differential Thermal Analysis of Nickel-base superalloys.* Superalloys 1996, pp. 259-270.
- F.Sun, J.X.Zhang (2011). *Topologically Close-Packed Phase Precipitation in Ni-Based Superalloys.* AMR 2011; volume 320, pp. 26–32.
- ThermoCalc, (2021). "The CALPHAD Methodology." Last modified September 28. https://thermocalc.com/about-us/methodology/the-calphad-methodology/
- S.Tin, T.M.Pollock, W.Murphy, (2001). *Stabilization of Thermosolutal Convective Instabilities in Ni-Based Single-Crystal Superalloys: Carbon Additions and Freckle Formation.* Metallurgical and Materials Transactions A: Physical Metallurgy and Materials Science, volume 32, pp. 1743-1753.
- J.Wahl, K.Harris, (2018). *Improved 3rd Generation Single Crystal Superalloy CMSX-4® Plus (SLS)-a study of evolutionary alloy development*. Proceedings of the international symposium on superalloys.
- W.S.Walston, J.C.Schaeffer, W.H.Murphy, (1996). *A NEW TYPE OF MICROSTRUCTURAL INSTABILITY IN SUPERALLOYS - SRZ.* TSuperalloys 1996, pp. 9-18.

- D.Wang, J.Zhang, L.Lou, (2010). *On the role of μ phase during high temperature creep of a second generation directionally solidified superalloy.* Materials Science and Engineering A, volume 527, issue 20, pp. 5161-5166.
- L.Wang, F.Pyczak, J.Zhang, L.H.Lou, R.F.Singer, (2012). *Effect of eutectics on plastic deformation and subsequent recrystallization in the single crystal nickel base superalloy CMSX-4.* Materials Science and Engineering A, volume 532, pp. 487-492.
- Y.Wang, Z.Liu, L.Qiao, S.Li, (2021). *Probing single crystal orientation by X-ray diffraction for nickel-based superalloys.* Results in Physics, volume 90, Article 104769.
- N.Wanderka, U.Glatzel, (1995). *Chemical composition measurements of a nickel-base superalloy by atom probe field ion microscopy.* Materials Science and Engineering: A, volume 203, issue 1-2, pp. 69-74.
- N. Warnken, (2016). *Studies on the Solidification Path of Single Crystal Superalloys.* Journal of Phase Equilibria and Diffusion, volume 37, issue 1, pp. 100-107.
- F.Whittle, (1930). *Improvements relating to the propulsion of aircraft and other vehicles.* Patent GB347206A.
- A.S.Wilson, (2017). *Formation and effect of Topologically close-packed phases in nickel-base superalloys.* Materials Science and Technology, pp. 1108-1118.
- B.C.Wilson, J.Hickman, G.E.Fuchs, (2003). *The effect of solution heat treatment on a single-crystal Ni-based superalloy.* JOM, volume 55, issue 4, pp. 35-40.
- A.Yeh, C.M.F Rae, S.Tin, (2006). *Effects of Ru on the high-temperature phase stability of Ni-base single-crystal superalloys.* Metallurgical and Materials Transactions A. volume 37, pp. 2621-2631.

- L.Zhonglin, Z.Dandan, S.Xianglin, X.Qingyan, L.Baicheng, (2016). *Role of as-cast dendritic microstructure in recrystallization of a Ni-based single crystal superalloy.* Journal of Alloys and Compounds, volume 660, pp. 115-124.
- L.C.Zhou, M.Huang, J.Xiong, J.Li, J.Zhu (2015). *Sub-solvus cellular recrystallization and P phase formation in a single-crystal superalloy containing Re.* Acta Metallurgica Sinica, volume 28, issue 1, pp.72-76.

9. APPENDIX

Appendix A, showing TCP phases present in CMSX-4 after 8 hours at solutioning conditions. A1 possessing several TCP phases in conjunction, whilst A2 demonstrating the small size and depletion of high Z value elements around the TCP phase.

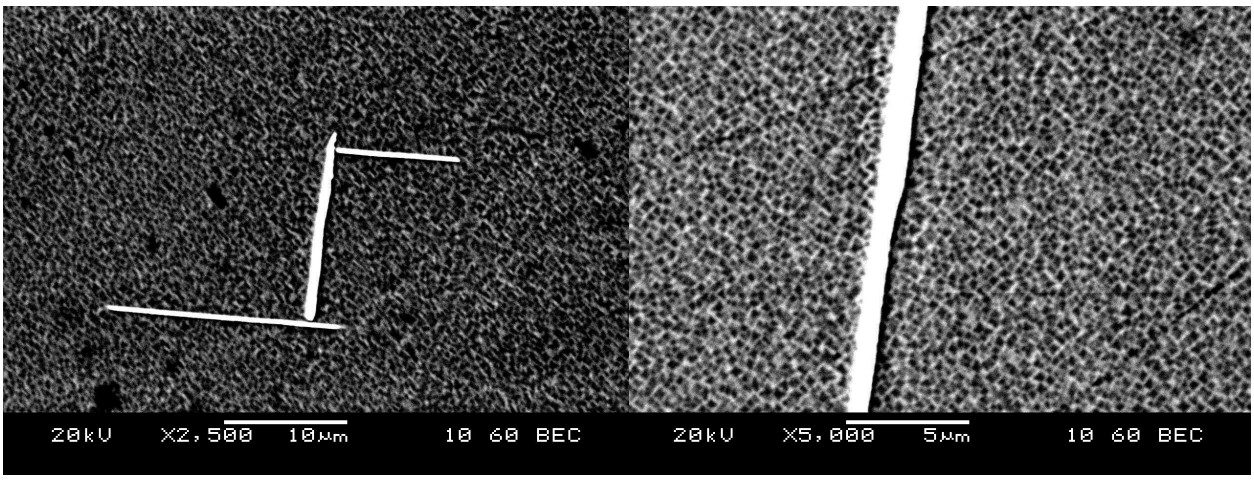

Appendix B, demonstrating the occurrence of TCP phases outside the dendrite core.

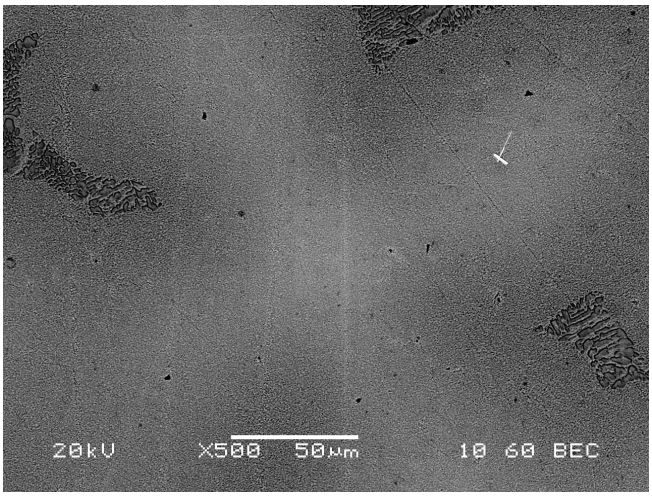

Appendix C, showing TCP phases throughout the CMSX-10K+ sample.

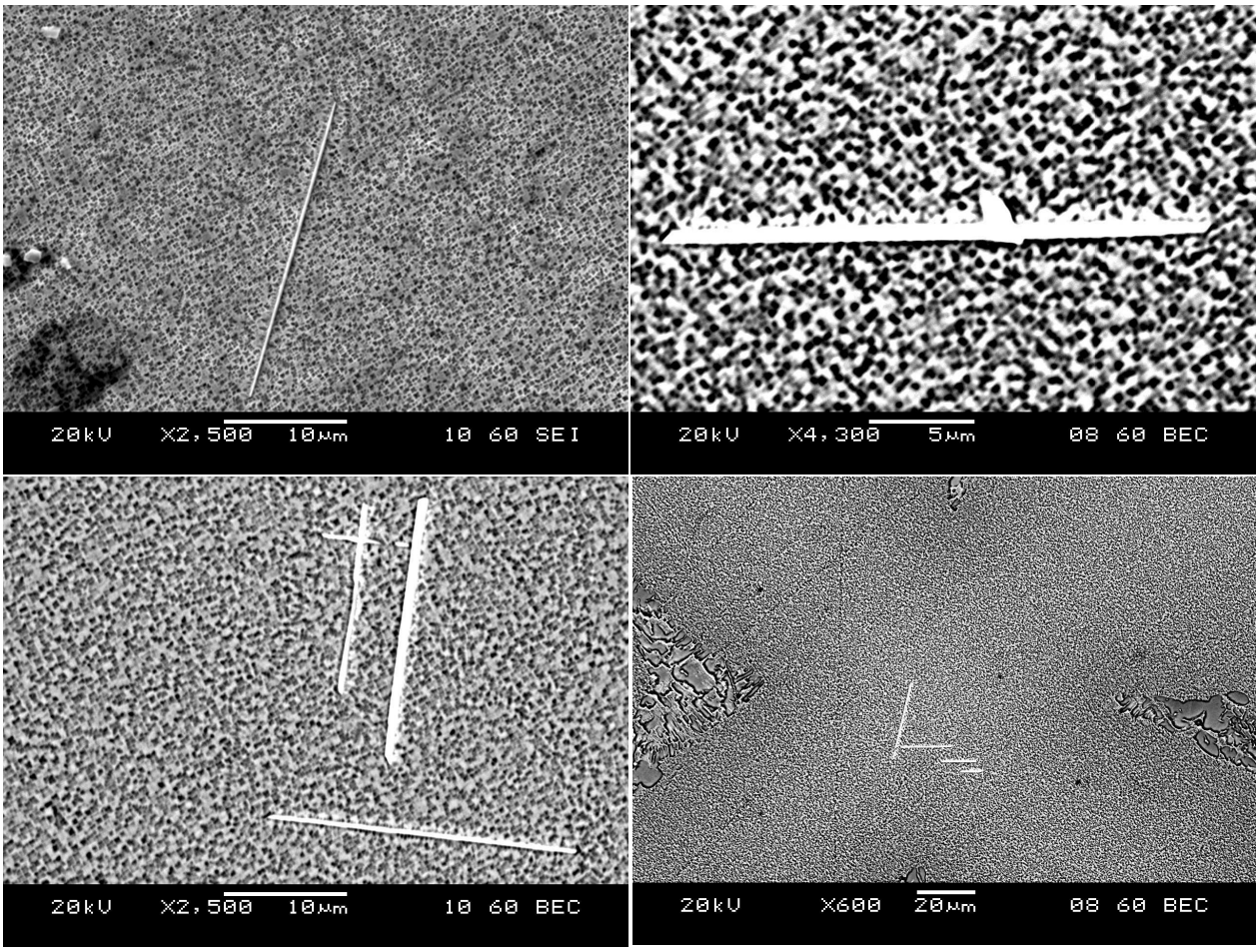

Appendix D, large number of high Z value element precipitates.

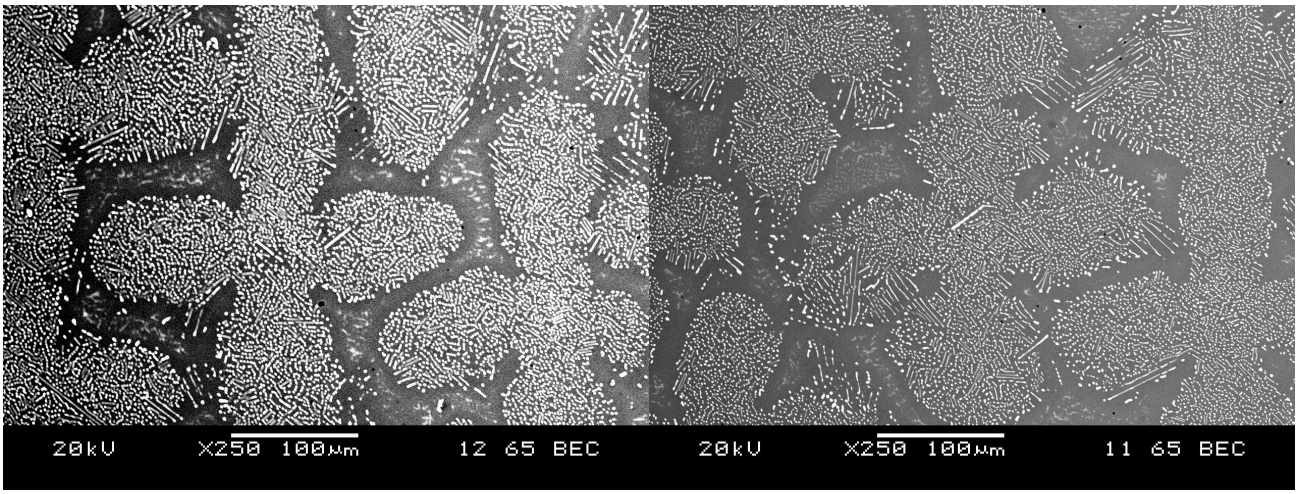

Appendix E, a step by step schematic of the TCP precipitation and dissolution process